STUDIES ON HYDROAMINATION REACTIONS USING HETEROGENEOUS CATALYSTS

A thesis submitted to the

UNIVERSITY OF PUNE

for the degree of

DOCTOR OF PHILOSOPHY

(in Chemistry)

BY

Ganapati V. Shanbhag

**CATALYSIS DIVISION
NATIONAL CHEMICAL LABORATORY
PUNE- 411008, INDIA**

January 2008

CERTIFICATE

Certified that the work incorporated in the thesis entitled **"Studies on hydroamination reactions using heterogeneous catalysts"** submitted by **Mr. Ganapati V. Shanbhag**, for the Degree of **Doctor of Philosophy**, was carried out by the candidate under my supervision in the Catalysis Division, National Chemical Laboratory, Pune - 411008, India. Materials obtained from other sources have been duly acknowledged in the thesis.

Dr. S. B. Halligudi

(Research Supervisor)

Dedicated to…

My beloved parents and teachers

ACKNOWLEDGEMENT

"Research is the art of seeing what others see, but thinking what others don't think"

- Ralph Waldo

Contents

ABBREVIATIONS

BET	Brunauer-Emmett-Teller
BJH	Barret–Joyner–Halenda
EA	Ethylacrylate
FTIR	Fourier-transform Infrared
GC	Gas Chromatography
GCMS	Gas Chromatography-Mass Spectroscopy
HA	Hydroamination
HPA	Heteropoly acid
LCT	Liquid Crystal Template
MAS	Magic angle spinning
MCM	Mobil composite material
MPA	Molybdophosphoric acid
MS	Mesoporous silica materials
NMR	Nuclear magnetic resonance
PhAc	Phenylacetylene
RT	Room Temperature
SEM	Scanning electron microscopy
SBA	Santa Barbara Amorphous
STA	Silicotungstic acid
TCD	Thermal conductivity detector
TEM	Transmission electron microscopy
TEOS	Tetraethyl orthosilicate
TG-DTA	Thermogravimetry-Differential Thermal Analysis
TPA	Tungstophosphoric acid
TPD	Temperature programmed desorption
TPR	Temperature programmed reduction
XRD	X-ray diffraction

CHAPTER I

1.1. Hydroamination

The search for new reactions as well as the application of known catalysts or reagents towards new targets is still important research areas in chemistry. If the reaction does not give the desired product in 100% yield, often waste is produced, which is unavoidable because it results in low atom economy [1] or atom efficiency [2]. Due to the drive towards the so-called "green chemistry" [3], the synthetic chemist in the future will be more and more concerned about atom economy and feedstock compared to present scenario. Although a number of "classic" organic reactions developed in the first half of the 20th century, e.g., pericyclic reactions, proceed with 100% atom efficiency, nowadays it is especially the catalysts that offer possibilities to achieve atom efficiency in organic synthesis.

The catalytic formations of carbon-carbon or carbon-hydrogen bonds are particularly important in hydrogenations, telomerisations, hydroformylations, hydrocyanations, etc [4, 5]. On the other hand, the atom efficient formation of carbon-heteroatom bonds, e.g., carbon-nitrogen bonds, are rare. This is surprising if one considers the fundamental importance of amines and their derivatives as natural products, pharmacological agents, fine chemicals, and dyes [6-9]. Hence, there is a considerable interest in the development of new efficient synthetic protocols for the construction of carbon-nitrogen bonds. One such synthetic route which utilizes cheap and readily available feedstock of olefins and amines and proceeds theoretically with 100% atom efficiency, thus offering economic and environmental benefits compared to other classical organic synthetic methods is called "Hydroamination."

Hydroamination is defined as a reaction, which involves the addition of N-H bonds across C-C multiple bonds. 100% atom economy makes hydroamination more attractive as no by-products such as salts or water are produced. Hydroamination reaction merges perfect atom economy with thermodynamic feasibility. However, this reaction has a considerable kinetic barrier and hence the use of catalyst is a desired option. The metals and metal complexes are known to catalyze hydroamination reactions [10]. To catalyze these reactions the possible approaches employed are either activation of an amine or an olefin.

        In principle, the addition of amines gives two regioisomeric products *viz.* Markovnikov and *anti*-Markovnikov products depending on the stability of the intermediate. (Although the original Markovnikov rule [11] is limited to the addition of hydrogen halides, clearly this rule can be used in a much wider context. A more generalized statement is "A positive part (electrophile) of the addendum prefers to add to that carbon atom of the unsymmetrical alkene (or alkyne), which contains maximum number of hydrogen atoms). For the amine addition of unactivated alkenes and alkynes, the Markovnikov product is generally favored due to the higher stability of intermediate carbocation. There are two types in hydroamination viz. intermolecular which involves the addition of an amine to olefin (Scheme 1.1) and intramolecular in which C-C multiple bond and amine group are part of the same molecule (Scheme 1.2). Intramolecular hydroamination results in cyclization leading to nitrogen heterocyclic compound, which makes it an important route in the synthesis of natural products, fine chemicals and drugs.

        Hydroamination of alkenes and alkynes offers the most attractive route to numerous classes of organo-nitrogen molecules such as alkylated amines, enamines or imines [12, 13]. These compounds are of significant industrial importance as chemical intermediates in the area of natural products, pharmaceuticals, fine chemicals, dyes, polymers and surfactants. To name few examples, this reaction is used in the synthesis of the medicinal drugs like amantadine, memantine, carmantadine, and amantocillin, tromaril, natural products such as (-) menthol, (±) pinidine, (R)-coniine, fine chemicals such as 2-methylpiperidine, indole etc [14-16].
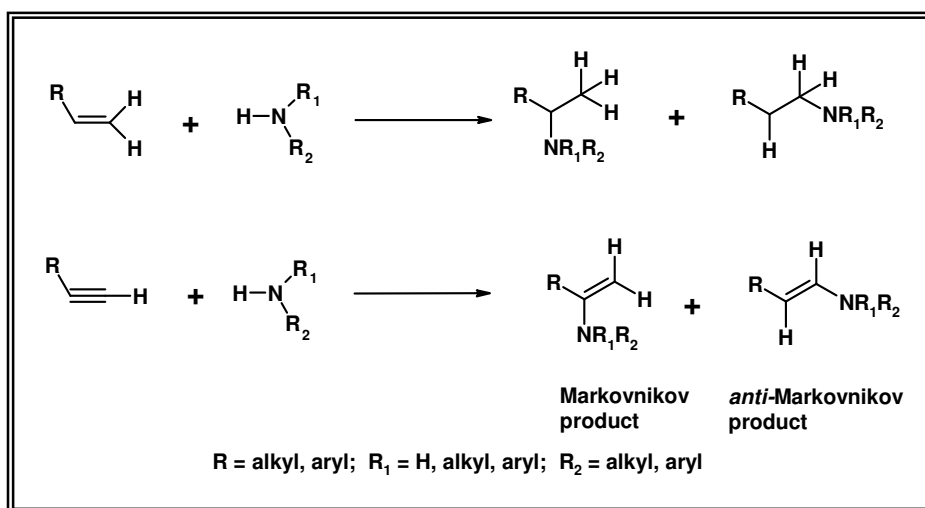
Scheme 1.1. Intermolecular hydroamination reactions
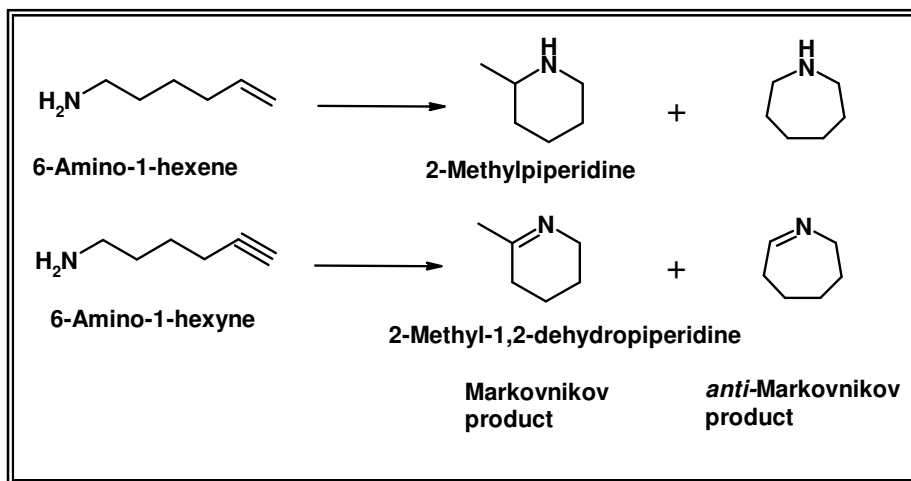
Scheme 1.2. Intramolecular hydroamination reaction

1.1.1. Mechanism and coordination chemistry

The direct addition of amines to olefins and alkynes is thermodynamically feasible. However, the absence of strong interaction between the reactants, which arises mainly from the symmetry forbidden of a HOMO-LUMO overlap, a high activation barrier exists which prevents the reaction in normal conditions [10]. The reaction entropy for hydroamination of simple unactivated alkenes with amines is highly negative.

To catalyze the direct hydroamination of alkenes and alkynes two basic approaches have been employed involving the activation of amine or olefin.

1.1.1.1. N-H bond activation of amine

One possible way to activate amine for catalysis is by transforming into much stronger nucleophile (amide ion) by deprotonation [17]. Thus the amides of strongly electropositive metals such as alkali metals are able to react with C-C multiple bond under appropriate conditions by nucleophilic addition to the corresponding β-aminoalkyl metal compounds as very reactive intermediates with a strong carbanion activity [Scheme 1.3].

An alternate method of amine activation is via oxidative addition of NH bond to an appropriate transition metal in a lower oxidation state. In case of addition to olefins, β-aminoalkyl compound is formed by the insertion of olefins into metal-nitrogen bond in the first step. Alkyl amine is generated in the second step by the reductive elimination. Thus reformed reduced metal catalyst can run again.
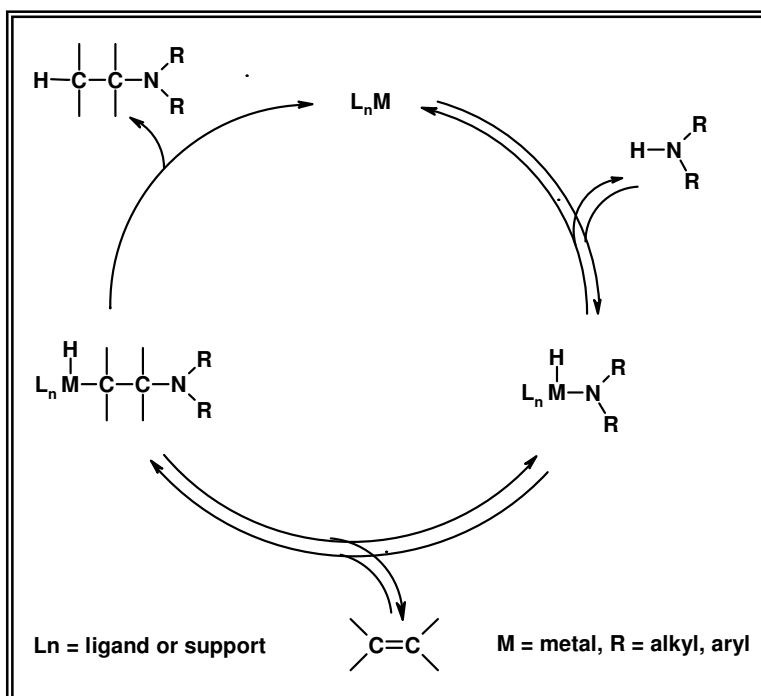
Scheme 1.3. Catalytic cycle for hydroamination via activation of amine

1.1.1.2. C-C multiple bond activation

Nucleophilic addition to the C-C multiple bond can be promoted by π-coordination complex with the metal center in the first step as shown in Scheme 1.4. The addition of amine in the second step forms β-ammonioethyl complex. The evidence of the formation can be drawn from the fact that in some cases such complexes are isolated. From this intermediate, catalytic cycle for the hydroamination is completed by intramolecular protolytic splitting reaction of metal-carbon bond as shown in scheme 1.4 via route (B). If the transition metal is d-electron rich and can receive the proton by oxidative addition, then the alkyl amine can be easily regenerated by reductive eliminaton with the regeneration of the catalyst (Scheme 1.4, route (B)).
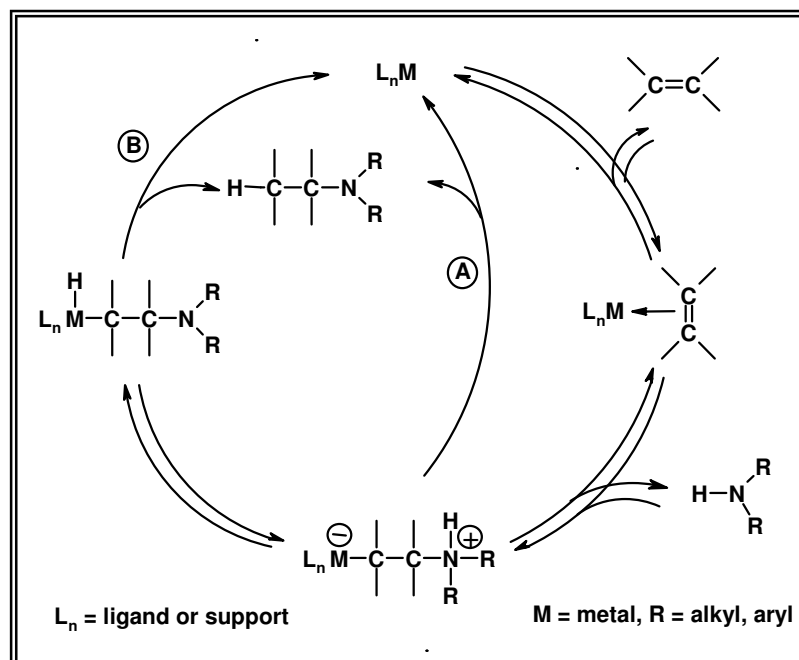
Scheme 1.4. Catalytic cycle for hydroamination via activation of olefin

1.1.1.3. Hydroamination of activated olefins

Hydroamination of activated olefins with amines is a Michael type addition reaction where N-H bond of amines is added over C=C of activated olefins (also known as acrylates or α, β-unsaturated compounds) [18]. When the C-C double bond is in conjugation with the electron withdrawing groups such as C=O, C≡N, COOH, COOEt, such molecules are termed as activated olefins. The examples are ethyl acrylate, acrylic acid, acrylonitrile etc. Here, C-C π-bond is activated by adjacent groups through electron conjugation, which makes β-carbon acidic. Amine being basic, then added preferably over β–carbon that results in *anti*-Markovnikov product in major quantity.

1.1.2. Advantages over conventional routes

The industry produces amines following various synthetic routes especially the reaction between ammonia or amine with alcohol or alkyl halide as shown in

Scheme 1.5 [19]. These methods suffer from drawbacks such as by-product formation (less atom efficiency) as well as poor product selectivity. Reaction 1 gives side products like hydrogen halides, which are not environmental friendly. Moreover the product, secondary amine further reacts with alkyl halide to give *tert.* amine which further gives quartenary ammonium salt thus reduces the product selectivities. Condensation of ketones with amines (reaction 2) is the textbook route to prepare enamines and imines but this reaction produces water as a by-product and hence limits its use in the domino reactions such as direct nucleophilic addition of organometallic reagents. Also aromatic ketones react slowly compared to aliphatic ketones and methyl ketones are sensitive to aldol type side reactions [20]. Hence, synthesis of imines from acetophenone always ends up in unsatisfactory yields [21-22].

$$R\text{-}X \ + \ H_2N\text{-}R' \ \longrightarrow \ R\text{-}NH\text{-}R' \ + \ H\text{-}X \ \text{-------} (1)$$

$$R\text{-}CO\text{-}R' + H_2N\text{-}R'' \ \longrightarrow \ RR'C{=}N\text{-}R'' + H_2O \ \text{---------} (2)$$

(R, R' = alkyl, aryl, X= halogen, -OH)
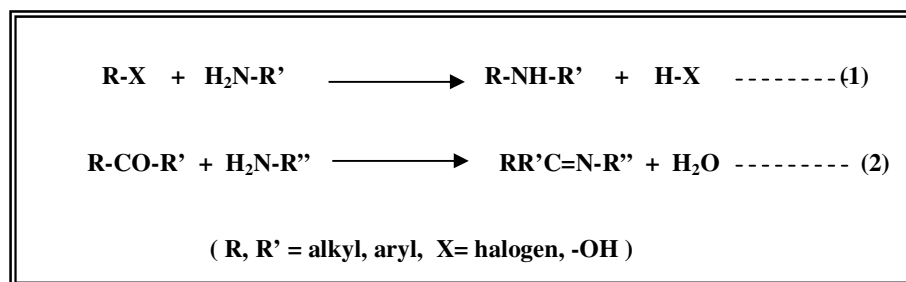
Scheme 1.5. Conventional routes for synthesizing alkylated amines and imines

1.1.3. Homogeneous catalysts for hydroamination

Some important reports on hydroamination using homogeneous catalysts are cited here out of huge literature database. The formation of highly nucleophilic alkali metal amides has been used for the hydroamination of unactivated simple alkenes, aromatic olefins and dialkenes such as 1, 3-butadienes [23-27]. Hydroamination of alkenes dates back as early as 1954 where Howk et al reported sodium or lithium metals as catalysts for the reaction of ethylene with ammonia to form ethyl amine under high temperature (~200 °C) and pressure (~1000 bar) conditions but only 0.7% conversion of ammonia was achieved [28]. Compared to olefins and alkynes, the amination of allenes has received only limited attention. Recently, Bergman and co-

workers found that zirconium bisamide complexes of the form $Cp_2Zr(NHAr)_2$ catalyze the hydroamination of allene [29].

Intermolecular addition of N-H to vinylarenes can proceed with different regioselectivity, depending on the catalyst employed: anti-Markovnikov addition of aryl/ alkylamines occurs in the presence of strong Brönsted bases [30] organolanthanide [31] rhodium [32] or ruthenium [33] catalysts to furnish the linear product. Conversely, branched regioisomers result from the addition of aromatic amines effected by Pd-(II)-diphosphine/triflic acid [34] or $TiCl_4$ [35]. Thus far, general catalyzed additions of non-nucleophilic sulfonamides to vinylarenes are rare. Recently, Pt(II) and Au(I)/Ag(I) complexes have been reported to catalyze these additions, but only in low to moderate yields (45 and 51%) [36, 37]. Transition metal complexes of Rh (I) and Pd (II) have been used for intermolecular hydroamination of alkenes [38, 39]. Recently some of the Lewis acidic metal salts such as $Cu(OTf)_2$ [40], $TiCl_4$ [41], $InCl_3$ [42], $FeCl_3$ [43] have been shown to catalyze for hydroamination of alkenes under homogeneous conditions. Some non-metal based homogeneous catalysts like N-bromosuccinimide have also been reported [44].

1.1.4. Heterogeneous catalysts for hydroamination

Compared to homogeneous catalysts, very few heterogeneous catalysts for hydroamination reactions are reported in the literature [10].

Zeolites have been shown to catalyze hydroaminations at high temperatures and pressures [45, 46]. The reaction of ammonia with ethylene or higher alkenes can be catalyzed by proton-exchanged zeolites of, e.g., ZSM-5 or mordenite structure [47]. Amination of 2-methylpropene can be catalyzed to give *tert*-butylamine in high selectivities (99%), but only low conversion (<1.73%) is achieved [48, 49]. The conversion is limited by the thermodynamic equilibrium between starting materials (2-methylpropene and ammonia) and the product (*tert*-butylamine) [50]. The activity of the zeolites generally increases with the ratio of Si^{4+} ions to Al^{3+} ions which determines the number of acidic sites. The Brønsted acidity of the zeolite is the main controlling factor for the activity of the zeolite [49, 51]. The activity and selectivity also depends on the zeolite structure and the pore size. In all cases reported the reaction gives the Markovnikov products and most likely proceeds through carbocation intermediates which are formed by interaction of the alkene with a surface proton or ammonium ion [47, 52]. The synthesis of alkylamines in the

presence of zeolites has been the subject of many patents and is used industrially by BASF to produce *tert*-butylamine.

Recent studies using heterogeneous catalysts for hydroamination reactions include transition metal ions exchanged zeolites especially Zn exchanged H-beta catalyst [53-57]. Pd (I) complex immobilized on the silica matrix was also reported as catalyst for hydroamination reaction [58]. There are few reports where supported ionic liquids are used for hydroamination reactions [59, 60]. Cation exchange resins can be used for hydroamination of vinylpyridines [61]. Recently Corma et. al. have reported Gold (I) supported on a biopolymer as catalyst for alkyne hydroamination [62]. Recent reports indicate that heteropoly compounds can also be used effectively as heterogeneous catalysts for hydroamination [63]. Hydroamination of activated olefins such as ethyl acrylate is also gaining importance due to its application in the synthesis of β-amino acids and lactums. Heterogeneous catalysts such as Cu-Al hydrotalcite, Na-Y and H-beta have been used for hydroamination of activated olefins so far [64-66].

Further sections give the general introduction of the heterogeneous catalysts *viz.* clays, mesoporous materials and heteropoly compounds, which are used for hydroamination reactions.

1.2. Clays

Clay minerals are hydrous aluminium phyllosilicates, sometimes with variable amounts of iron, magnesium, alkali metals, alkaline earths and other cations [67, 68]. Clays have structures similar to the micas and therefore form flat hexagonal sheets. Clay consists of layered structure composed of polymeric sheets of SiO_4 tetrahedra linked to sheets of $(A1, Mg, Fe)_6$ octahedra in two dimensional form. The geochemical importance of clay minerals stems from their omnipresence in soils and sediments, high specific surfaces, and ion-exchange properties [69, 70]. Existence of clays is as early as the existence of the earth. Although the properties of clays such as ion exchange, sorptivity and medicinal properties have been exploited for thousands of years, it is only in the 20th century that clay mineral properties have been utilized in catalytic applications. Today clay is an important material with a large variety of applications in ceramics, oil drilling, liners for waste disposal, and the metal and

paper industry. Clay is furthermore used as adsorbent, decoloration agents, ion exchanger, and molecular sieve catalyst [71, 72].

1.2.1. Clays as micro reactors

Besides advantages endowed on clays due to their heterogeneous nature, there are many other attractive attributes associated with clays that make them unique. The prominent and remarkable aspect of clays is their surface acidity. It is seldom appreciated and not a common knowledge that a pinch of dirt from one's garden has (or made to display by proper treatment) the acidity that makes it equal to some of the strongest inorganic acids. These surface acidity for natural clays with Na^+ or NH_4^+ as interstitial cations range from +1.5 to -3. Simple washing of the clay with mineral acid exchanging the interlamellar Na^+, K^+, NH_4^+ cations with proton brings their surface acidity to Ho values (Hammett. acidity) between -5.6 to -8 which is between that for conc. nitric acid (Ho= -5) and that for conc. sulfuric acid (Ho= -12) [73]. Clays have coordinatively unsaturated atoms, broken bonds around the edges of the silica-alumina units that give rise to unsaturated charges which are balanced by adsorbed cations. They are responsible for acidity in clays. Clays have the presence of both Bronsted and Lewis acid sites. The clay interface bears an electrical double layer. The negatively charged tetrahedral layer attracts positively charged counter cations. Clays have internal pools of water in between the layers and thus are promising catalysts for reactions such as Diels-Alder cyclloaddition [74]. Also according to the requirements, clays can be modified by certain methods such as ion-exchange, mineral acid treatment to improve acidity, calcination, impregnation of metallic salt on the surface, pillaring by bulky metal ions, anchoring of metal complexes [75-78].

Most commonly, the modification of clays is carried out either by exchanging the cations present in the clay with any other suitable cations like Fe, Zn, Pd, Cu, Ru, Rh, Ce, *etc*. or by increasing the interlameller space by pillaring [79, 80]. Cation-exchanged clays were prepared by stirring a mixture of the clay and a metal salt in aqueous medium or aqueous acetone at room temperature or above.

Table 1.1. Classification of selected common hydroxylated phyllosilicates

Layer type	Interlayer species	Layer charge	Octahedral-sheet type	Mineral name	Formula
1:1	None or H_2O only	~0	Dioctahedral Trioctahedral	Kaolinite Chrysotile	$Al_4Si_4O_{10}(OH)_8$ $Mg_6Si_4O_{10}(OH)_8$
2:1	None	~0	Dioctahedral Trioctahedral	Pyrophylite Talc	$Al_4Si_8O_{20}(OH)_4$ $Mg_6Si_8O_{20}(OH)_4$
	Hydrated exchangeable cations	0.4-1.2	Dioctahedral Dioctahedral Dioctahedral Trioctahedral Trioctahedral Trioctahedral	Montmorillonite Beidellite Nontronite Saponite (F-) Hectorite Stevensite	$M_{x/n}{}^{n+}[Al_{4-x}Mg_x][Si_8]O_{20}(OH)_4.nH_2O$ $M_{x/n}{}^{n+}[Al_4][Si_{8-x}Al_x]O_{20}(OH)_4.nH_2O$ $M_{x/n}{}^{n+}[Fe_4][Si_{8-x}Al_x]O_{20}(OH)_4.nH_2O$ $M_{x/n}{}^{n+}[Mg_6][Si_{8-x}Al_x]O_{20}(OH)_4.nH_2O$ $M_{x/n}{}^{n+}[Mg_{6-x}Li_x][Si_8]O_{20}(OH)_4.nH_2O$ $M_{x/n}{}^{n+}[Mg_{6-}Vacancy_x][Si_8]O_{20}(OH)_4.nH_2O$
		1.2-1.8	Intermediate trioctahedral	Vermiculite Vermiculite	$[Mg,Ca]_{x/2}{}^{2+}[Al_{4-x}Mg_x][Si_8]O_{20}(OH)_4.8H_2O$ $[Mg,Ca]_{x/2}{}^{2+}[Mg_6][Si_{8-x}Al_x]O_{20}(OH)_4.8H_2O$
	Non-hydrated cations	1.8-2.0	Dioctahedral Trioctahedral	Paragonite Phlogopite	$Na_2[Al_4][Si_6Al_2]O_{20}(OH)_4$ $K_2[Mg,Fe]_6[Si_6Al_2]O_{20}(OH,F)_4$
	Hydroxyl sheet	0.4-2.0	Trioctahedral Trioctahedral	Clinochlore thuringite	$[(Al_xMg_{6-x})(OH)_6[Mg_6][Si_{8-x}Alx]O_{20}(OH)_4$ $[(Fe^{3+}{}_xFe^{2+}{}_{6-x})(OH)_6][Fe^{2+}{}_{6-y}Mg_y][Si_{8-x}Al_x]O_{20}(OH)_4$

26

1.2.2. Origin of clays

Most clay minerals are the result of weathering of some pre-existing rock. The bulk of clay present in sedimentary rocks was derived by the weathering of silicate minerals composing igneous rocks. Some clay minerals are hydrothermal in origin (dickite, rectorite, and halloysite), whereas others form from the alteration of other types of clay (example – nontronite) [81, 82]. The important mineral, bentonite predominately consists of smectites and has the properties governed by them [83]. Montmorillonite is a major constituent of bentonite mineral (~ 80-90%), remaining being the mineral impurities such as quartz, crystoballite, feldspar and other clay minerals depending on the geological origin. Although montmorillonite clay is well-known and extensively used by the catalysis community, bentonites have also been used as commercial catalysts [84-86].

1.2.3. Classification of clays

Mineralogically, clays are divided into 3 principal groups – kaolinite-serpentine, illite, and smectite. There are about 30 minerals included in the 3 clay groups [87]. Certain other minerals are included with the clays as a group and consist of a clay mineral regularly interstratified on an atomic level with sheet-type non-clay minerals, usually micas. Clays can also be classified based on their layered structures. Smectites, micas, vermiculites, talc, and pyrophyllite are characterized by a 2:1 layer structure in which two tetrahedral sheets form on either side of an octahedral sheet through sharing of apical oxygens (Table 1.1). As the apical oxygens from the tetrahedral sheet form ditrigonal or hexagonal rings, one oxygen from the octahedral sheet is located in the center of each ring and is protonated to yield a structural hydroxyl. In 2:1 phyllosilicates, isomorphous substitution of cations having different valences can lead to charge imbalances within a sheet. These may be partly balanced by the opposite type of charge imbalance in the adjacent sheet (e.g., a positively charged octahedral sheet may offset some of the negative charge associated with a tetrahedral sheet). The net charge imbalance on a 2:1 layer, if it occurs, is negative. This charge is referred to as the layer charge of the mineral and is balanced by larger cations *(e.g.,* Na^+, K^+ Ca^{2+} and Mg^{2+}) that coordinate to the basal surfaces of the tetrahedral sheets from adjacent layers. The 2:1 phyllosilicates are distinguished chiefly on the basis of their layer charge. The least complicated clay minerals are the

1:1 clay minerals composed of one tetrahedral (T) layer and one octahedral (O) layer. The 1:1 clay minerals are referred to as TO minerals. The TO package has a basal spacing of 0.7 nm (7Å). For example, kaolinite refer to the dioctahedral (1:1)-mineral, it has Al^{3+} filling two of three octahedral sites.

1.2.4. General aspect of clays.

Clay particles generally give well-defined X ray diffraction patterns from which the mineral composition and the basal distances are determined [88]. Particle size, shape, nature and the distribution of amount of both mineral and organic impurities, nature and amount of exchangeable ions and degree of crystal perfection are all known to affect the properties of clays profoundly [89]. Many clays absorb water between their layers, which move apart and the clay swells. For efficient swelling, the energy released by cations and layer solvation must be sufficient to overcome the attractive forces such as hydrogen bonding, between the layers. The swelling property in many ways is responsible for exchange of cations from external solutions. Between the two TOT layers, large cationic species can be inserted by cation exchange, which form pillared clays. The pillaring in clays increases the thermal stability and interlayer distance but may decrease the acidity [76].

1.2.5. Montmorillonite clay

Montmorillonite is the most widely used smectite clay which belongs to TOT type (dioctahedral) clays. The structure of montmorillonite K-10 is   shown in Fig 1.1 which represents schematic representation of crystal lattice of montmorillonite. They have an octahedral aluminate layer sandwiched between two tetrahedral silicate layers (TOT or 2:1 layer) [90]. The layers contain Fe^{3+} and Mg^{3+}, which present in small amounts as impurities.
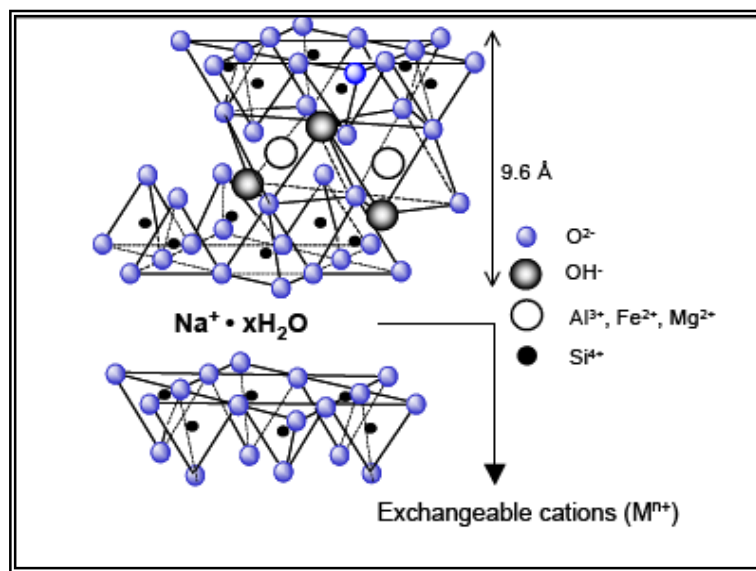
Fig. 1.1. Structure of montmorillonite K-10

The interstitial cations such as Na^+, K^+ and Ca^{2+} are too large to be accommodated in the interior of the crystal and are trapped as freely moving ions between negatively charged planes. These charge compensating cations on the layer surfaces can be easily replaced by other cations when available in solution and hence they are called exchangeable cations and the process is referred to as ion exchange. The concentration of these cations expressed in milli equivalents per 100 gram of dry clay, is called CEC (Cation Exchange Capacity). Natural montmorillonite has limited catalytic activity. An acid treatment can increase this activity many folds [91].

A wide variety of acid treated montmorillonite clays manufactured by Sud Chemie AG (and marketed by Aldrich and Fluka Chemie) such as montmorillonite K5, K10, K20, K30, KSF, KSFO etc. are prepared from naturally occurring clay, Bavarian montmorillonite through patented acid treatment and activation procedures.

1.2.6. Application of clays as catalysts

Starting from the beginning of petrochemical industry, clays have been used as catalysts. The first hydrocracking process developed over 80 years ago was based on acid-treated clays [92], but later and still now, zeolites and aluminosilicates were used. However, in few cases such as in treating some heavy fractions, clays are still

used. In addition, the clays such as kaolin or bentonite are still used as additives in current fluid catalytic cracking (FCC) [93–96]. Modification of these clays by pillaring the sheets with metal-oxide or of intercalating between the sheet anions, complexes, and organic chemicals represent a breakdown in the catalytic chemistry of these materials because they introduced new possibilities in mastering the properties and reactivity [97–101]. Today a large spectrum of structural, textural and compositional modifications are possible for layered materials, allowing a fine-tuning and control of the catalytic reactivity [102–109]. This makes these materials very interesting for catalytic applications. Worth noting, clays appear to have a relevant role also in catalyzing the starting of the life on the earth [110]. In fact, is known that the clay montmorillonite catalyzes the polymerization of RNA from activated ribonucleotides [111]. Hanczyc et al. [110] observed that montmorillonite accelerates the spontaneous conversion of fatty acid micelles into vesicles.

1.3. Mesoporous materials

There is an ever-growing interest in expanding the pore sizes of zeolite materials (microporous, crystalline aluminosilicates which consist of corner sharing TO_4 tetrahedra (T = Si, Al)) from micropore region to mesopores (pore size >20 Å) region in response to the increasing demands in both industrial and fundamental studies. Examples are treating heavy feeds, separating and selective synthesizing large molecules and intra zeolite fabricating technology [112-113]. Zeo-type materials, typically have a surface area of ca. >700 m^2g^{-1}, which are not truly crystalline like microporous zeolites but because of rapid growth of the research on those materials make them to be classified as mesopore zeolites, with the majority of this surface inside the pores and accessible only through apertures of well-defined dimensions [114]. In 1992, researchers at Mobil Corporation discovered the M41S family of silicate/aluminosilicates mesoporous molecular sieves with exceptionally large uniform pore structures, which has resulted in a worldwide resurgence in this area [115, 116]. Three different mesophases in this family have been identified, i.e. lamellar [117], hexagonal [116], and cubic phases [118], in which the hexagonal mesophase, MCM-41, possesses highly regular arrays of uniform-sized channels whose diameters are in the range of 15-100 Å depending on the templates used, the addition of auxiliary organic compounds (co-template) and the reaction parameters.

The pores of this novel material are nearly as regular, yet considerably larger than those present in crystalline materials such as zeolites, thus offering new opportunities for applications in catalysis [119] and advanced composite materials [120]. Accordingly, MCM-41 has been investigated extensively because the other members in this family are either thermally unstable or difficult to obtain.
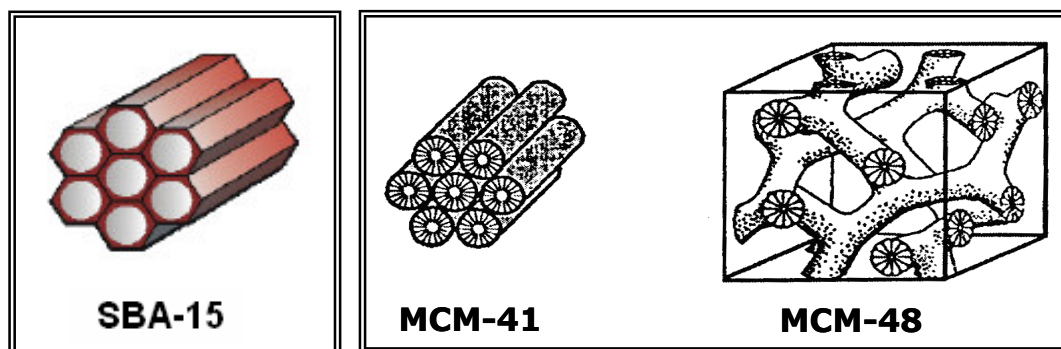
Fig. 1.2. Structures of mesoporous materials

1.3.1. M41S and SBA-15

Mesoporous silica materials like MCM-41, MCM-48, MCM-50 and SBA-15 (Fig. 1.2.) had received considerable research interests in shape selective heterogeneous catalysis and as host for various kinds of molecules due to their large surface area, uniform pore size and high density internal surface silanols. Ordered mesoporous silica was first reported independently by Mobil scientists [121, 122] and by Kuroda's group [123, 124] in the early 1990s. These materials are characterized by a regular array of pores, in the 2.0–10.0nm range, with uniform diameter, high specific surface area, and pore volume, which are advantageous for the adsorption and catalytic conversion of bulky molecules. The number of research papers dealing not only with mesoporous silica, but also with other oxides, such as alumina, titania, and zirconia, has grown tremendously during the last decade [125-127]. Obviously when new type of materials such as these are discovered, an explosion of scientific and commercial development swiftly follows, and new investigations on every conceivable aspect of their nature, the synthesis procedures and synthesis mechanisms, heteroatom insertion, characterization, adsorption, and catalytic properties, rapidly occurs [128].

SBA-15 has recently been synthesized by Stucky and co workers [129], in an acidic medium with poly(alkylene oxide) triblock copolymers, such as poly(ethylene oxide)–poly(propylene oxide)–poly(ethylene oxide) (PEO–PPO–PEO) and found to have uniform and large tubular channels up to 30 nm in diameter [130]. Since SBA-15 also possesses thick pore walls, the hydrothermal stability is much higher than MCM-41. Such features may provide high potential as supports for catalytic applications.

The purpose and advantages of synthesizing mesoporous materials is as follows.

1. To overcome the diffusional constraints with zeolites.

2. Very high surface are (>1000 m^2/g) and pore size distribution (20-100 Å).

3. Good host material for guest species (i.e. heterogenization of homogeneous species or metal complexes on the walls).

4. Easier to monitor the changes made with active species via surface area measurement and pore size distribution experiment.

1.3.2. Synthesis and mechanism of formation

Mesoporous materials such as MCM-41 are invariably synthesized by using organic structure directing agents called templates. *e.g*., cationic surfactants containing long alkyl chain quaternary ammonium compounds containing 10-20 carbons often followed with addition of co-surfactants. Even though synthesis parameters such as temperature and time have a role in the formation of the materials, the surfactant or polymer template certainly plays a dominating factor for obtaining a specific structure. The surfactants have a hydrophilic head group and a long chain hydrophobic tail group, within the same molecule, and in solution they will aggregate and self-organize in such a way so as to minimize the contact between the incompatible ends. Therefore, the mechanism responsible for the formation of M41S materials from its precursors had attracted much scientific attention.

Different synthesis mechanisms have been postulated in the literature to explain the formation mechanism of mesoporous materials.

1.3.3. Mechanism of formation of M41S molecular sieve

Two Synthesis mechanisms were proposed by Mobil researchers [121, 122]. In the first route, the cationic surfactant species organize into lyotropic liquid crystal

phase, which can serve as template for the formation of hexagonal structure. Surfactant micelles aggregate into hexagonal array of rods, followed by the interaction of silicate anions present in the reaction mixture with the cationic head groups of the surfactant species. The condensation of the silicate species further leads to the formation of an inorganic polymeric species. The template is removed by calcination to get hexagonally arranged inorganic hollow cylinders (Scheme 1.6).
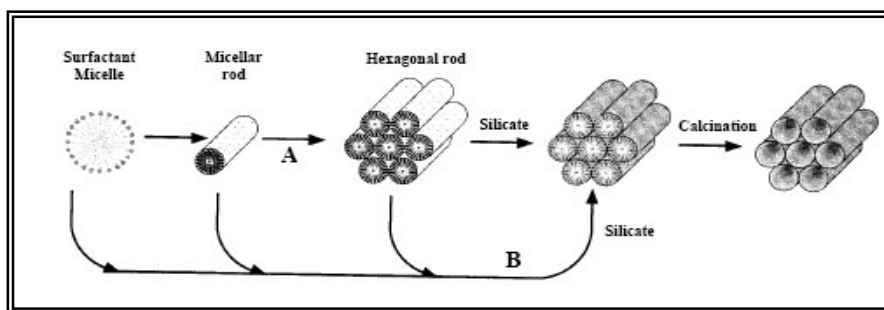
Scheme 1.6. Liquid Crystal Templating mechanism proposed for the formation of mesoporous MCM-41: (A) liquid crystal phase initiated and (B) silicate anion initiated. [*Source*: Ref. 116]

In the second route, the hexagonal ordering is assumed to be initiated by the presence of silicate species in the reaction mixture. Chen *et al.* [131] proposed that randomly distributed surfactant micelles interact with silicate oligomers by columbic interactions which results in randomly oriented surfactant micelles surrounded by two or three silica monolayers. These species spontaneously pack into a highly ordered mesoporous phase with an energetically favorable hexagonal arrangement, accompanied by silicate condensation. Further condensation between silicate species on adjacent rods occurs on heating and the inorganic wall continues to condense to form the stable hexagonal network.

Some other mechanisms for the formation of mesoporous silica like charge density matching, folded sheet mechanism and silicatropic liquid crystal models have also been proposed.

1.3.4. Mechanism of formation of SBA-15 molecular sieves

Monnier et al. [132] and Tanev [133] showed that the assembly of mesoporous materials can also be driven by hydrogen bonds in the case of neutral templates such as nonionic poly (ethylene oxide) (PEO) surfactants and inorganic precursors. The assembly of the mesoporous silica organized by non-ionic alkyl-ethylene oxide surfactants or poly (alkene oxide) triblock copolymer species in acid media occurs through an (S^0H^+) (X^-I^+) path way. First, alkoxysilane species are hydrolysed at a pH less than 2.

$$\text{Si(OEt)}_4 \ + \ n\,H_3\overset{+}{O} \ \xrightarrow[\text{pH} < 2]{\text{Hydrolysis}} \ \text{Si(OEt)}_{4-n}\,(\overset{+}{O}H_2)n \ + \ n\text{EtOH}$$

This is followed by partial oligomerisation of the silica. The EO moieties of the surfactant in strong acid media associating with hydronium ions

$$\text{REO}_m \ + \ y\text{HX} \ \xrightarrow{\ H_2O\ } \ \text{REO}_{m-y}[(\text{EO})H_3\overset{+}{O}]_y \ + \ y\overset{-}{X}$$
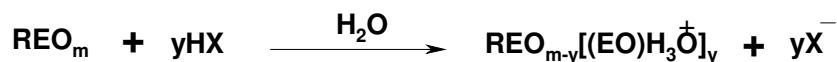
Where R = alkyl, poly (propylene oxide) and X- = Cl$^-$, Br$^-$, I$^-$, NO$_3^-$, H$_y$SO$_4^{-2+y}$, H$_y$PO$_4^{-3+y}$

Zhao et al. [130] proposed that the formation of SBA-15 occurs through a scheme where the silica source is first hydrolyzed at low pH to form Si(OMe)$_{4-n}$(OH$_2^+$)n species and the PEO moieties of the block copolymer associate with hydronium ions. Then, the charged PEO units and the cationic silica species are assembled together, via Cl$^-$, by a combination of electrostatic, hydrogen bonding and van der Waals interactions to form REO^{m-y}[(EOH$_3$O$^+$]y…yX$^-$….I$^+$, which can be designated as $(S^0H^+)(X^-I^+)$. Coordination sphere expansion around the silicon atom by anion (e.g. Cl$^-$) coordination of the form X$^-$Si$^-$OH$_2^+$ may play an important role [134]. Further condensation of the silica species and the organization of the surfactant and inorganic species result in the formation of the lowest energy silica-surfactant mesophase structure allowed by the solidifying inorganic network [135]. Furthermore, the time required for silica mesopore precipitation depends on the acid anion and is found to be the shortest in the presence of Cl$^-$ anion when used in the form of hydrochloric acid. It was shown that the EO-length determines which mesostructure is formed [136]. The length of the hydrophilic EO-block determines the silica

mesostructure and influences the wall thickness of SBA-15. The hydrophobic PO-block affects the pore diameter and further, the PO-block length influences the templating ability as a longer PO-block results in more highly ordered domains and better defined particles.

1.3.5. Aluminium substituted mesoporous molecular sieves

Ion-exchange, catalytic and adsorptive properties of molecular sieve materials originate from acid sites which arise from the presence of accessible hydroxyl groups associated with tetrahedral framework aluminium in a silica matrix [137, 138] Purely siliceous molecular sieve materials have an electrically neutral framework and consequently no acid sites. Much effort has therefore been devoted to the introduction of aluminium into silica frameworks [137-141]. Typically, aluminium is incorporated into the framework of a silicate material via a so called "direct synthesis" procedure in which an aluminium precursor is added into the gel prior to hydrothermal synthesis. This direct synthesis method often requires specialized synthesis conditions depending on the respective structures of the materials, and the incorporation of aluminium into the silica matrix usually causes a decrease in the structural ordering.

SBA-15 is a purely siliceous phase synthesized in strong acidic media (2 M HCl solution). Since most aluminium sources dissolve in strong acids, precipitation to incorporate framework aluminium into SBA-15 by direct synthesis seems unlikely. Previous studies have shown that aluminium can be effectively incorporated into siliceous MCM-41 materials via various post-synthesis procedures by grafting aluminium onto MCM-41 wall surfaces with anhydrous $AlCl_3$ [142] or aluminium isopropoxide in non-aqueous solution [143] or with sodium aluminate [144] in aqueous solution followed by calcination. The authors claimed that the materials produced via these postsynthesis procedures have superior structural integrity, acidity and catalytic activity to those of materials having aluminium incorporated during synthesis. Aluminium incorporated molecular sieves, AlSBA-15 in particular, have been shown to catalyze wide variety of organic transformations such as alkylation, acylation, hydrodesulfurization, oxidative ring opening and cracking, with high activity and selectivity [145-153]. They are also used as supports for metal oxides and complexes and used in many organic transformations [154-158]. Acid sites generated from Al incorporation in the framework of MCM-41 and SBA-15 can be exchanged

with metal ions and metal complexes, which in turn makes them more versatile in catalytic applications [159-162].

1.4. Heteropoly compounds

Heteropolyacids (HPAs) are hydrogen forms of heteropolyanions produced by the condensation of more than two kinds of oxoanions. HPAs have several advantages as catalysts, which make them economically and environmentally attractive. On the one hand, HPAs have a very strong Brönsted acidity; on the other, they are efficient oxidants under rather mild conditions [163]. HPAs have a very high solubility in polar solvents and fairly high thermal stability in the solid state. These properties render HPAs potentially promising acid, redox, and bifunctional catalysts in homogeneous as well as in heterogeneous systems. HPAs are widely used as model systems for fundamental research, providing unique opportunities for mechanistic studies on the molecular level. The catalytic function of heteropoly compounds has attracted much attention in recent years and design of the catalyst is possible at atomic or molecular level. The elucidation of catalytic processes is also possible at the atomic/molecular level due to their molecular nature. Out of a large number of heteropoly acids, the relatively inexpensive and most commonly used in catalytic applications are Keggin heteropolyacids such as tungstophosphoric acid, silicotungstic acid and phosphomolybdic acid.

1.4.1. Structure of Keggin heteropoly compounds

In solid state, HPAs show hierarchic structure [164, 165]. The structure divided into three levels – primary, secondary and tertiary.

1.4.1.1. Primary structure

The structure of a heteropolyanion or polyoxoanion molecule itself is called a primary structure [166]. In solution, heteropolyanions are present in the unit of the primary structure, being coordinated with solvent molecules and/or protonated. Based on primary structure, different polyoxoanion structures exist.

Keggin structures [167-171] are anionic metal-oxygen cluster compounds having the molecular formula $XM_{12}O_{40}$, where "X" is a central, tetrahedrally coordinated atom connecting twelve peripheral, octahedrally coordinated "M" metal

atoms (Fig. 1.3). Berzelius synthesized the first Keggin structure (ammonium 12-molybdophosphate) in 1826. Keggin correctly deduced its geometry based on powder X-ray diffraction patterns in 1933 [167]. The acid and salt forms of the structure have proven to be industrially important: as ion-exchange materials; as analytical reagents for the determination of environmental contaminant concentrations; as protein precipitants; and as catalysts.
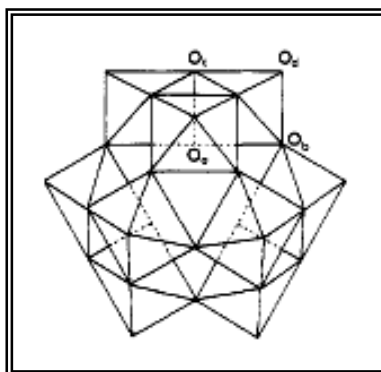
Fig. 1.3. Primary structure of Keggin heteropoly anion, $XM_{12}O_{40}^{n-}$

The ideal Keggin structure of the α type has T_d symmetry and consists of a central XO_4 tetrahedron (X = heteroatoms or central atom, most commonly Si^{IV}, P^V, or Ge^{IV}) surrounded by twelve MO_6 octahedra (M = addenda atom, most commonly Mo or W).

Interestingly, the same structure was suggested for the structurally similar HPA salts, e.g., $Cs_3PW_{12}O_{40}$, in which the Cs^+ ions each have four equivalent terminal oxygens as the closest neighbors [172]

The researchers prepared many HPAs whose structures were different from Keggin. Lot of research is involved in deducing the structures of newly synthesized HPAs. Other important structures reported for HPAs are Lacunary Keggin [173], Dawson [174] and Anderson [175].

1.4.1.2. Secondary and tertiary structure

Heteropoly compounds in the solid state are ionic crystals (sometimes amorphous) consisting of large polyanions, cations, water of crystallization, and other molecules. This three-dimensional arrangement is called the "secondary structure" (Fig. 1.4). The secondary structure is variable for the group A salts. For example, $H_3PW_{12}O_{40}$. XH_2O, is cubic for n = 0-6 and orthorhombic for n = 21. The crystal

structures of Cs and NH$_4$ salts are the same as the cubic H$_3$PW$_{12}$O$_{40}$.6H$_2$O, with cations at the sites of H$^+$(H$_2$O)$_2$ sites.
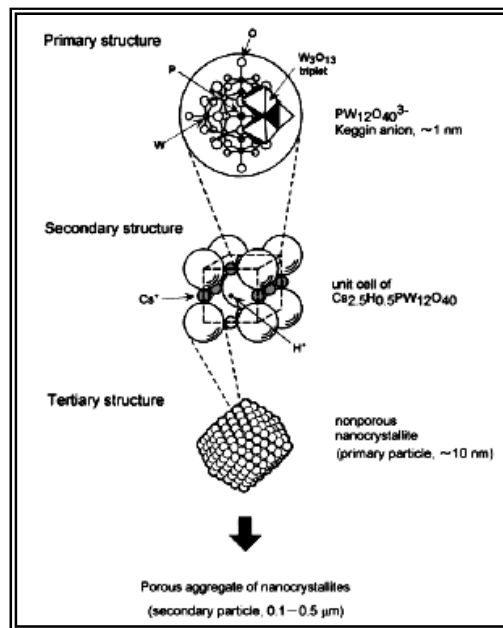
Fig. 1.4. Primary, secondary and tertiary structures; hierarchical structure of heteropoly compounds (HPAs) in the solid state.

Tertiary structure is the structure of solid heteropoly compounds as assembled. The size of the primary and secondary particles, pore structure, distribution of protons and cations, etc. is the elements of the tertiary structure (Fig. 1.4). Counter cations greatly influence the tertiary structure of HPAs. The surface area of the crystalline heteropolyacids is small (3-8 m^2 g^{-1}), but some of their salts with appropriately large cations such as ammonium, cesium and rubidium show surface areas of the order of 100 to 200 m^2 g^{-1}.

1.4.2. Synthesis

The simplest way to prepare heteropolyanions involves the acidification of an aqueous solution containing the oxoanions and the heteroatom [168, 176, 177].

$$12 \text{ WO}_4^{2-} + \text{HPO}_4^{2-} + 23 \text{ H}^+ \longrightarrow [\text{PW}_{12}\text{O}_{40}]^{3-} + 12 \text{ H}_2\text{O}$$
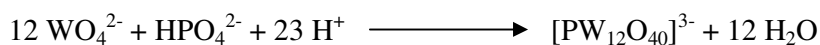
Control of the pH and X/M (central atom/addenda atom) ratio is necessary in order to obtain the desired structure, i.e., the Keggin HPA, the Wells-Dawson HPA, the Anderson HPA, a lacunary compound or the desired specific isomer. Free acids are synthesized primarily by following two methods: (1) by extraction with ether from acidified aqueous solutions and (2) by ion exchange from salts of heteropoly acids.

1.4.3. Heterogeneous catalysis

1.4.3.1. Surface-type catalysis

Surface-type catalysis is the ordinary heterogeneous catalysis, where the reactions take place on the two-dimensional surface (outer surface and pore wall) of solid catalysts (Fig. 1.5 (a)). The reaction rate is proportional to the surface area in principle. For example. The rates of double-bond isomerization of olefins are proportional to the surface area of $H_3PMo_{12}O_{40}$ [178].

1.4.3.2. Bulk-type catalysis

In the bulk-type (I) catalysis, e.g., acid-catalyzed reactions of polar molecules over the HPA and group A salts at relatively low temperatures, the reactant molecules are absorbed in the interpolyanion space of the ionic crystal and react there, and then the products desorb from the solid (Fig. 1.5 (b)) [166, 179, 180]. Polar molecules like alcohols and amines are readily absorbed into the solid bulk by substituting for water molecules and/or by expanding the distance between polyanions. The solid behaves like a solution and the reaction field becomes three-dimensional. This is known as "pseudoliquid" catalysis first proposed in 1979 [181-183].
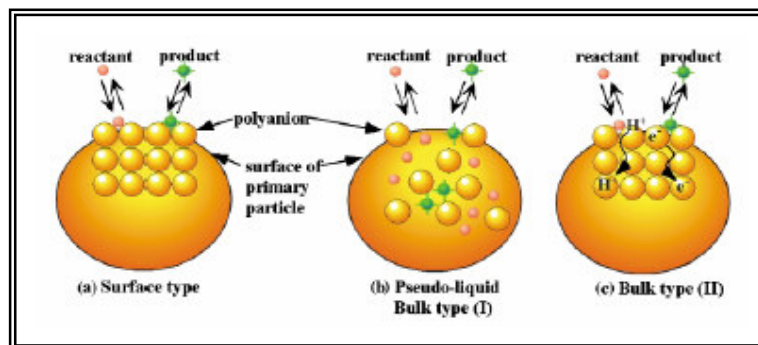
Fig. 1.5. Three types of catalysis for solid heteropoly compounds: (a) surface type, (b) pseudoliquid: bulk type (I), (c) bulk type (II).

Certain oxidation reactions like oxidative dehydrogenation and oxidation of hydrogen at high temperatures exhibit bulk-type (II) catalysis (Fig. 1.5 (c) [184, 185]. In this type of catalytic oxidation, although the principal reaction may proceed on the surface, the whole solid bulk takes part in redox catalysis owing to the rapid migration of redox carriers such as protons and electrons. The rate is proportional to the volume of catalyst in the ideal bulk-type (II) catalysis [165].

1.4.4. Acidic properties

Acidic properties of heteropoly compounds in the solid state are sensitive to counter cations, constituent elements of polyanions, and tertiary structure. Typical heteropolyacids having the Keggin structures, such as, $H_3PW_{12}O_{40}$ and $H_4SiW_{12}O_{40}$, are strong acids; protons are dissociated completely from the structures in aqueous solution. Heteropolyacids are much stronger acids than H_2SO_4, HBr, HCl, HNO_3, and $HClO_4$. Since, in heteroplyanions the negative charge of similar value is spread over much larger anions than those formed from mineral acids, the electrostatic interaction between proton and anion is much less for heteropolyacids than for mineral acids [164]. An additional important factor is the dynamic delocalizability of the charge or electron.

1.4.5. Salts of heteropoly acids

The nature of counter cation in HPA salts is critical with respect to their acidity, solubility, porosity, and thermal stability. Salts with rather small cations resemble the parent HPAs; they are readily soluble in water, nonporous, and possess surface areas under 10 m^2g^{-1} (Table 1.2) [186]. In contrast, water-insoluble salts with large monovalent cations, such as NH_4^+, K^+, Cs^+, etc., have a rigid microporous/ mesoporous structure and surface areas over 100 m^2g^{-1}. Even if these solids are prepared (by precipitation from aqueous solutions) to be stoichiometric, residual quantities of protons still remain, which are apparently responsible for the catalytic activity of these salts [187]. As demonstrated by Misono, Okuhara et al. [188], acidic Cs salt, $Cs_{2.5}H_{0.5}TPA$, has strong acid sites and high surface area (100-200 m^2g^{-1}) and is an efficient solid acid catalyst for a variety of organic reactions, especially

promising for liquid-phase reactions. Various methods of the preparation of bulk and supported HPA salts have been described [189, 190].

Certain "neutral" HPA salts can also gain proton sites upon the interaction with the reaction medium. Two mechanisms of the proton generation in heteropoly salts are distinguished: the dissociation of coordinated water (for salts with the cations like Al^{3+}, Zn^{2+}, etc.) and the reduction of the metal cation (for, e.g., Ag^{+}, Cu^{2+}, and Pd^{2+}) [191, 192]. Ono et al. have studied Pt(II) and Pd(II) salts of TPA these are capable of acting as bifunctional catalysts in alkane isomerization [192]. $Cs_{2.5}H_{0.5}TPA$ catalyzes the n-butane isomerization to isobutane at 300 °C [193]; combining the Cs salt with noble metals such as Pt enhances the activity in the presence of H_2 [194]. Copper salt of molybdovanadophosphoric acid was impregnated on MgO and used effectively for oxidative dehydrogenation of hexanol [195]. Copper salt of silicotungstic acid has been used as a catalyst in hydroxylation of phenol [196]. Some heteropoly compounds have also been employed as catalysts for hydrogenation of propanoic acid [197].

Table 1.2. Physicochemical Properties of HPA Salts [163]

Cation	Ionic radious (Å)	Solubility	Surface area, m^2g^{-1}
Li^{+}	0.68	S	<10
Na^{+}	0.97	S	<10
Ag^{+}	1.26	S	<10
Mg^{2+}	0.66	S	<10
Ca^{2+}	0.99	S	<10
Cu^{2+}	0.72	S	<10
Zn^{2+}	0.74	S	<10
Al^{3+}	0.51	S	<10
Fe^{3+}	0.64	S	<10
La^{3+}	1.02	S	<10
Ce^{3+}	1.03	S	<10
K^{+}	1.33	S	>100
Rb^{+}	1.47	N	>100
Cs^{+}	1.67	N	>100
NH_4^{+}	1.43	S	>100

Solubility in water: S = soluble, N = insoluble

1.5. Outline of the thesis

The thesis has been divided into six chapters

CHAPTER I

Chapter I gives a general introduction about hydroamination reactions and their importance. It also gives an introduction to homogeneous and heterogeneous hydroamination catalysts. It further gives an introduction to the catalysts used for hydroamination reactions viz. montmorillonite clays, AlSBA-15 and heteropoly salt based catalysts. A review of the literature to date in these areas is included. Finally, the aim of the thesis is outlined briefly.

CHAPTER II

This chapter describes the preparation and characterization of hydroamination catalysts viz. M^{n+} exchanged montmorillonite clays, modified SBA-15 based catalysts and heteropoly salts such as copper 12-silicotungstate. These catalysts were characterized by different techniques such as N_2 sorption, AAS, XRF, XRD, TEM, SEM, FTIR pyridine adsorption and ^{27}Al MAS NMR, 29Si MAS NMR, H_2-TPR and EPR. For each technique, its theory and experimental procedures are described briefly.

CHAPTER III

Chapter III is divided into two parts

Part A describes the preparation and characterization results of Cu^{2+} and Zn^{2+} exchanged montmorillonite K-10 catalysts. Catalysts were characterized by surface area, XRD and FTIR pyridine adsorption and the results are discussed. The catalysts are used in the intermolecular hydroamination of phenyl acetylene with aniline in the liquid phase. The catalytic activities of different metal ion exchanged catalysts and effect of different supports on the catalytic activity are discussed. The most active catalyst is used to study different reaction parameters like temperature, molar ratio, catalyst weight and effect of time on conversion. Hydroamination of different alkynes and amines are performed with Cu^{2+} exchanged montmorillonite K-10 to know the general applicability of the catalyst.

Part B describes intermolecular hydroamination of activated olefines catalyzed by K-10 montmorillonite clay. Catalysts were characterized by surface area (N_2 sorption), XRD and FTIR pyridine adsorption and the results are discussed. These catalysts are used in intermolecular hydroaminations of ethyl acrylate with aniline. The most active

catalyst is used to study different reaction parameters like temperature, molar ratio, catalyst weight and effect of time on conversion. The general applicability of the K-10 montmorillonite catalyst is determined by taking different α, β-unsaturated compounds and different amines for hydroamination reaction.

Chapter IV

It describes the preparation and characterization results Cu^{2+} ion exchanged AlSBA-15 catalysts. Catalysts were characterized by N_2 sorption, XRD, TPR, SEM, TEM, ^{27}Al MAS NMR, ^{29}Si MAS NMR, FTIR pyridine adsorption and EPR and the results are discussed. The catalysts were used in the intermolecular hydroamination of phenyl acetylene with 2, 4-xylidine. The effect of Si/Al ratio and Cu^{2+} ion concentration on the catalytic activity is compared. The most active catalyst is used to study different reaction parameters like temperature, molar ratio, catalyst weight and effect of time on conversion. Hydroamination of different alkynes and amines are performed with Cu^{2+}/AlSBA-15 to know the general applicability of the catalyst.

Intermolecular hydroaminations of activated olefines catalyzed AlSBA-15 catalysts were discussed. Catalysts were characterized by N_2 sorption, XRD, NH_3-TPD, and FTIR pyridine adsorption and the results are discussed. These catalysts are used in intermolecular hydroaminations of ethyl acrylate with aniline. The catalytic activity of AlSBA-15 is compared with CuAlSBA-15 and ZnAlSBA-15 catalysts. The most active catalyst is used to study different reaction parameters like temperature, molar ratio, catalyst weight and effect of time on conversion.

Chapter V

Synthesis and characterizations of metal salts of heteropoly acids such as copper 12-silicotungstate are discussed. Intra and intermolecular hydroaminations of alkynes catalyzed by heteropoly salts are carried out in the liquid phase. Catalysts were characterized by techniques such as XRD, FTIR and TG-DTA and the results are discussed. Different alkynes and amines are used for heterogeneous hydroamination reaction in the liquid phase. The most active catalyst is used to study different reaction parameters like temperature, molar ratio, catalyst weight and effect of time on conversion.

CHAPTER VI

This chapter summarizes the conclusions reached in this thesis.

1.6. References

1.   B.M. Trost, Science 254 (1991) 1471.

2.   B.M. Trost, 1998. In: Beller, M., Bolm, C. (Eds.), Transition Metals for Organic Synthesis. Wiley-VCH, vol. 1, p. 1.

3.   R.A. Sheldon, Chem. Technol. (1994) 38.

4.   B. Cornils, W.A. Herrmann, "Applied Homogeneous Catalysis with Organometallic Compounds". VCH, Weinheim 1996 (Chapter 7.4,17.1)

5.   M. Beller, C. Bolm, (Eds.), 1998. "Transition Metals for Organic Synthesis", Wiley-VCH.

6.   M.S. Gibson, 1968. In: Patai, S. (Ed.), The Chemistry of the Amino Group. Wiley/Interscience, New York, p. 61.

7.   B.M. Trost, T.R. Verhoeven, 1982. In: G. Wilkinson, F.G.A. Stone, E.W. Abel, (Eds.), Comprehensive Organometallic Chemistry. Pergamon Press, Oxford, UK, vol. 8, p. 892.

8.   J.P. Collman, L.S. Hegedus, J.R. Norton, R.G. Finke, 1987. Principles and Applications of Organotransition Metal Chemistry. University Science Book, Mill Valley.

9.   J.J. Brunet, D. Neibecker, F. Niedercorn, J. Mol. Catal. 49 (1989) 235.

10.   T.E.Müller, M. Beller, Chem. Rev. 98 (1998) 675.

11.   V. Markovnikov, C. R. Acad. Sci. 85 (1875) 668.

12.   M. B. Gasc, A. Laites, J. J. Perk, Tetrahedron 39 (1983) 703.

13.   K.C. Hultzsch, Adv. Synth. Catal. 347 (2005) 367.

14.   M. Beller, C. Breindl, Chemosphere 43 (2001) 21.

15.   H. Trauthwein, A. Tillack, M. Beller, Chem. Commun. (1999) 2029.

16.   G. A. Molander, E. D. Dowdy, S. K. Pack, J. Org. Chem. 66 (2001) 4344.

17.   R. Taube, Reactons with nitrogen compounds, B.Cornils, W.A. Herrmann (Eds.) "Applied homogeneous catalysis with organometallic compounds" V3, 2002, p. 513.

18.   L.L. Anderson, J. Arnold, R.G. Bergman, J. Am. Chem. Soc. 127 (2005) 14543.

19.   K.Tanabe, W.F.Hoelderich, Appl. Catal A Gen. 181 (1999) 399.

20.   R.W. Layer, Chem.Rev. 63 (1963) 489.

21.   J.J. Eisch, R.Sanchez, J.Org.Chem, 51 (1986) 1848.

22.   A.Cobas, E.Guitian, L.Castedo, J.Org.Chem. 58 (1993) 3113.

23.   G.P. Pez, J.E. Galle, Pure Appl. Chem. 57 (1985) 1917.

24.   R.K. Razdam, Chem. Commun. (1969) 770.

25.   B.W. Howk, E.L. Little, S.L. Scott, G.M. Whitman, J. Am. Chem. Soc. 76 (1954) 1899.

26.   R. Stroh, J. Ebersberger, H. Haberland, W. Hahn, Angew. Chem. 69 (1957) 124.

27.   J. Wollensak, R.D. Closson, Org. Synthesis 43 (1963) 45.

28.   B.W. Howk, E.L. Little, S.L. Scott, G.M. Whitman, J. Am. Chem. Soc. 76 (1954) 1899.

29.   P.J. Walsh, A.M. Baranger, R.G. Bergman, J. Am. Chem. Soc. 114 (1992) 1708.

30.   K. Kumar, D. Michalik, I.G. Castro, A. Tillack, A. Zapf, M. Arlt, T. Heinrich, H. Bottcher, M. Beller, Chem. Eur. J. 10 (2004) 746.

31.   J.S. Ryu, G.Y. Li, T.J. Marks, J. Am. Chem. Soc. 125 (2003) 12584.

32.   M. Utsunomiya, R. Kuwano, M. Katwatsura, J.F. Hartwig, J. Am. Chem. Soc. 125 (2003) 5608.

33.   M. Utsunomiya, J.F. Hartwig, J. Am. Chem. Soc. 126 (2004) 2702.

34.   M. Kawatsura, J.F. Hartwig, J. Am. Chem. Soc. 122 (2000) 9546.

35.   L.T. Kaspar, B. Fingerhut, L. Ackermann, Angew. Chem., Int. Ed. 44 (2005) 5972.

36.   H. Qian, R.A. Widenhoefer, Org. Lett. 7 (2005) 2635.

37.   J. Zhang, C.G. Yang, C.J. He, J. Am. Chem. Soc. 128 (2006) 1798.

38.   J.J. Brunet, D. Neibecker, K. Philippot, Tet. Lett. 34 (1993) 3817.

39.   O. Lober, M. Kawatsura, J. F. Hartwig, J. Am. Chem. Soc. 123 (2001) 4366.

40.   J. G. Taylor, N. Whittall, K. K. Hii, Org. Lett. 8 (2006) 3561.

41.   L. Ackermann, L. T. Kaspar, C. J. Gschrei, Org. Lett. 6 (2004) 2515.

42.   J.M. Huang, C.M. Wong, F.X. Xu, T.P. Loh, Tet. Lett. 48 (2007) 3375.

43.   J. Michaux, V. Terrasson, S. Marque, J. Wehbe, D. Prim, J.M. Campagne, Eur. J. Org. Chem. 16 (2007) 2601.

44.   S.K. Talluri, A. Sudalai, Org. Lett. 7 (2005) 855.

45.   J.J. Brunet, D. Neibecker, F. Niedercorn, J. Mol. Catal. 49 (1989) 235.

46.   M. Deeba, M.E. Ford, T.A. Johnson, In: Catalysis of Org.Reactions; Blackburn, D. W., Ed.; Dekker: New York, 1990; p 241.

47.   M. Deeba, M.E. Ford, T.A. Johnson, J. Chem. Soc. Chem.Commun. 8 (1987) 562.

48.   M. Tabata, N. Mizuno, M. Iwamoto, Chem. Lett. (1991) 1027.

49.   N. Mizuno, M. Tabata, T. Uematsu, M. Iwamoto, J. Catal. 146 (1994) 249.

50.   M. Deeba, M.E. Ford, J. Org. Chem. 53 (1988) 4594.

51.   N. Mizuno, M. Tabata, T. Uematsu, M. Iwamoto, J. Chem. Soc. Faraday Trans. 1 89 (1993) 3513.

52.   P. Fink, J. Datka, J. Chem. Soc. Faraday Trans. 1 85 (1989) 307.

53.   J. Penzien, T.E. Muller, J.A.Lercher, Chem.Commun. (2000) 1753.

54.   J. Penzien, C. Haebner, A. Jentys, K. Köhler, T.E. Müller, J. Lercher, J. Catal. 221 (2004) 302.

55.   J. Penzien, T.E.Muller, J.A.Lercher, Micropor. Mesopor. Mater. 48 (2001) 285.

56.   J. Penzien, R.Q. Su, T.E.Muller J. Mol. Catal A: Chem. 182 (2002) 489.

57.   T.E. Muller, J.A. Lercher, N.V. Nhu, AIChE, 49 (2003) 214.

58.   M.K. Richmond, S.L. Scott, H. Alper, J. Am. Chem. Soc. 123 (2001) 10521.

59.   S. Breitenlechner, M. Fleck, T.E. Muller, A. Suppan, J. Mol. Catal. A. Chem. 214 (2004) 175.

60.   O. Jimenez, T.E. Muller, C. Sievers, A. Spirkl, J.A. Lercher, Chem.Commun. (2006) 2974.

61.   M.J. Bhanushali, N.S. Nandurkar, M.D. Bhor, B.M. Bhanage, Catal. Commun. 9 (2008) 425.

62.   A. Corma, P. Concepción, I. Domínguez, V. Forné, M.J. Sabater, J.Catal. 251 (2007) 39.

63.   N. Lingaiah, N. S. Babu, K. M. Reddy, P. S. S. Prasad, I. Suryanarayana, Chem. Commun. (2007) 278.

64.   M.L. Kantam, B. Nilima, C.V. Reddy, J. Mol. Catal. A Chem. 241 (2005) 147.

65.   J. Horniakova, K. Komura, H. Osaki, Y. Kubota and Y. Sugi, Catal. Lett. 102 (2005) 191.

66.   K. Komura, J. Tsutsui, R. Hongo, Y. Sugi, Stud. Surf. Sc. and Catal. 170 (B) (2007) 1111.

67.   P. Laszlo, Pure & Applied Chem, 62 (1990) 2027.

68.   P. Laszlo, Science, 235 (1987) 1473.

69.   A. Corma, Chem. Rev. 97 (1997) 2373.

70.   A. Cornelis, P. Laszlo, Synlett (1994) 155.

71.   L. Fowden, R.M. Barrer, R.B. Tinker, eds. Philosophical Transactions of the
       Royal Society of London, Series A, Mathematical and Physical Sciences, 1984,
       pp 311.

72.   H.H. Murray, Proceedings of the 10th International Clay Conference, Adelaide,
       Australia, 1993, G.J. Churchman, R.W. Fitzpatrick, and R.A. Eggleton, eds.,
       CSIRO Publishing, 1995, pp 49.

73.   R.S. Verma, Tetrahedron, 58 (2002) 1235.

74.   P. Laszlo, H. Moison, Chem. Lett. (1989) 1031.

75.   O. S. Ahmed, Langmuir 19 (2003) 5540.

76.   H.J. Chae, I.S. Nam, S. W. Ham, S.B. Hong, Catal. Today 68 (2001) 31.

77.   G. D. Yadav, N.S. Asthana, Appl. Catal. A: Gen. 244 (2003) 341.

78.   I.K Biernacka, A.R. Silva, A.P. Carvalho, J. Pires, C. Freire, J. Mol. Catal. A
       Chem. 278 (2007) 82.

79.   C. R. Reddya, P. Iyengara, G. Nagendrappab, B.S. J. Prakasha, J. Mol. Catal. A
       Chem. 229 (2005) 31.

80.   B. M. Choudary, M. Sateesh, M. L. Kantam, K. V. R. Prasad, Appl. Catal. A:
       Gen. 171 (1998) 155.

81.   M.D. Nikalje, P. Phukan, A. Sudalai Org. Prep. Procedure. Int. 32 (2000) 1.

82.   L. Stixrude, D.R. Peacor, Nature 420 (2002) 165.

83.   R.J. Merriman, Clay Miner. 41 (2006) 473.

84.   N. Gungor, T. Tulun, J. Sci. Ind. Res. 55 (1996) 268.

85.   Z. Xiong, Y. Xu, L. Zhu, J. Zhao, Langmuir 21 (2005) 10602.

86.   J.G. Carriazo, L.M. Martínez, J.A. Odriozola, S. Moreno, R. Molina, M.A.
       Centeno, Appl. Catal. B: Environ.72 (2007) 157.

87.   J. T. Kloprogge, S. Komarenent, J. E. Amonette, Clays Clay Miner. 47 (1999)
       529.

88.   J.P. Butrille, T.J. Pinnavaia, Catal. Today 14 (1992) 141.

89.   J.T. Kloprogge, E. Booy, J.B.H. Jansen, J.W. Geus, Clay Miner. 29 (1994)
       153.

90.   L.M. Barclay, D.W. Thompson, Nature 222 (1969) 263.

91.   G.A. Mills, J. Holmes, E.B. Cornelius, J. Phy. Coll. Chem. 54 (1950) 1170.

92.   M.L. Occelli, R.J. Rennard, Catal. Today 2 (1988) 309.

93.   M.L. Occelli, S.A.C. Gould, Chemtech 24 (1994) 24.

94.   S. Maitra, S. Ray, N. Bandyopadhyay, Interceram 55 (2006) 12.

95.   M.L. Occelli, S.D. Landau, T.J. Pinnavaia, J. Catal. 90 (1984) 256.

96.   M.L. Occelli, F. Baldiraghi, J.P. Olivier, A. Auroux, Stud. Surf. Sci. Catal. 149 (2004) 323.

97.   D.E.W. Vaughan, Catal. Today 2 (1988) 187.

98.   F. Figueras, Catal. Rev.-Sci. Eng. 30 (1988) 457.

99.   P. Sidheswaran, A.N. Bhat, Indian J. Chem., Sec. A 35A (1996) 870.

100. A. Clearfield, Chem. Mater. 10 (1998) 2801.

101. M. Curini, O. Rosati, U. Costantino, Curr. Org. Chem. 8 (2004) 591.

102. E.M. Serwicka, K. Bahranowski, Catal. Today 90 (2004) 85.

103. S. Albertazzi, F.D. Basile, A. Vaccari, Int. Sci. Technol. 1 (2004) 496.

104. A. Vaccari, Appl. Clay Sci. 14 (1999) 161.

105. X. Guo, W. Hou, Q. Yan, Y. Chen, Chi. Sci. Bull. 48 (2003) 101.

106. D.E. de Vos, J. Wahlen, B.F. Sels, P.A. Jacobs, Synlett (2002) 367.

107. D. Tichit, F. Fajula, Stud. Surf. Sci. Catal. 125 (1999) 329.

108. A. Tanaka, J.N. Kondo, K. Domen, Crit. Rev. Surf. Chem. 5 (1995) 305.

109. L. Xu, C.-W. Hu, E.-B. Wang, J. Nat. Gas Chem. 6 (1997) 155.

110. M.M. Hanczyc, S.M. Fujikawa, J.W. Szostak, Science 302 (2003) 618.

111. K. Kawamura, J.P. Ferris, Origins of Life and Evolution of the Biosphere, vol. 29, Kluwer Academic Pub, the Netherlands, 1999, p. 563.

112. G.A. Ozin, C. Gil, Chem. Rev. (1989) 1749.

113. M.E. Davis, R.F. Loba, Chem. Mater. 4 (1992) 756.

114. X.S. Zhao, G. Q. Lu, G. J. Millar, Ind. Eng. Chem. Res. 35 (1996) 2075.

115. C.T. Kresge, M.E. Leonowicz, W.J. Roth, J.C. Vartulli, J.S. Beck, Nature 359 (1992) 710.

116. J.S. Beck, J.C. Vartulli, W.J. Roth, M.E. Leonowicz, C.T. Kresge, K.D. Schmitt, C.T.W. Chu, D.H. Olson, E.W. Sheppard, S.B. McCullen, J.B. Higgins, J.L. Schlenker, J. Am. Chem. Soc. 114 (1992) 10834.

117. M.Dubois, Th. Gulik-krzywicki, B. Cabane, Langmuir 9 (1993) 673.

118. J.C. Vartulli, K.D. Schmitt, C.T. Kresge, W.J. Roth, M.E. Leonowicz, S.B.

McCullen, S.D. Hellring, J.S. Beck, J.L.Schlenker, D.H. Olson, E.W. Sheppard, Chem. Mater. 6 (1994) 2317.

119.   A. Corma, A. Martinez, Adv. Mater. (1995) 137.

120.   C. Huber, K. Moller, T. Bein, J. Chem. Soc. Chem. Commun. (1994) 2619.

121.   C.T. Kresge, M.E. Leonowicz, W.J. Roth, J.C. Vartulli, J.S. Beck, Nature 359 (1992) 710.

122.   J.S. Beck, J.C. Vartulli, W.J. Roth, M.E. Leonowicz, C.T. Kresge, K.D. Schmitt, C.T.W. Chu, D.H. Olson, E.W. Sheppard, S.B. McCullen, J.B. Higgins, J.L. Schlenker, J. Am. Chem. Soc. 114 (1992) 10834.

123.   T. Yanagisawa, T. Shimizu, K. Kuroda, Bull. Chem. Soc. Jpn. 1990, 63, 988.

124.   S. Inagaki, Y. Fukushima, K. Kuroda, J. Chem. Soc., Chem. Commun. 1993, 680.

125.   J.M. Thomas, Angew. Chem. Int. Ed. 38 (1999) 3588.

126.   A. Taguchi, F. Schuth, Micropor. Mesopor.Mat. 77 (2005) 1.

127.   J.A. Melero, R.V. Grieken, G. Morales, Chem. Rev.106 (2006) 3790.

128.   P.J. Langley, J. Hulliger, Chem. Soc. Rev. 28 (1999) 279.

129.   D. Zhao, J. Feng, Q. Huo, N. Melosh, G.H. Fredrickson, B.F. Chmelka, G.D. Stucky, Science 279 (1998) 548.

130.   D. Zhao, Q. Huo, J. Feng, B.F. Chmelka, G.D. Stucky, J. Am. Chem. Soc. 120 (1998) 6024.

131.   C. Y. Chen, S. L. Burkett, H. X. Li, M. E. Davis, Microporous Mater. 2 (1993) 27.

132.   A. Monnier, F. Schuth, Q. Huo, D. Kumar, D. Margolese, R.S. Maxwell, G. Stucky, M. Krishnamurty, P. Petroff, A. Firouzi, M. Janicke, B. Chmelka, Science 261 (1993) 1299.

133.   P. T. Tanev and T. J. Pinnavaia, Science 267 (1995) 865.

134.   D.H. Olson, G.D. Stucky, J. C. Vartuli, U.S. Patent, 5, 364, 79 (1994).

135.   A. Firouzi, F. Atef, A.G. Oertli, G.D. Stucky, B.F. Chmelka, J. Am. Chem. Soc. 119 (1997) 3596.

136.   P. Kipkemboi, A. Fogden, V. Alfredsson, K. Flodstrom, Langmuir 17 (2001) 5398.

137.   A. Corma, V. Forne, M.T. Navarro, J.P. Pariente,. J. Catal. 148 (1994) 148.

138.   V. Luca, D.J. MacLachlan, R. Bramley, K. Morgan, J. Phys. Chem. 100

(1996) 1793.

139.   C.Y. Chen, H.X. Li, M.E. Davis, Microporous Mater. 2 (1993) 17.

140.   R. Schmidt, D. Akporiaye, M. Sto¨cker, O.H. Ellestad, J. Chem.Soc., Chem. Commun. (1994) 1493.

141.   Z. Luan, H. He, C.F. Cheng, W. Zhou, J. Klinowski, J. J. Phys. Chem. 99 (1995) 1018.

142.   R. Ryoo, S. Jun, J.M. Kim, M.J. Kim, Chem. Commun. (1997) 2225.

143.   R. Mokaya, W. Jones, Chem. Commun. (1997) 2185.

144.   H. Hamdan, S. Endud, H. He, M.N.M. Muhid, J. Klinowski, J. Chem. Soc., Faraday Trans. 92 (1996) 2311.

145.   Y. Kanda, T. Aizawa, T. Kobayashi, Y. Uemichi, S. Namba, M. Sugioka, Appl. Catal. Environ. 77 (2007) 117.

146.   Y. Zheng, J. Li, N. Zhao, W. Wei, Y. Sun, Micropor. Mesopor.Mater. 92 (2006) 195.

147.   B. Jarry, F. Launay, J.P. Nogier, J.L. Bonardet, Stud. Surf. Sci. Catal. 158 B (2005) 1581.

148.   A. Vinu, G.S. Kumar, K. Ariga, V. Murugesan, J. Mol. Catal A Chem. 235 (2005) 57.

149.   A. Vinu, B.M. Devassy, S.B. Halligudi, W. Bohlmann, M. Hartmann , Appl. Catal. A: Gen. 281 (2005) 207.

150.   W. Hu, Q. Luo, Y. Su, L. Chen, Y. Yue, C. Ye, F. Deng, Micropor. Mesopor. Mat. 92 (2006) 22.

151.   Y. Yue, A. Gedeon, J.L. Bonardet, N. Melosh, J.B. Despinose, J. Fraissard, Chem. Commun. (1999) 1967.

152.   A. Sakthivel, S.K. Badamali, P. Selvam, P. Micropor. Mesopor. Mater. 39 (2000) 457.

153.   S.G. Wang, Y. Li, Y.J. Gong, D. Wu, Y.H. Sun, B. Zhong, Acta.Phys. Chim. Sin. 17 (2001) 399.

154.   S. Sahoo, P. Kumar, F. Lefebvre, S.B. Halligudi, J. Mol. Catal. A Chem. 273 (2007) 102.

155.   A. Bordoloi, A. Vinu, S.B. Halligudi, Chem.Commun. (2007) 4806.

156.   K.S. Oh, S.I. Woo, Catal.Lett.110 (2006) 247.

157.   A. Hu, H.L. Ngo,W. Lin, J. Am. Chem. Soc. 125 (2003) 11490.

158.   D. Wu, E. Linder, H.A. Mayer, Z. Jiang, V. Krishnan, H. Bertagnolli, Chem. Mater. 17 (2005) 3951.

159.   Y. Wan, P. McMorn, F.E. Hancock, G.J. Hutchings, Catal. Lett. 91 (2003) 145.

160.   V. Hulea, F. Fajula, J. Catal. 225 (2004) 213.

161.   S.E. Park, H.S.M. Suh, D.S. Kim, J. Ko, J. Catal. 225 (2004) 213.

162.   S. Sinlapadech, R.M. Krishna, Z. Luan, L. Kevan, J. Phys. Chem. B 105 (2001) 4350.

163.   I.V. Kozhevnikov, Chem. Rev. 98 (1998) 171.

164.   T. Okuhara, N. Mizuno, M. Misono, Adv. Catal. 41 (1996) 113.

165.   N. Mizuno, M. Misono, Chem. Rev. 98 (1998) 199.

166.   M. Misono, Catal. Rev. Sci. Eng. 29 (1987) 269.

167.   J.F. Keggin, Nature (London) 131 (1933) 908.

168.   G.A. Tsigdinos, Top. Curr. Chem. 76 (1978) 1.

169.   M.T. Pope, "Heteropoly and Isopoly Oxometalates". Springer-Verlag, Berlin, 1983.

170.   M.T. Pope, A. Muller, Angew. Chem. Int. Ed. Engl. 30 (1991) 34.

171.   "Polyoxometallates: From Platonic Solids to Anti-Retroviral Activity." (M.T Pope and A. Muller, Eds.). Kluwer, Dordrecht, 1994.

172.   G.M. Brown, M.R. Noe-Spirlet, W.R. Bushing, H.A. Levy, Acta Crystallogr. Sect. B 33 (1977) 1038.

173.   L. Pettersson, I. Anderson, L.O. Ohman, Inorg. Chem. 25 (1986) 4726.

174.   B. Dawson, Acta Crystallogr. 6 (1953) 113.

175.   J.S. Anderson, Nature 140 (1937) 850.

176.   G.A. Tsigdinos, Ind. Eng. Chem. Prod. Res. Dev. 13 (1974) 267.

177.   B. Gruttner, and G. Jander, in "Handbook of Preparative Inorganic Chemistry," 2nd Ed. (G. Brauer, Ed.), Academic Press, New York, 1976, Vol. 2, p. 1716.

178.   M. Misono, Y. Konishi, M. Furuta, Y. Yoneda, Chem. Lett. (1978) 709.

179.   M. Misono, N. Mizuno, K. Katamura, A. Kasai, Y. Konishi, K. Sakata, T. Okuhara, Y. Yoneda, Bull. Chem. Soc. Jpn. 55 (1982) 400.

180.   T. Okuhara, S. Tatematsu, K.Y. Lee, M. Misono, Bull. Chem. Soc. Jpn. 62 (1989) 717.

181.   M. Misono, K. Sakata, Y. Yoneda, W.Y. Lee, in "Proc. 7th Int. Congr. Catal.

Tokyo, 1980," Kodansha, Tokyo, Elsevier, Amsterdam, 1981; p. 1047.

182. K. Sakata, M. Furuta, M. Misono, Y. Yoneda, ACS/CSJ Chemical Congr. Honolulu, April, 1979.

183. M. Misono, 1st Japan-France Catal. Seminar, July (1979).

184. T. Komaya, M. Misono, Chem. Lett. (1983) 1177.

185. M. Misono, N. Mizuno, T. Komaya, In Proc. 8th Int. Congr. Catal. 1984; Verlag Chemie: Weinheim, 5 (1984) 487.

186. H. Niiyama, Y. Saito, S. Yoshida, E. Echigoya, Nippon Kagaku Kaishi 4 (1982) 569.

187. J.B. Moffat, . J. Mol. Catal. 52 (1989) 169.

188. T. Okuhara, T. Nishimura, H. Watanabe, M. Misono, Stud. Surf. Sci. Catal. 90 (1994) 419.

189. S. Soled, S. Miseo, G.B. McVicker, J.E. Baumgartner, W.E. Gates, A. Gutierrez, J. Paes, Symposium on Advanced Techniques in Catalyst Preparation; 209th National Meeting of the American Chemical Society; Anaheim, CA; April 2-7, American Chemical Society: Washington DC, 1995; p 122.

190. J.M. Tatibouet, C. Montalescot, K. Bru¨ckman, Appl. Catal. A 138 (1996) L1.

191. Y. Ono, In Perspectives in Catalysis; J.M. Thomas, K.I. Zamaraev, Eds.; Blackwell: London, 1992; p 431.

192. M. Misono, Catal. Rev. Sci. Eng. 29 (1987) 269.

193. K. Na, T. Okuhara, M. Misono, Chem. Lett. (1993) 1141.

194. K. Na, T. Okuhara, M. Misono,. J. Chem. Soc., Chem. Commun. (1993) 1422.

195. G. Zhou, X. Yang, J. Liu, K. Zhen, H. Wang, T. Cheng, J. Phys. Chem. B 110 (2006) 9831.

196. H. Zhang, X. Zhang, Y. Ding, L. Yan, T. Ren, J. Suo, New J. Chem. 26 (2002) 376.

197. H. Benaissa, P.N. Davey, Y.Z. Khimyak, I.V. Kozhevnikov, J. Catal. 253 (2008) 244.

CHAPTER II

2.1. Introduction

The successful heterogeneous catalysts should possess high catalytic activity for the desired reaction, high selectivity for the desired product and acceptable commercial life. The characterization of catalytic material is a very important step in the process of catalyst development, which gives insight into the relation between physical and chemical properties of the catalyst and its activity. If the structure and composition of the catalyst can be correlated with its activity and selectivity, the working of the catalyst can be understood.

In this work, the catalysts were prepared by impregnation method and characterized by various techniques such as surface area, X-ray diffraction, N_2-sorption, FTIR pyridine adsorption, TPD of ammonia, DRUV-vis spectroscopy, NMR etc. The theory and experimental procedure of various characterization techniques used are briefly described in the following sections.

2.2. Catalyst preparation

2.2.1. SBA-15

In a typical synthesis, 4 g of amphiphilic triblock copolymer, poly(ethylene glycol)-block-poly(propylene glycol)-block-poly(ethylene glycol), (average molecular weight = 5800) was dispersed in 30 g of water and 120 g of 2 M HCl solution was added while stirring. It was followed by the addition of 8 g of tetraethyl orthosilicate to the homogeneous solution with stirring. This gel mixture was continuously stirred at 40 °C for 24 h, and finally crystallized in a Teflon-lined autoclave at 100 °C for 2 days. After crystallization the solid product was filtered, washed with distilled water, and dried in air at room temperature. The material was calcined in static air at 550 °C for 24 h to decompose the triblock copolymer and obtain a white powder (SBA-15).

2.2.2. AlSBA-15

Silica SBA-15 (1 g) was combined with 25 ml of dry ethanol containing various amounts of $AlCl_3$ with magnetic stirring at 80 °C for 10 h. The solid material was then filtered, washed vigorously with dry ethanol, and dried at room temperature in air. It was calcined in static air at 550 °C for 5 h.

2.2.3. AlMCM-41

8.67 g of cetyl trimethyl ammonium bromide (CTMABr) and 29 g of water were mixed and stirred for 30 min. Thereafter, 9.31 g of sodium silicate solution was added drop wise to the surfactant solution with vigorous stirring. After stirring for 30 min, 0.12 g of sodium aluminate dissolved in 2 g of water was added to the synthesis mixture and the resulting gel was stirred for another 15 min. Then, 0.6 g of conc. H_2SO_4 in 2.5 g of water was added to the above mixture to reduce the pH to 11.5 and stirred for 1 h. The homogeneous gel having composition

10 SiO_2: 5.4 CTMABr: 0.0125 Al_2O_3: 4.25 Na_2O: 3 H_2SO_4: 480 H_2O

was then transferred to a 150 cm^3 Teflon-lined stainless steel autoclave and heated for 24 h at 110 °C. The solid was filtered and thoroughly washed with deionized water, dried at 90 °C and then calcined in continuous flow of nitrogen at 540 °C for 10 h. The calcined product is finally ion-exchanged by stirring for 6 h (three times) in an ethanol solution of 1M NH_4NO_3 (50 ml/g) at 50 °C and subsequently washed and dried at 90 °C. This was further calcined at 450 °C for 6 h and used for experiments.

2.2.4. Metal exchanged catalysts.

The metal exchanged catalysts were prepared by suspending a known amount of dried precursor in an aqueous metal salt solution by ion exchange method. precursor supports under study include montmorillonite K-10, AlSBA-15, AlMCM-41, H-beta, and silica. In a typical synthesis Zn/K-10, 10 g known amount of montmorillonite K-10 was stirred with 0.1 M zinc acetate solution prepared in water (50 ml) at 80 °C for 10 h and then cooled to room temperature and the exchanged clay was separated by filtration. The above procedure was repeated to ensure maximum zinc exchange. The residue obtained was filtered and washed repeatedly with distilled water. This zinc exchanged K-10 was dried at 120 °C for 12 h and then calcined in air (RT-300 °C, 3 °C min^{-1}; for 4 h at 300 °C and ground well. All samples were calcined in shallow quartz boats placed inside a 3 cm diameter quartz tube placed in a tubular furnace. A series of catalysts with different metal exchange were prepared by changing the conditions such as metal concentration and exchange time. Calcination

programme for metal exchanged mesoporous materials and H-beta was RT-500 °C, 5 °C min⁻¹; for 4 h at 500 °C ; cooled at 5 °C min⁻¹ to RT.

2.2.5. Heteropoly salts

Stoichiometric amounts of metal carbonates and HPA are used for the synthesis of copper salts of HPAs. In a typical synthesis of $Cu_2SiW_{12}O_{40}$, 10 g (0.005 mole) of $H_4[SiW_{12}O_{40}]$ was dissolved in 20 ml of water and 0.3 g (0.0075 mole of copper) of copper carbonate (basic) was added to the acid solution. Since no apparent evolution of gas occurred after the addition of the carbonate, the mixture was heated slowly to 65 °C at which point evolution of carbon dioxide began to occur. The reaction mixture was then stirred for 0.5 h with cooling and filtered. A solid was obtained upon evaporation of the solution to dryness in the open. Then it was calcined to 250 °C for 5h.

2.3. Catalyst characterization – Theory and experimental procedure

2.3.1. Elemental analysis

Si/Al ratio of the catalyst samples were determined by XRF spectroscopy (Shimadzu XRF-1700 sequential XRF spectrometer). The amount of exchanged metal ions on supports was determined by atomic absorption spectrophotometer (AAS-Hitachi Model Z-8000) except for Pd (determined by ICP-OES) by following the standard procedure.

2.3.2. Surface area measurement by BET method

The common method of measuring surface area of catalyst materials is based on the theory developed by Brauner, Emmett and Teller in 1938 considering the concept of multilayer adsorption. The isotherm points are transformed into the linear version of BET equation [1, 2]:

$$P/V(P_0-P) = 1/V_mC + [(C-1)/V_mC] (P/P_0) \qquad (2.1)$$

Where, P is the adsorption equilibrium pressure, P_0 is the saturation vapor pressure of the adsorbate at the experimental temperature, V is the volume of gas adsorbed at pressure P, V_m is the volume of adsorbate required for monolayer coverage and C, a constant that is related to the heat of adsorption and liquefaction.

The specific surface areas of the catalysts were measured by N_2 physisorption at liquid nitrogen temperature with Omnisorb 100 CX Coluter instrument. Samples were dried at 300 °C in a dynamic vacuum for 2 h before N_2 physisorption measurements. The specific surface area was determined by using the standard BET method on the basis of adsorption data. The pore size distributions were calculated from both adsorption and desorption branches of the isotherms using BJH method [3] and the corrected Kelvin equation. Pore volume values were determined by using the t-plot method of De Boer.

2.3.3. X-ray diffraction

X-ray diffraction (XRD) is used to identify bulk phases, if desired under *in situ* conditions and to estimate particle sizes. In catalyst characterization, diffraction patterns are mainly used to identify the crystallographic phases that are present in the catalyst [4]. This method involves the interaction between the incident monochromatized X-rays (like Cu Kα or Mo Kα source) with the atoms of a periodic lattice. X-rays scattered by atoms in an ordered lattice interfere constructively in directions given by Bragg's law [5]:

$$n\lambda = 2\ d\ sin\theta;\ n = 1, 2, 3,\ldots \tag{2.2}$$

Where, λ is the wavelength of the X-rays, d is the distance between two lattice planes, θ is the angle between the incoming X-rays and the normal to the reflecting lattice plane and n is the integer called order of the reflection.

The width of the diffraction lines can be used to estimate the crystal size by the relation, Debye-Scherrer formula [1],

$$D_{hkl} = 0.9\lambda/\beta cos\theta \tag{2.3}$$

where, D_{hkl}, λ, β and θ are the volume averaged particle diameter, X-ray wavelength, full width at half maximum (FWHM), and diffraction angle respectively.

Powder X-ray diffraction patterns of the clay catalysts were recorded using a Rigaku (Model D/MAXIII VC, Japan), setup with Cu Kα radiation and graphite monochromatic with scan speed 16 °/min and scanning in the 2θ range from 5 to 50 θ. Silicon was used to calibrate the instrument.

Low angle X-ray diffraction patterns of mesoporous samples were collected on a Philips X' Pert Pro 3040/60 diffractometer using Cu Ka radiation (l = 1.5418 Å), nickel filter and an X'celerator as detector which employs the RTMS (Real Time

Multiple Strip) detection technique. XRD patterns were collected in the range of 2θ = 0.5-5.

2.3.4. Microscopic analysis

Transmission electron microscopy is typically used for high resolution imaging of thin films of a solid sample for micro structural and compositional analysis. The technique involves: (i) irradiation of a very thin sample by a high-energy electron beam, which is diffracted by the lattices of a crystalline or semi crystalline material and propagated along different directions, (ii) imaging and angular distribution analysis of the forward scattered electrons (unlike SEM where backscattered electrons are detected) and (iii) energy analysis of the emitted X-rays [6].

Scanning electron microscopy is a straightforward technique to probe the morphological features of mesoporous molecular sieve materials. SEM scans over a sample surface with a probe of electrons (5-50 eV) and detects the yield of either secondary or back-scattered electrons as a function of the position of the primary beam. Contrast is generally caused by the orientation that parts of the surface facing the detector appear brighter than parts of the surface with their surface normal pointing away from the detector. The interaction between the electron beam and the sample produces different types of signals providing detailed information about the surface structure and morphology of the sample [7].

TEM photographs were taken from JEOL Model 1200 EX instrument operated at an accelerating voltage at 120 kV. Samples were prepared by placing droplets of a suspension of the sample in isopropanol on a polymer micro grid supported on a Cu grid for TEM measurements. SEM was employed to characterize the surface morphology with Leica stereoscan, Cambridge 440 Microscope (UK) with a Kevex model EDAX system.

2.3.5. Infrared adsorption studies - Pyridine adsorption

The most common application of IR in catalysis is to identify adsorbed species and to study the way in which these species are chemisorbed on the surface of the catalyst [8-10]. More specifically, IR spectroscopy has been used to study the adsorption of typical probe molecules like ammonia, pyridine and other bases,

hydrocarbons, carbon dioxide which can monitor either the acidic or basic sites on oxide catalysts [11]. Investigation of adsorbed species in relation to their behavior in catalytic reactions is the main field of application of IR spectroscopy.

The nature of acid sites (Brönsted and Lewis) of the catalyst samples with different loading were characterized by *in-situ* Fourier transform infrared (FTIR) spectroscopy with chemisorbed pyridine in drift mode on an FTIR-8300 Shimadzu SSU-8000 instrument with 4 cm^{-1} resolution and averaged over 500 scans. These studies were performed by heating pre-calcined powder samples in-situ from room temperature to 400 °C with a heating rate of 5 °C min^{-1} in a flowing stream (40 ml min^{-1}) of pure N_2. The samples were kept at 400 °C for 3 h and then cooled to 100 °C; then pyridine vapors (20 μl) were introduced under N_2 flow. The infrared (IR) spectra were recorded with resolution 4cm^{-1} and 500 scans after degassing the sample at 200 °C for 30 minutes.

.

2.3.6. Temperature programmed desorption (TPD) of ammonia

Temperature programmed desorption (TPD), reduction (TPR), oxidation (TPO) and reaction spectroscopy (TPRS) typically involves monitoring surface or bulk processes between the solid catalyst and its gaseous environment via continuous analysis of the gas phase composition as the temperature is raised linearly with time. Instrumentation for temperature-programmed investigations consists of a reactor charged with catalyst in a furnace that can be temperature programmed and a thermal conductivity detector (TCD) to measure the concerned active gas of the gas mixture before and after interaction.

The acidity of the catalysts were measured by temperature programmed desorption of NH_3 (NH_3-TPD) using a micromeritics AutoChem-2910 instrument. It was carried out after ~ 0.5 g of the catalyst sample was dehydrated at 500 °C in helium flow (30 cm^3 min^{-1}) for 1 h. The temperature was decreased to 100 °C and NH_3 was adsorbed by exposing the samples treated in this manner to a stream containing 10 % NH_3 in helium for 1 h at 100 °C. It was then flushed with helium for another 1 h to remove physisorbed NH_3. The desorption of NH_3 was carried out in helium flow (30 cm^3 min^{-1}) by increasing the temperature to 600 °C at 10 °C min^{-1} measuring NH_3 desorption using TCD detector.

2.3.7. Temperature programmed reduction (TPR)

The reducibility of the calcined catalysts was measured by TPR method with Micromeritics AutoChem 2910 instrument. About 300 mg of the catalyst was mounted in a quartz tube and calcined in argon flow at 500 °C for 1 h (temperature-programmed rate of 10 °C min^{-1}) with the aim to remove the substances physisorbed. It is then cooled to ambient temperature in argon prior to the reduction by a mixing gas of hydrogen and helium (5% H_2 in volume percentage). In the H_2-TPR analysis, the heating rate was 10 °C min^{-1} and the gas flow was 10 ml min^{-1}. The cold trap consisted of liquid nitrogen and 2-propanol. The hydrogen consumed during the reduction was detected by a thermal conductivity detector.

2.3.8. Diffuse reflectance UV-visible spectroscopy

Diffuse reflectance spectroscopy (DRS) is a spectroscopic technique based on the reflection of light in the ultraviolet (UV), visible (VIS) and near-infrared (NIR) region by a powdered sample. In a DRS spectrum, the ratio of the light scattered from an "infinitely thick" closely packed catalyst layer and the scattered light from an infinitely thick layer of an ideal non-absorbing (white) reference sample is measured as a function of the wavelength λ. The scattered radiation, emanating from the sample, is collected in an integration sphere and detected [12]. The disadvantage is that the DRS signals are usually broad and overlap with each other, leading to a biased spectral analysis.

Diffuse reflectance UV-vis (DRUV–vis) spectra of catalyst samples were obtained using a Shimadzu UV-2101 PC spectrometer equipped with a diffuse-reflectance attachment, with $BaSO_4$ as the reference. The reflectance spectra were converted into the Kubelka-Munk function, *F(R)*, which is proportional to the absorption coefficient for low values of *F(R)*. The spectra were measured in the range of 200-800 nm in air at room temperature.

2.3.9. Solid-state nuclear magnetic resonance spectroscopy

In solid-state NMR, the line shape is determined by dipolar and quadrupolar interactions. The lines are usually broader because the rigid structure of the solid phase prevents the averaging of the dipolar interaction (H_D) by motions. Since, the first order quadrupolar and dipolar interactions are proportional to ($3 \cos^2\theta - 1$), where, θ is the angle between an internuclear vector and the magnetic field, these

interactions can be removed, to a first order approximation, by spinning the sample around the so-called magic angle β with respect to the external magnetic field, for which $3 \cos^2\beta - 1 = 0$, i.e. $\beta = 54.74^o$. This technique is known as Magic Angle Spinning (MAS) [13].

Magic angle spinning (MAS) NMR spectra for ^{27}Al and ^{29}Si nuclei were recorded on BRUKER DSX300 spectrometer at 7.05 T (resonance frequencies 59.63 MHz, rotor speed 4000 Hz, number of scans 5275, external reference $Si(OCH_3)_4$ and 78.19 MHz, rotor speed 6000 Hz, number of scans 2800, external reference $Al(H_2O)_6^{3+}$ for ^{29}Si and ^{27}Al, respectively).

2.3.10. Electron paramagnetic resonance spectroscopy

Electron Paramagnetic Resonance (EPR), often called Electron Spin Resonance (ESR), is a branch of spectroscopy in which electromagnetic radiation (usually of microwave frequency) is absorbed by molecules, ions, or atoms possessing electrons with unpaired spins, *i.e.* electronic spin S > 0. EPR is similar to Nuclear Magnetic Resonance (NMR) [14]. In both EPR and NMR, the sample material is immersed in a strong static magnetic field and exposed to an orthogonal low-amplitude high-frequency field. ESR usually requires microwave-frequency radiation (GHz), while NMR is observed at lower radio frequencies (MHz). With ESR, energy is absorbed by the sample when the frequency of the radiation is appropriate to the energy difference between two states of the electrons in the sample, but only if the transition satisfies the appropriate selection rules. In EPR, because of the interaction of the unpaired electron spin moment (given by two projections, $m_s = \pm 1/2$, for a free electron) with the magnetic field, the so-called Zeeman effect, there is different projections of the spin gain different energies.

$$E_{ms} = g m_B B_o m_s \qquad (2.4)$$

Here B_o is the field strength of the external magnetic field. The SI units for magnetic field is tesla,T, but, historically in EPR, gauss (1 G = 0.0001 T) is still used. Other terms in Eq.(2.4): m_s - is a spin projection on the field ($m_s = \pm 1/2$ for a free electron), m_B is the Bohr magneton:

EPR spectra were recorded on a Bruker EMX spectrometer operating at Xband frequency and 100-kHz field modulation. Measurements at variable temperatures were done using a Bruker BVT 3000 temperature controller.

2.3.11. Thermal analysis

Thermo analytical techniques involve the measurements of the response of the solid under study (energy or mass released or consumed) as a function of temperature (or time) dynamically by application of a linear temperature program. Thermogravimetry (TG) is a technique measuring the variation in mass of a sample when it undergoes temperature scanning in a controlled atmosphere. This variation in mass can be either a loss of mass (vapor emission) or a gain of mass (gas fixation). Differential thermal analysis (TGA) is a technique measuring the difference in temperature between a sample and a reference (a thermally inert material) as a function of time or temperature, when they undergo temperature scanning in a controlled atmosphere. The DTA method helps to determine any transformations and provides information on exothermic and endothermic reactions, taking place in the sample, which include phase transitions, dehydration, decomposition, redox or solid-state reactions. Further, for molecular sieves, it provides informations about the desorption of water, oxidative decomposition of occluded organic template species and dehydroxylation of silanol groups in the channel walls [15].

Thermogravimetric and differential thermal analysis (TG-DTA) of the samples were performed on a Setaram TG-DTA 92 apparatus from room temperature to 1000 ^{o}C in flowing dry air (ca. 50 ml min^{-1}), using α-Al_2O_3 as reference. In each experiment, 25-30 mg of the sample was used with a heating rate of 10 ^{o}C min^{-1}. TGA curves are depicted as first derivative DTG of the direct weight loss traces.

2.4. References

1.   J. M. Thomas, W. J. Thomas, Principles and Practice of Heterogeneous catalysis, VCH, Weinheim, 1997.

2   S. Brunauer, P. H. Emmett, E. Teller, J. Am. Chem. Soc. 1938, 60, 309.

3   E. P. Barrett, L. G. Joyner, P. P. Halenda, J. Am. Chem. Soc. 1951, 73, 373.

4   S. Biz, M. Occelli, Catal. Rev-Sci. Eng. 1998, 40, 329.

5   W. H. Bragg, W. L. Bragg, The Crystalline State, Vol. 1, McMillan, New York, 1949.

6   J. R. Fryer, Chemical Applications of Transmission Electron Microscopy, Academic Press, San Diego, 1979.

7   J. I. Goldstein, H. Yakowitz (Eds.), Practical Scanning Electron Microscopy, Plenum Press, New York, 1975

8   M. D. Baker, Catal. Rev. Sci. & Eng., 29 (1987) 269.

9   J. A. Lercher, C. Grundling and G. Eder-Mirth, Catal. Today, 27 (1996) 353.

10   J. C. Lavalley, Catal. Today, 27 (1996) 377.

11   M. C. Kung and H. H. Kung, Catal. Rev. Sci. & Eng., 27 (1985) 425.

12   R. A. Schoonheydt, Diffuse Reflectance Spectroscopy, Chapter 4, in: Characterization of Heterogeneous Catalysts, F. Delannay (Ed.), Marcel Dekker, New York, 1984.

13   R. A. Wind, in A. I. Popov, K. Hallenga (Eds.), Modern NMR Techniques and Their Application in Chemistry, Marcel Dekker, Inc., New York, 1991, p. 156,

14   J. C. Vedrine, Electron Spin Resonance, Chapter 5 in: Characterization of Heterogeneous Catalysts, F. Delannay (Ed.) Marcel Dekker, New York, 1984.

15   C-Y. Chen, H-X. Li, M. E. Davis, Microporous Mater. 2 (1993) 17.

CHAPTER III

Part A

3.1. Intermolecular hydroamination reactions catalyzed by transition metal ion exchanged clays

3.1.1. Introduction

Montmorillonite K-10 clay is an inexpensive and non-corrosive acid activated clay, which has been used as an efficient catalyst for wide variety of reactions [1]. It is mesoporous in nature with basal spacing dL between tetrahedral silicate and octahedral aluminate layers which may vary between 1 and 5 nm depending on the amount of intercalated water in the interlamellar space. The interlayer cations such as Na^+, K^+, Ca^{2+} and Mg^{2+} present in K-10 can undergo exchange with cations from external solutions [2]. By replacing the interlayer ions with high charge density cations like Al^{3+}, Zn^{2+} and Fe^{2+} acidity can be imparted in the clay and can be utilized for a broad range of organic transformations [3-6].

The catalytic intermolecular hydroamination of alkynes have been carried out in the presence of Hg and Tl salts [7-9]. Later, alkali metals [10], zirconocenes [11], complexes of lanthanides and actinides [12-15], have been designed to promote these reactions. In recent studies, moisture- and air- sensitive titanium complexes [16-18] and more expensive metal complexes of Ru, Rh, Ir, Pd, and Au have been the most used catalysts for hydroamination of alkynes [19-28]. However, homogeneous methods suffer from tedious work-up procedures and low recyclability of the catalyst. There are a few reports available on the use of heterogeneous catalysts for hydroamination of alkynes. Müller and co-workers have developed metal exchanged zeolites for alkyne hydroamination, which favored Markovnikov addition products [29-31]. Also, Pd complexes immobilized on a silica support have been reported for intramolecular cyclization of amino-alkynes [32].

This section deals with the preparation and characterization of transition metal ion exchanged montmorillonite clay catalysts by X-ray diffraction (XRD), atomic absorption spectroscopy (AAS), SEM, surface area, FTIR (Fourier transform infrared)

pyridine adsorption, and diffuse reflectance ultraviolet-visible (DRUV-vis) spectroscopy. These catalysts have been used in the liquid-phase intermolecular hydroamination of phenylacetylene with aniline to give phenyl(1-phenylethylidene)amine. The general performance of the catalyst has been determined by reacting with different alkynes and amines. Role of acidity on the formation of N-(1-phenylethylidene)aniline in hydroamination reaction has also been discussed.

3.1.2. Preparation

In a typical synthesis, 10 g of montmorillonite K-10 (hereafter K-10) was stirred with 0.1 M zinc acetate solution prepared in water (50 ml) at 80 °C for 10 h and then cooled to room temperature and the exchanged clay was separated by filtration. The above procedure was repeated once to ensure maximum zinc exchange. The residue obtained was filtered and washed twice with 100ml of distilled water. Zn^{2+} exchanged K-10 was dried at 120 °C for 12 h and calcined (RT-300 °C, 3 °C min^{-1}; for 4 h at 300 °C). The other transition metal ion catalysts were prepared by exchanging with the pre decided stock solutions of the corresponding metal acetate by following the above procedure.

3.1.3. Chemicals and reagents

K-10 was purchased from Fluka AG, Switzerland. Phenylacetylene and other alkynes were purchased from Aldrich. Aniline and other amines, metal acetates and toluene were purchased from Merck (India) Ltd. H-beta (Si/Al = 15) was obtained from CPP, NCL Pune. Silica gel was prepared by hydrolysis of tetraethyl orthosilicate (Aldrich) in presence of catalytic amount of con. HNO_3. Toluene used in the reaction was distilled over sodium wire before use.

3.1.4. Characterization - Results and discussion

The   details of surface area of the catalysts and amount of exchanged transition metal ion contents with different metal acetates and zinc with different stock zinc acetate   concentrations is listed in Table 3.1.

Table 3.1. Metal content and surface area of different catalysts.

S. No.	Catalyst	Metal acetate concn.	Metal content (mmol/g)	Specific Surface area (m^2/g)
1	Zn/ K-10	0.5	0.60	177
2	Zn/ K-10	0.2	0.51	201
3	Zn/ K-10	0.1	0.38	213
4	Zn/ K-10	0.05	0.22	224
5	Zn/ K-10	0.02	0.10	227
6	Zn/ K-10	0.01	0.04	230
7	Zn/ Silica	0.1	0.37	151
8	Zn/ H-beta	0.1	0.38	481
10	Pd/ K-10	0.1	0.37	221
12	Cu/K-10	0.1	0.36	220
13	Co/ K-10	0.1	0.39	223
14	Mn/ K-10	0.1	0.38	220
15	ZnO	-	-	10
16	Clay	-	-	232
17	H-beta	-	-	550
18	Silica	-	-	201

3.1.4.1. The structure and texture characterization

The X-ray diffractograms of the montmorillonite K10, Cu/K-10 and Zn/K-10 with different Zn concentrations are shown in Fig. 3.1. The catalysts show their first peak at $2\theta = 8.9$, which is assigned to the basal reflection (plane (d_{001}). The XRD profile of K-10 clay showed a layered structure with a basal spacing (d_{001}) of 3.33 Å. XRD of Zn/ K-10 and Cu/K-10 showed that the layered structure is retained and the basal spacing of (d_{001}) was estimated to be 3.35 Å (for 0.22 mmol Zn/K-10), which is comparable to that of the parent K-10 clay. SEM photographs of K-10 and Zn/K-10 is represented in Fig. 3.2. Both the samples contain flake like structures with a randam-sized particles. It appears that the particle size is increased approximately from 1 to 2 μm after incorporation of metal in the clay.
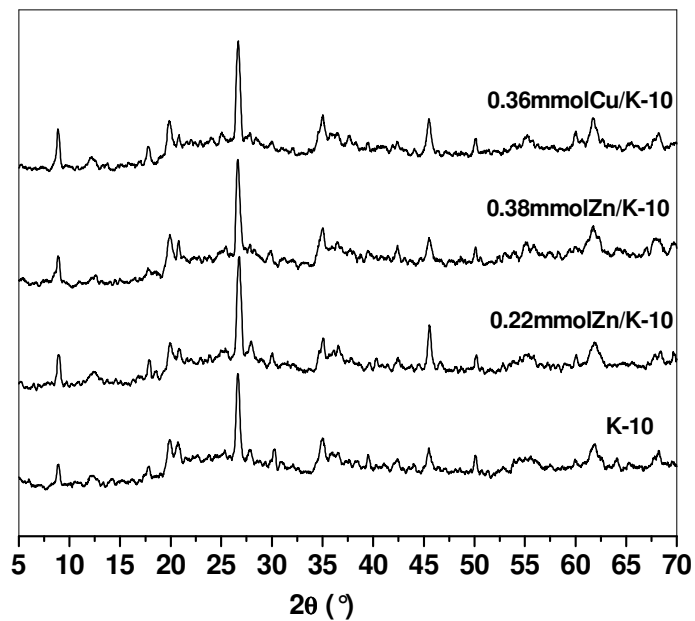
Fig. 3.1. XRD patterns of K-10 and exchanged K-10 catalysts
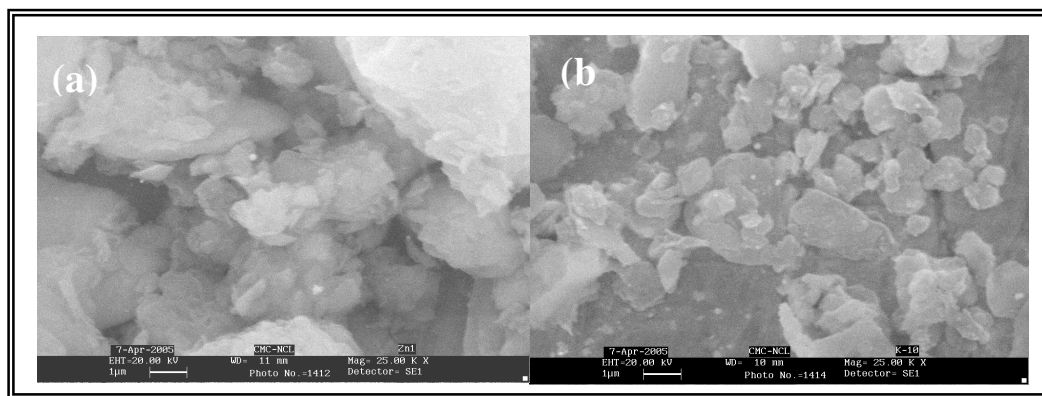
Fig. 3.2. SEM photographs of (a) Zn/ K-10, (b) K-10

3.1.4.2. Diffuse Reflectance UV -vis spectroscopy

The diffuse reflectance UV-Vis spectrum of K-10 and Cu-K-10 is depicted in the Fig. 3.3. K-10 does not have any absorption band above 400 nm. However, Cu-K10 exhibits a strong band with a maximum at 549 nm, which is attributed to the d-d transitions of Cu(II).
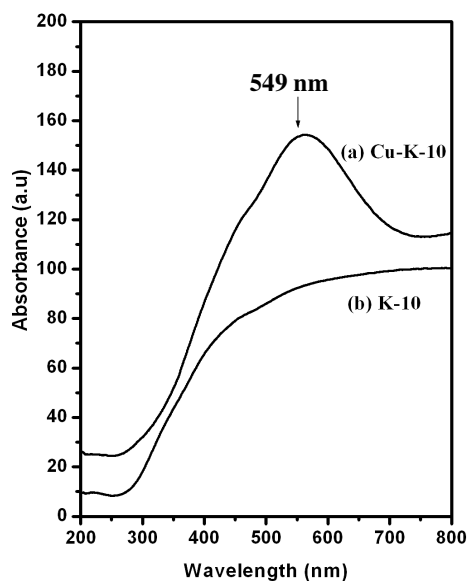
Fig. 3.3. Diffuse reflectance UV-vis Spectra of (a) K-10 (b) Cu/ K-10
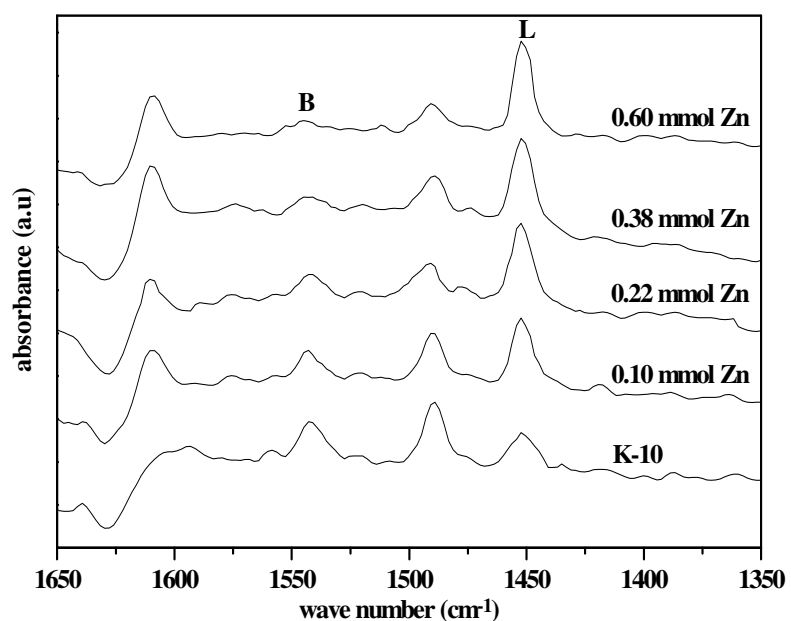
Fig. 3.4. FT-IR pyridine adsorption experiments on K-10 and Zn/ K-10 catalysts showing Brönsted (B) and Lewis acid sites (L).

3.1.4.3. Acidity measurements by FTIR pyridine adsorption

Pyridine adsorption *in-situ* FT-IR spectroscopy was performed for K-10 and Zn incorporated K-10 catalysts and the spectra recorded after outgassing at 200 °C are represented in Fig. 3.4. Adsorption of pyridine on the parent K-10 clay resulted in absorption bands at 1540 cm^{-1} and 1450 cm^{-1}, which can be assigned to pyridine molecules interacting with Bronsted and Lewis acid sites, respectively. Incorporation of zinc led to an increase in Lewis acidity as shown in Fig. 3.4. In contrast, there is decrease in concentration of Bronsted acid sites with increase in zinc loading in the range 0.1 –0.6 mmol of Zn per gram of K-10.

3.1.5. Intermolecular hydroamination of phenylacetylene with aniline

3.1.5.1. Experimental procedure

In a typical reaction, the reaction mixture consisting of phenylacetylene (hereafter referred as PhAc) (1.77 g), aniline (3.23 g), toluene (12 ml) and catalyst (0.25 g) placed in a 50 ml round bottom flask was kept in an oil bath, which was refluxed (110 °C) under N_2 atmosphere. Toluene was used as a solvent since it prevents metal ion leaching into the reaction mixture besides having other common advantages of a solvent. Samples were withdrawn at regular intervals of time and analyzed for its contents by Shimadzu 14B gas chromatograph, equipped with a flame ionization detector using HP-5 capillary column (cross linked 5 % ME silicone, 30 m x 0.53 x 1.5 μm film thickness). The authenticity of the product was confirmed by GC-MS and conversion of phenylacetylene was estimated in weight percentage. The reactions above the reflux temperature were carried out in Parr autoclave.

enamine intermediate   phenyl-(1-phenyl ethylidene)amine
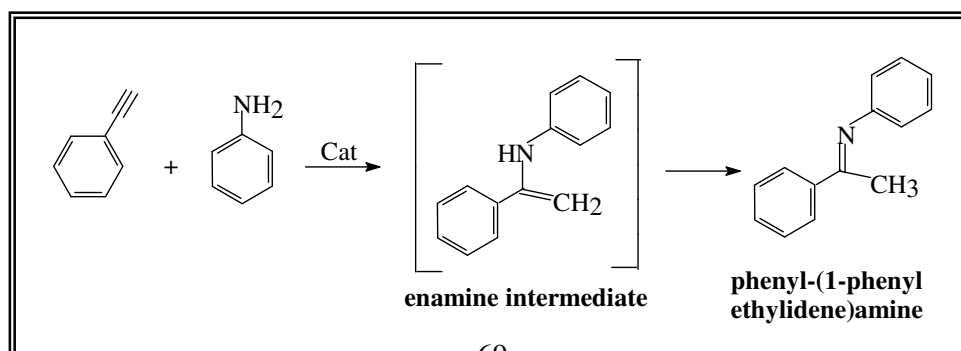
Scheme 3.1. Hydroamination of phenylacetylene with aniline

3.1.5.2. Results and discussion

3.1.5.2.1. Influence of metal ions and supports on the catalytic activity.

Intermolecular hydroamination of PhAc by aniline to give phenyl-(1-phenylethylidene)amine (Scheme 3.1) was chosen as a model reaction for testing the performance of metal exchanged K-10 as a catalyst and compared its performance with other supports like H-beta and silica. In the above reaction, enamine was formed as an intermediate, which being unstable undergoes rearrangement to form stable phenyl-(1-phenylethylidene)amine. This reaction is highly regioselective and only Markovnikov addition product was formed under the reaction conditions studied.
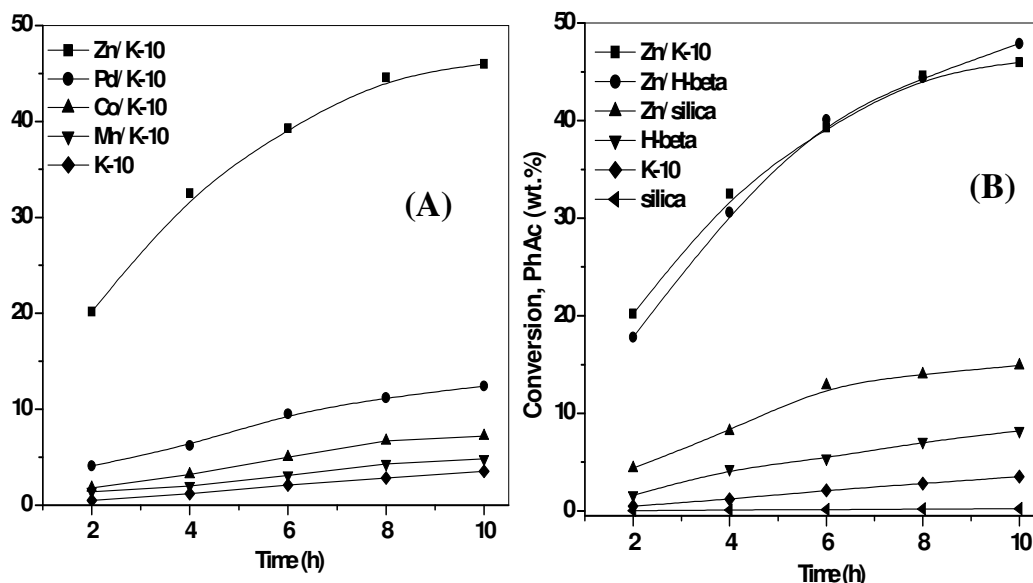
Fig 3.5. (A) Effect of support on the activity of the catalyst in hydroamination of PhAc by aniline. (Conditions: temperature = 110 °C, aniline to PhAc mole ratio = 2, catalyst wt. = 0.25 g, total reactants wt. = 5g).

(B) Time-PhAc conversion profile for different metal exchanged on K-10 catalysts. (Conditions: temperature = 110 °C, aniline to PhAc mole ratio = 2, catalyst wt. = 0.25 g, total reactants wt. = 5g).

In order to find the influence of divalent transition metals exchanged with K-10 catalysts on the intermolecular hydroamination of PhAc by aniline, the catalysts prepared with different divalent transition metals such as Zn, Cu, Pd, Co, Mn were

tested and their performance is shown in Fig.3.5 (A). It is seen that Cu/ K-10 and Zn / K-10 showed highest activities with 56% and 46 % conversion, respectively and the others followed as Pd/K-10 (12.4 %), Co/K-10 (7.2 %) and Mn/K-10 (4.8 %) after 10 h of reaction. Zinc exchanged H-beta has been used as a catalyst for hydroamination reaction and H-beta was found to be the best support among zeolites [29]. The catalytic performance of Zn/ K-10 has been compared with supports H-beta and silica containing similar zinc concentrations and the results are presented in Fig 3.5. (B). The conversion of PhAc after 10 h for Zn/ H-beta (47.9 %) was marginally higher in comparison with Zn/K-10 (46 %) under similar reaction condition, while Zn/ silica is at least three times less active than the other two.

The effect of Zn^{2+} concentration on the catalytic activity of the Zn/ K-10 was carried out with Zn^{2+} concentrations ranging from 0.04 - 0.60mmol/g and the results are shown in Fig 3.6. The conversion of PhAc increased linearly up to 0.22 mmol/g of zinc and further increase has marginal effect on the catalytic activity. Zn^{2+} is exchanged with interlayer cations as well as the Brönsted acid sites up to a concentration of 0.22 mmol/g. The higher loading results in incorporation of zinc species as ZnO after calcination, which does not contribute to the catalytic activity [22]. This was confirmed by independent experiment (shown in Fig. 3.6.) and no activity of ZnO in hydroamination reaction could be because of its basic nature.
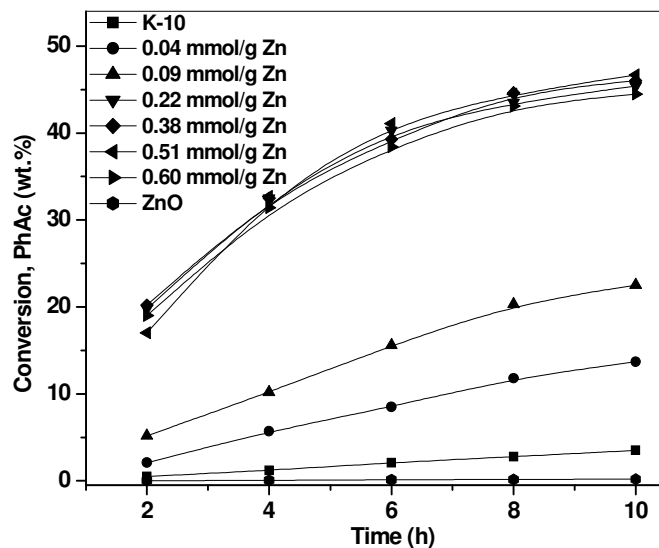
Fig. 3.6. Influence of zinc ion concentration on the activity of K-10 supported catalysts and activity of ZnO. (Conditions: temperature = 110° C, aniline to PhAc mole ratio = 2, catalyst wt. = 0.25 g, total reactants wt. = 5g).

3.1.5.2.2. Plausible mechanism of hydroamination catalyzed by $Zn^{2+/}K$-10

Two approaches are possible for transition metal catalyzed hydroamination reactions, which involve primarily the activation of either, an amine or an alkyne. Amine activation takes place via oxidative addition of the N-H bond by transition metal in a lower oxidation state. Insertion of alkyne into the metal nitrogen bond results in β-aminoalkenyl metal complex, which further gives final product by reductive elimination. But this approach is least possible for Zn considering its stable solitary +2 oxidation state. Hence, the most probable mechanism for hydroamination of PhAc by aniline catalyzed by Zn^{2+} ion exchanged K-10 can be explained via alkyne activation as shown in Scheme 3.2. PhAc forms a π-coordination complex with Zn^{2+} ion (step I). This makes the π-electron system more vulnerable to nucleophilic attack of aniline. Hence, nucleophilic addition of aniline (Markovnikov addition as shown in step II) results in β-ammonioalkenyl zinc complex. 1,3-Proton shift in β-ammonioalkenyl zinc complex gives enamine (A) as hydroamination product (step III). Enamine being unstable rearranges itself to give stable imine (B) in step IV, while regenerating the catalyst in a cycle.
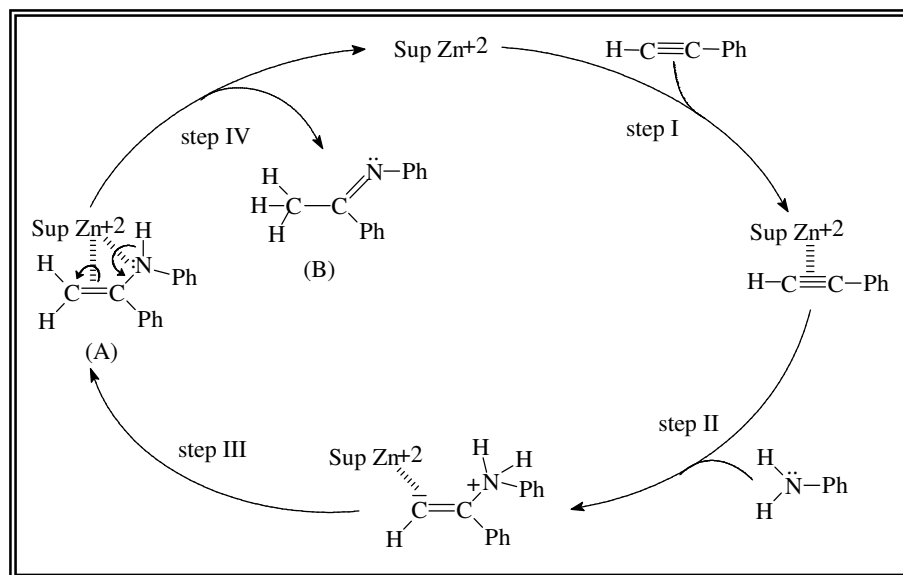
Scheme 3.2. Proposed mechanism for hydroamination of PhAc by aniline catalyzed by Zn/ K-10

3.1.5.2.3. Why Cu^{2+} and Zn^{2+} are highly active for hydroamination of alkynes compared to other metals?

The strength of Lewis acidity of metal ions plays an important role in hydroamination reactions [23]. If the metal cation is a very soft Lewis acid, the formation of catalyst-substrate complex is either hindered or may not form at all. In contrast, if the metal cation is a hard Lewis acid, catalyst-substrate complex possibly too stable to undergo subsequent reactions. In other words, the intermediate Lewis acidity of the metal center facilitates the activation of the alkyne group in the presence of amines followed by coordination of the alkyne to the metal center and subsequent nucleophilic attack by the amine becomes possible. Zn^{2+} ion is known as "moderate Lewis acid" cation owing to its moderate hardness, which explains the reason for higher activities shown by Zn/K-10 and Zn/H-beta catalysts in hydroamination of PhAc by aniline. Lewis acids like Al^{3+} present in K-10 as well as H-beta and other metal ions present in a little amount such as Na^+, K^+ and Ca^{2+}, Mg^{2+} in K-10 are responsible for smaller but noticeable activity shown by K-10 and H-beta. But lower activity shown by these metal ions may be due to their hardness property. Brönsted acidity decreases with increase in zinc ion concentration on K-10 (Fig. 3.4.). Müller

and co-workers studied in detail the role of Brönsted acidity in hydroamination reactions and the co-catalysis between Brönsted and Lewis acidity [24]. Brönsted acidity though doesn't seem to have profound effect in Zn/K-10 catalyzed hydroamination reaction, it appears that protons are involved in step III and step IV of the reaction (Scheme 3.2). It may facilitate 1,3- proton shift in 2-ammonioalkenyl zinc complex through protonation of the carbon attached to the metal and in turn helps in the cleavage of metal-carbon bond (step III). Brönsted acidity can also facilitate the formation of final product imine by the rearrangement of intermediate enamine in the last step. Moreover, reversible protonation of amines can enhance the possibility of the selective interaction of acetylenic bond with the metal center in the step I of the reaction.
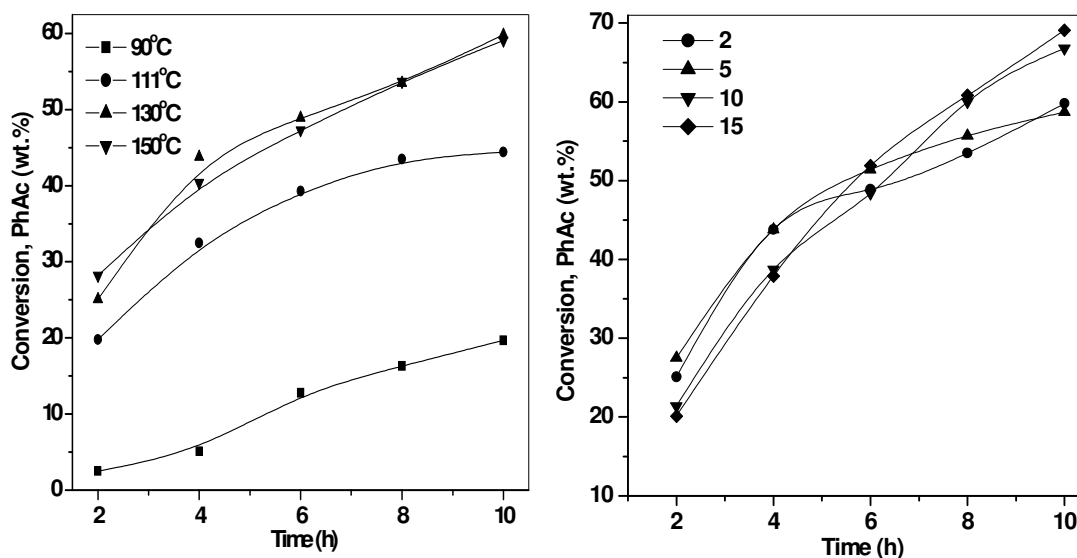
Fig. 3.7. (A) Effect of reaction temperature. (Conditions: catalyst = 0.22 mmol Zn/ K-10, aniline to PhAc mole ratio = 2, catalyst wt. = 0.25 g, total reactants wt. = 5 g).
(B) Effect of anline to PhAc mole ratio. (Conditions: catalyst = 0.22 mmol Zn/ K-10, temperature = 130 °C, catalyst wt. = 0.25 g, total reactants wt. = 5 g).

3.1.5.2.4. Optimization of reaction conditions

Zn/ K-10 with 0.22 mmol/g zinc concentration was used to optimize the reaction conditions of intermolecular hydroamination of PhAc by aniline.

The reaction was studied by varying the temperature in the range (90-150 °C), keeping constant catalyst 0.25 g (5 % of the total reactants weight) and Aniline to PhAc mole ratio of 2. Conversion of PhAc as a function of temperature is shown in Fig.3.7. (A). The Markovnikov addition product phenyl-(1-phenylethylidene)amine formed with 100% selectivity. The conversion of PhAc increased sharply when temperature was increased to 130 °C. There was not much change in conversion with further increase in temperature. Conversion of PhAc decreased below reflux temperature (90 °C). Hence, 130 °C was found to be suitable for the reaction and used for further optimization.
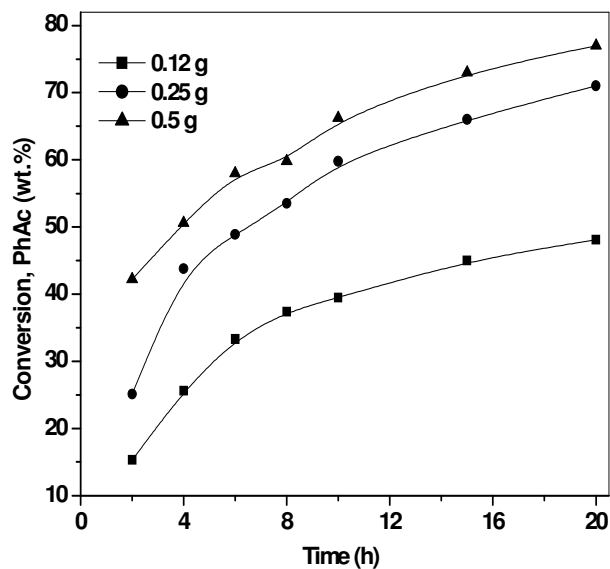
Fig. 3.8. Effect of catalyst concentration and reaction time. (Conditions: catalyst = 0.22 mmol Zn/ K-10, temperature = 110 °C, aniline to PhAc mole ratio = 2, total reactants wt. = 5g).

75

The reaction was carried out with aniline to PhAc molar ratios varied between 2 to 15 keeping constant catalyst (0.25g) and 130 °C and the results are shown in Fig.3.7. (B). Data collected over 10 h shows that change in aniline to PhAc mole ratio (from 2 to 5) has marginal influence on the conversion of PhAc. However, conversion increased by 8 % as the mole ratio increased from 5 to 10 and no change in conversion thereafter. After 6 h, conversion of PhAc was the same for all mole ratios studied. Hence, higher concentration of aniline in the reaction must be hindering the rate of hydroamination preventing the π coordination of PhAc with the metal center (Scheme 3.2.).

To study the effect of catalyst concentration on hydroamination, the reaction was carried out at 110 °C with aniline to PhAc mole ratio 2 by varying catalyst weight (0.12-0.5 g) and the results are shown in Fig 3.8. The conversion increased with increase in catalyst concentration as expected. There was linear increase in conversion of PhAc up to 6 h and later there was marginal increase in the range 6-20 h. At the end of 20 h, maximum conversion of PhAc (77%) was obtained for 0.5 g of catalyst with 100% selectivity for phenyl-(1-phenylethylidene)amine. The catalyst recycling was performed thrice by following the standard procedure and the conversion of PhAc was the same as that of the fresh catalyst in all the cycles.

3.1.6. Hydroamination of alkynes and amines catalyzed by Cu/K-10

3.1.6.1. Experimental Procedure

Typical procedure for M^{2+}/K-10 catalyzed hydroamination reaction: Synthesis of *N*-(1-phenylethylidene)-2,4,6-trimethylaniline (entry 5, Table 3.4.): phenylacetylene (5.37 mmol, 0.55 g) and 2,4,6-trimethylaniline (10.73 mmol, 1.45 g) were added to a stirred mixture of Cu/K-10 (0.2 g) in toluene (4 mL). The reaction mixture was stirred at 110 °C for 20 h under N_2 atmosphere in an oil bath. The mixture was then cooled and filtered to remove the catalyst and the solvent was removed by distillation. The mixture was dried *in vacuo* and purified by column chromatography on neutral alumina as the stationary phase (petroleum ether/ethyl acetate, 200/1). Yield: 91%, light brown oil: ^{1}H NMR (CDCl$_3$, 200 MHz): δ (ppm)= 7.86-8.01 (m, 2H), 7.31-7.48 (m, 3H), 6.80 (s, 2H), 2.21 (s, 3H), 1.99 (s, 3H), 1.92 (s,

6H). ^{13}C NMR (CDCl$_3$): δ (ppm) = 165.57 (C), 146.5 (C), 139.33 (C), 131.96 (C), 130.43 (CH), 128.56 (CH), 128.43 (CH), 127.12 (CH), 125.63 (C), 20.81 (CH$_3$), 17.96 (CH$_3$), 17.48 (CH$_3$). FT IR (neat, cm^{-1}): 3025, 2940, 1638, 1207, 1025, 856, 762, 629. GCMS *m/z* (relative intensity): 237 (64) [M$^+$], 222 (100), 207 (47), 103 (52), 91 (55), 77 (40).

3.1.6.2. Results and discussion

All catalysts were prepared by ion exchange of K-10 with aqueous metal acetate solutions under identical conditions. Reactions were conducted in a round bottom flask with toluene as a solvent unless otherwise stated. Among different M^{+2} exchanged K-10, Cu^{+2} gave the highest yields for hydroamination of 1a with *p*-toluidine (Table 3.2.) and hence was used as a catalyst in further studies. The higher activity of Cu^{2+} and Zn^{2+} in hydroamination is due to their moderately hard Lewis acidity. The reaction proceeded with high regioselectivity, only the Markovnikov addition product being observed in all the cases.

Table 3.2. Intermolecular hydroamination of phenylacetylene with *p*-toluidine.[a]

Ph—≡—H + *p*-CH$_3$C$_6$H$_4$NH$_2$ $\xrightarrow[\text{toluene, 110 °C}]{\text{Catalyst}}$

N–*p*-Tol

Ph

Markovnikov product

1a
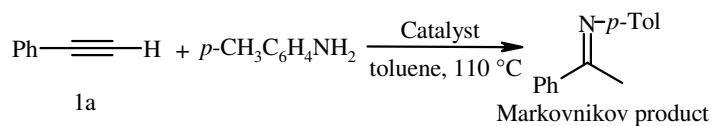
Entry	Catalyst	Yield %
1	Cu-K-10	64
2	Zn-K-10	52
3	Pd-K-10	8
4	Co-K-10	5
5	Ni-K-10	3
6	Mn-K-10	3
7[b]	H$^+$-K-10	2

[a] Reaction conditions: Amine/alkyne = 2, 4 ml toluene, 110 °C, 10 wt.% catalyst, 4h. All yields were determined by GC analysis and referred to alkyne. 100% selectivity for Markovnikov product.

[b] Unexchanged clay.

Table 3.3. Hydroamination of alkynes with aniline [a]

Entry	Alkynes	Temp (°C)	Time (h)	Yield %
1	1-Hexyne	80	20	5
2[b]	1-Hexyne	110	20	45
3[b]	1-Heptyne	110	20	55
4[b]	3-Hexyne	110	48	NR
5	Phenylacetylene	110	10	93
6	Diphenylacetylene	110	48	NR
7	4-Ethynyltouene	110	10	87
8	4-Ethynylanisole	110	10	84
9	1-Ethynyl-2-nitrobenzene	110	20	32

[a] Reaction conditions: aniline/alkyne = 2, 4 ml toluene, 10 wt.% catalyst. Yields were determined by GC analysis and referred to alkyne. NR = no reaction, 100% selectivity for Markovnikov product.

[b] Reaction was carried out in a Parr autoclave under N$_2$.

To gain more insight into the scope and limitations of our method, we examined the reactions of different alkynes with aniline (Table 3.3.). Aromatic alkynes were more reactive than aliphatic alkynes, while terminal alkynes gave the highest yields. Internal alkynes (entries 4, 6) did not undergo the reaction probably due to the steric hindrance by the bulky groups attached to the triple bond. The activated alkynes with electron-donating substituents, CH_3- and CH_3O- gave better yields (entries 7, 8), where as alkyne with electron-withdrawing substituent, NO_2 was less reactive (entry 9).

Table 3.4. Hydroamination of phenylacetylene with aromatic amines [a]

$$Ph\text{---}\equiv\text{---}H \; + \; RNH_2 \xrightarrow[\text{toluene, 110 °C}]{\text{Cu-K-10}}$$

Markovnikov
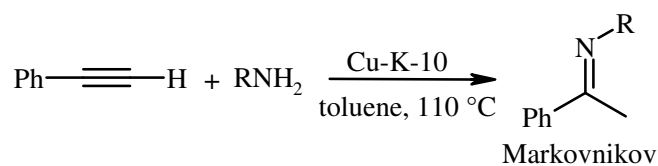
Entry	R	Time (h)	Yield %
1	C_6H_5	10	93
		20	99
2	$2\text{-}CH_3C_6H_4$	10	84
		20	99
3	$4\text{-}CH_3C_6H_4$	20	98
4	$2,4\text{-}(CH_3)_2C_6H_3$	20	99
5	$2,4,6\text{-}(CH_3)_3C_6H_2$	20	95
		20^b	91
6	$2\text{-}i\text{Pr}C_6H_4$	20	99
7	$4\text{-}i\text{Pr}C_6H_4$	20	99
8	$4\text{-}CH_3OC_6H_4$	20	95
9	$2\text{-}ClC_6H_4$	20	32
10	$4\text{-}BrC_6H_4$	20	68
11^c	$4\text{-}O_2NC_6H_4$	48	NR
12^c	$4\text{-}HOCC_6H_4$	48	NR
13	1-Naphthyl	20	88

[a] Reaction conditions: Amine/alkyne = 2, 4 ml toluene, 110 °C, 10 wt.% catalyst, NR = no reaction, Yields were determined by GC analysis and referred to alkyne. 100% selectivity for Markovnikov product.
[b] Isolated yield.
[c] Solvent 1,4-dioxane, 100 °C.

The nature of the substituents on the anilines had a significant effect on the hydroamination reaction (Table 3.4.). The aniline derivatives with electron-donating groups at the *ortho* and *para* positions reacted smoothly with 1a (>90% yield) to give the corresponding imines. Interestingly, sterically demanding amines like 2,4,6-trimethylaniline and 2-isopropylaniline (entries 5, 6), gave higher imine yields indicating that bulkier groups around -NH_2 group do not affect the reactivity of amine. The amines with electron-withdrawing substituents, -Cl and -Br were less reactive (entries 9, 10), where as amines with stronger electron-withdrawing substituents, -NO_2 and -CHO, did not undergo the hydroamination reaction (entries 11, 12). This reaction also took place smoothly with 1-naphthylamine (entry 13).

Part B

3.2. Hydroamination of activated olefins catalyzed by montmorillonite clays

3.2.1. Introduction

The solid acid mediated hydroamination of acrylates with amines (Scheme 3.3.) is a simplistic approach towards the synthesis of amino acid derivatives that can be used in peptide analogues or as precursors to optically active amino alcohols, diamines and lactums. In the absence of the catalysts such reactions require very high temperatures and longer reaction times. The addition of various aliphatic amines with acrylates has been reported with different homogeneous and heterogeneous catalytic system [33-37]. Some of them have expressed the inability of aromatic amines to undergo hydroamination under their reaction conditions. Recently Sugi et. al have reported the hydroamination of acrylates with aromatic amines using zeolites as catalysts [38].

Different grades of acid-activated montmorillonite clays are tailored to different applications and can be purchased from a variety of commercial sources. The acid-treated clay K10 is produced by Süd Chemie AG of Moosburg, Bavaria (Germany), and has been obtainable from Fluka AG and Aldrich Chemical Co. for a number of years. The ease of availability of these acid activated clays explains why synthetic organic chemists have largely used these materials in a wide range of acid catalyzed reactions [1].

3.2.2. Chemicals and reagents

Montmorillonite clays were purchased from Fluka AG, Switzerland. Ethyl acrylate was purchased from Lancaster Chemicals, U.K. Methyl acrylate, acrylonitrile and acrylic acid were procured from Loba Chemicals, Mumbai. All the amines and toluene were purchased from S.D Fine Chem Ltd., Mumbai. All the chemicals were used as received. Toluene used in the reaction was distilled over sodium wire before use.
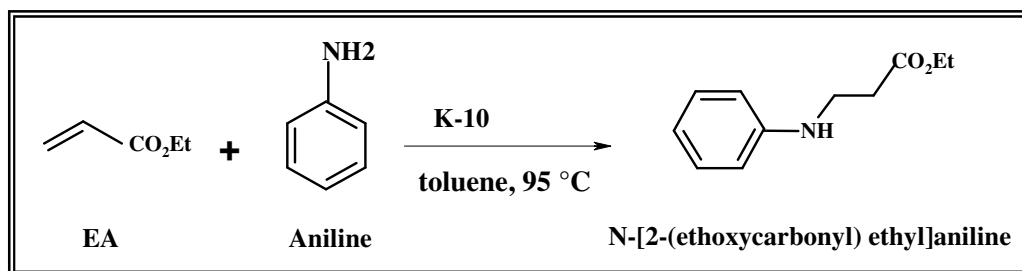
Scheme 3.3. Hydroamination of ethyl acrylate with aniline

3.2.3. Characterization- Results and discussion

The properties of various grades of acid-treated clays of the K series (K-10, K-20, K-30) catalysts and Al-pillared clay used in this work are listed in Table 3.5 and Table 3.6. Lewis and Brönsted acidity of clays have been determined using pyridine as

Table 3.5. Chemical analysis of clay catalysts

Catalyst	Chemical analysis (%)								
	SiO_2	Al_2O_3	Fe_2O_3	CaO	MgO	Na_2O	K_2O	Loss on ignition	Total
K-10	73.0	14.0	2.7	0.2	1.1	0.6	1.9	6.0	99.5
K-20	75.0	12.5	2.4	0.3	1.2	0.3	1.5	6.3	99.5
K-30	80.0	10.0	1.8	0.2	1.0	0.3	0.5	6.0	99.8
Al-Pillared Clay	69.8	24.5	1.8	0.2	2.5	0.3	0.9	-	100
Untreated clay	78	15.1	3.2	-	2.1	-	-	-	-

probe molecule by monitoring the bands in the range of 1350-1600 cm^{-1} arising from its ring vibration modes [39-40]. The characteristic absorption band for Brönsted acidity appeared at 1540 cm^{-1} and that due to Lewis acidity appeared at 1450 cm^{-1}. However, in the case of solid acids, as important as the number and type of acid sites is their acid strength since this will be responsible for the extent to which a given

bond in the reactant molecule will be polarized and, consequently, will determine the type of reaction that the solid acid will be able to catalyze.

Table 3.6. Characteristic properties of clay catalysts

Catalyst	Specific Surface area $(m^2 \, g^{-1})$	I(B)	I(L)	Acidity I(B)+ I(L)	B/L ratio (I(B)/I(L))
K-10	242	0.14	0.20	0.36	0.70
K-20	240	0.14	0.23	0.37	0.61
K-30	330	0.13	0.05	0.18	2.60
Al-pillared clay	250	0.07	0.25	0.32	0.28
Untreated clay	179	0.08	0.23	0.31	0.35

The surface area, pore volume, intensity of Brönsted acidity and Lewis acidity peaks and B/L ratio determined using pyridine is given in the Table 3.6. BET surface area increased in the order untreated clay < K10 < K20 < Al Pillared clay < K30. Taking into account of surface area, the acidity ((I(B) + I(L)) per unit surface area decreased in the order K10 ~ K20 > Al-pillered clay > K30 > untreated clay.

3.2.4. Intermolecular hydroamination of activated olefins catalyzed by montmorillonte clays.

3.2.4.1. Experimental procedure

The liquid phase hydroamination of α,β-ethylenic compounds with amines was carried out in a 50 mL two necked flask equipped with a nitrogen inlet for maintaining an inert atmosphere and an additional port with a septum for sample withdrawal. The temperature of the reaction vessel was maintained by placing the above assembly in thermostated oil bath. The reaction was carried out at selected reaction conditions i.e. at 95 °C with ethylacrylate hereafter indicated as EA, to aniline molar ratio of 1 and with 10 wt.% (total reaction mixture) of catalyst. The catalysts were activated at 100 °C in air for 15 h and cooled to room temperature prior to their use in the reaction. To the reaction mixture 1 ml toluene was added. The reaction mixture was magnetically stirred and heated to the required temperature

under atmospheric pressure. Samples were withdrawn at regular intervals and analyzed using a gas chromatograph (Shimadzu 14B) equipped with a cross linked 5% diphenyl-95% dimethylpolysiloxane capillary column (30m) and a flame ionization detector and the identity of the product was confirmed by GCMS (Shimadzu GCMS QP 5000) equipped with an identical column and a mass selective detector. Conversion was calculated based on amine.

Table 3.7. Properties of the catalysts in the hydroamination of aniline using ethyl acrylate at 95 °C.

Catalyst	Conversion (%)[*]	Selectivity (%)[#] (Mono-addition)[1a]	(Di-addition)[1b]	Rate constant k_I x 10^{-4} min^{-1}
No Catalyst	2[+]	100	-	-
H-β	39	100	-	-
K-10[a]	49	100	0	56.90
K-20[a]	37	99.83	0.13	39.12
K-30[a]	32	100	0	25.83
Al-pillared clay[a]	26.	99.84	0.13	25.57
Untreated clay	27	100	0	25.85

Reaction conditions: aniline:EA =1(molar ratio), Amount of catalyst: [a] 0.3g (dried at 100 °C for 15 h before use), * Conversion determined by GC analysis with respect to aniline, [#] Selectivity was determined by GC analysis. [1a] N-[2-(ethoxycarbonyl) ethyl]aniline (mono-addition product) , [1b] N,N-bis[2-(ethoxycarbonyl)ethyl]aniline, Time = 2 h. [+]Time = 12 h.

The reaction mixture was then cooled and filtered to remove the catalyst and volatiles were removed by distillation. The product was separated by column chromatography using neutral alumina as stationary phase and (petroleum ether/ethyl acetate 95 : 5) as eluent. The single product was characterized by NMR, GC-MS, and FT-IR analysis which confirmed the product to be N-[2-(ethoxycarbonyl) ethyl]aniline.

Yield: 90%, ^{1}HNMR (200MHz,CDCl$_3$): δ (ppm) = 7.21-7.06(m,2H), 6.68-6.53(m,3H), 5.21(s, 1H), 4.13-4.01(m, J= 3.72 Hz, 2H), 3.41-3.34(t, J= 6.45 Hz, 2H), 2.57-2.47(q, J = 6.32 Hz, 2H), 1.22-1.14(t, J = 7.07Hz, 3H) ; ^{13}C NMR (CDCl$_3$, 200 MHz,): δ (ppm) = 147.73 (C), 129.52 (CH), 129.34 (CH), 117.72 (CH), 113.10 (CH), 112.70 (CH), 60.64 (CH$_2$), 39.51(CH$_2$), 34.02 (CH$_2$), 14.24 (CH$_3$);FT-IR (neat cm^{-1}) υ

3409, 2985, 1731, 1604, 1504, 1373, 1319, 1249, 1176, 1099, 1029, 1864, 748, 694. GCMS: *m/z* (relative intensity): 193 (11.83), 118 (2.55), 106 (100), 93 (2.46), 77 (11.26), 65 (6.57), 51 (7.79).

3.2.4.2. Results and discussion

3.2.4.2.1. Catalytic activities of different clay catalysts

The conversion of aniline in the hydroamination with EA over different types of montmorillonite clays (K-10, K-20, K-30, untreated clay, Al-pillared clay) at 95 °C is shown in Table 3.7. Aniline reacted with EA to yield only *anti*-Markovnikov adduct N-[2-(ethoxycarbonyl)ethyl]aniline (mono-addition product) (1a) (Scheme 3.3.). No Markovnikov adduct (N-[1-(ethoxycarbonyl)ethyl]aniline and double addition product N,N-bis[2-(ethoxycarbonyl)ethyl]aniline (1b) were formed. For all the catalysts, the aniline conversion increased linearly with time up to a conversion of 70 – 95 %. K-10 clay gave the highest conversion (49 %) with respect to aniline over a period of 2h under the selected reaction conditions with a rate constant of 56.90 x 10^{-4} min^{-1}. Under the optimized reaction condition K-10 displayed exceptionally high catalytic activity and gave the highest conversion of 85 % over a period of 12 h. The apparent rate constants for the different catalyst declines in the following order: K-10 > K-20 > K-30 > untreated clay > Al-Pillared clay. The apparent rate constant for hydroamination over K-10 is 56.90 x 10^{-4} min^{-1} that of K-20 is 39.12 x 10^{-4} min^{-1} while Al-Pillared clay registered an apparent rate constant of only 25.57 x 10^{-4} min^{-1}. The acidity and the activities of clay catalysts can be correlated. The activity seems to depend upon Brönsted acid sites. As the I(B) decreased the activity of the catalysts also decreased with an exception of K-20 catalyst which showed lower activity compared to K-10 clay. The role of Brönsted acidity in hydroamination of activated olefins is explained in Scheme 3.5. A control experiment was carried out without adding any catalysts at a temperature of 95 °C. There was only 2% conversion without catalyst.

Table 3.8. Hydroamination of α, β-ethylenic compounds with aniline using K-10 at 95 °C.

Catalyst	Conversion (%)*	Selectivity (%) (Mono-addition)	(Di-addition)	Rate constant k_l x 10^{-4} min^{-1}
Ethyl acrylate	49.5	100	0	56.90
Methyl acrylate	31.1	100	0	31.00
Acrylonitrile	7.61	100	0	65.83
Acrylic acid	37	100	0	38.50

Reaction conditions: aniline:EA =1(molar ratio), Amount of catalyst: 0.3g (dried at 100 °C for 15 h before use), Time = 2 h. * Conversion determined by GC analysis with respect to aniline.

3.2.4.2.2. General performance of K-10 catalyst in hyrdoamination of activated olefins with amines

The liquid phase hydroamination of acrylates with amines was carried out using clay as catalysts and the reaction follows as shown in Scheme 3.4. Hydroamination of different α,β-ethylenic compounds like methyl acrylate, acrylonitrile, and acrylic acid with aniline using 10 wt % K-10, at 95 °C and aniline/acrylate molar ratio of 1. The conversion and product distributions for the hydroamination of different α,β-ethylenic compounds are given in Table 3.8. Under the selected reaction condition ethyl acrylate with aniline gave maximum conversion of 49.5 % over a period of 2 h.

The data on the catalytic performances of various aromatic amines with EA using clay (K-10) along with reaction conditions and the data on the catalytic activity are presented in Table 3.9. Hydroamination of EA with various aromatic amines mainly gave excellent chemoselectivity for mono-addition product. All reactions were exclusively regioselective giving the product of *anti*-Markovnikov addition of amine to CC double bonds. The high chemo selectivity in the hydroamination could be used for the synthesis of precursors for amino acids. The results indicate that the aniline derivatives that have electron-donating groups at the *-ortho* and *-para* positions reacted smoothly with EA to give corresponding hydroamination products.

Scheme 3.4. Hydroamination of α, β-ethylenic compounds with amines

Strongly electron-donating substituents having methoxy group gave slightly higher conversion as compared to methyl groups in the same positions. In contrast, the reaction of amines with electron withdrawing substituents like nitro group did not undergo hydroamination. However, 1-Naphthylamine reacted sluggishly with EA to give the hydroamination product (32 %) which could be because of the bulky nature of amine. On the other hand, in the course of investigations we found that EA reacted with N-methylaniline to yield 80 % mono-addition product, which demonstrates the feasibility of secondary amines to undergo this reaction. However, sterically hindered amines like 2,4,6-trimethyl aniline gave less yield for corresponding hydroamination product indicating that bulkier groups around NH_2 affect the activity of amines (Table 3.9.).

Table 3.9. Effect of substituents on benzene ring of aniline in the hydroamination of EA over K-10 at a reaction temperature of 110 °C.

Aromatic Amine	Time (h)	Conversion (%)*	*anti*-Markovnikov product selectivity (%)[#]		Rate constant k_1 x 10^{-4} min^{-1}
			Mono-addition	Di-addition	
Aniline	6	85	97	2.8	52.60
	12	94.5	95.1[1a]	4.8	40.18
4-Bromoaniline	6	60	100	0	25.42
	12	82	96.5[2a]	3.5	23.72
p-Anisidine	6	79	98.6	1.39	43.35
	12	94.6	94.3[3a]	5.6	40.53
2,4-Xylidene	6	60.9	96.7	3.28	26.08
	12	82.3	96.8[4a]	3.1	23.97
o-Nitroaniline	12	Nil	Nil	Nil	Nil
p-Isopropylaniline	6	61.5	98.2	1.6	26.43
	12	74.5	96.9[5a]	2.8	18.92
o-Chloroaniline	6	26	99.7	0.3	6.93
	12	40	99.2[6a]	0.79	
o-Toluidine	6	39.5	99.8	0.2	13.95
	12	60	98[7a]	2	12.72
p-Ethylaniline	6	70	97	2.8	33.43
	12	90	96[8a]	4	31.97
N-Methylaniline	6	59	100	-	24.77
	12	80	100	-	22.35
1-Naphthylamine	6	16	100	0	8.52
	12	32	99.5[10a]	0.5	5.35
2,4,6-Trimethylaniline	6	10	100	0	3.00
	12	15	100[11a]	0	2.25

Amine to EA ratio = 1 Amount of catalyst = 0.3 g (10 wt.% of total reaction mixture); * Conversion with respect to aniline and selectivity were determined by GC analysis, [1a] N-[2-(ethoxycarbonyl) ethyl]aniline (mono-addition product) , [2a] 4-Bromo-N-[2-(ethoxycarbonyl) ethyl]aniline, [3a] 4-methoxy-N-[2-(ethoxycarbonyl) ethyl]aniline, [4a] 2,4-dimethyl-N-[2-(ethoxycarbonyl) ethyl]aniline, [5a] 4-isopropyl-N-[2-(ethoxycarbonyl) ethyl]aniline, [6a] 2-Chloro-N-[2-(ethoxycarbonyl) ethyl]aniline, [7a] 2-methyl-N-[2-(ethoxycarbonyl) ethyl]aniline, [8a] 4-ethyl-N-[2-(ethoxycarbonyl) ethyl]aniline, [9a] N-Methyl-N-[2-(ethoxycarbonyl) ethyl]aniline, [10a] N-[2-(ethoxycarbonyl)ethyl]-1-Naphthylamine, [11a] 2,4,6-trimethyl-N-[2-(ethoxycarbonyl) ethyl]aniline.

Table 3.10. Hydroamination of aliphatic amines with EA over K-10 at room temperature.

Aliphatic Amine	Conversion (%)*	anti-Markovnikov product selectivity (%)[#]	
		Mono-addition	Di-addition
Morpholine	97	100	0
Piperidne	97	100	0
di-propylamine	96	100	0
n-propylamine	96	92.2	7.8
Benzylamine	95	99.9	0.1

Reaction conditions: Amine to EA ratio = 1. Amount of catalyst = 0.1 g (5 wt.% of total reaction mixture), * Conversion determined by GC analysis with respect to aniline, [#] Selectivity was determined by GC analysis, Temperature =25 °C, Time = 1 h

Encouraged by the results with aromatic amines we turned our attention to aliphatic amines and as we expected they were more reactive for addition with α,β-ethylenic compounds compared to the aromatic amines. Table 3.10. summarizes the results obtained by the hydroamination of EA with aliphatic amines. Interestingly, under the selected reaction conditions using 5 wt % of K-10, amine/acrylate molar ratio of 1 and in the absence of any solvent, all the aliphatic amines gave excellent conversion for hydroamination product at room temperature. Morpholine and piperidine reacted with EA to yield 97 % hydroamination product over a period of 1 h. Primary aliphatic amine (n-propylamine) however, gave a mixture of mono and di-addition product with a selectivity of 92 % for mono-addition and 8 % to di-addition product over a period of 1 h. On the contrary reaction of benzylamine with EA in the presence of clay showed high conversion of amine and excellent chemo-selectivity for mono-addition product.

Table 3.11. Influence of reaction temperature on hydroamination of EA with aniline over clay K-10 and catalyst regeneration data.

Temperature (°C)	Conversion (%)[*]	Selectivity (%)[#] (Mono-addition) [1a]	(Mono-addition) [1b]	Rate constant k_I x 10^{-4} min^{-1}
85	20.2	100	0	18.85
95	49.5	100	0	56.90
105	58.4	99.5	0.5	73.28
110	67.1	99	1	92.63
Regeneration of K-10 at 95 °C.				
Fresh catalyst	49.5	100	0	-
1st recycle	48.4	100	0	-
2nd recycle	48.9	100	0	-
3rd recycle	48	100	0	-

Reaction conditions: aniline: EA =1(molar ratio), Amount of catalyst = 0.3g (10 wt.% of total reaction mixture);* Conversion determined by GC analysis with respect to aniline, # Selectivity was determined by GC analysis. [1a] N-[2-(ethoxycarbonyl) ethyl]aniline (mono-addition product) , [1b] N,N-bis[2--(ethoxycarbonyl)ethyl]aniline, Time = 2 h.

3.2.4.2.3. Optimization of reaction conditions

The dependence of reaction temperature on conversion and product selectivities was studied in the range of 85-110 °C as a function of time and the results are presented in Figure 3.9. (a-c). The results show that the performance of the catalyst increases substantially with increasing reaction temperature. Figure 3.9. (a-c) and Table 3.11. illustrates that with increase in temperature, aniline conversion increases linearly with time up to 95 % (constant k_1 increased from 18.85 x 10^{-4} min^{-1} at 85 °C to 92.63 x 10^{-4} min^{-1} at 110 °C). The rate constants calculated at different temperatures are presented in Table 3.11.. It is seen that k_1 increases with increase in temperature.

It is seen that at reaction temperature upto 95 °C, the selectivity for product 1a is 100% for a period of 6 h (Fig. 3.9. (b)). After 6h very small amount of product 1b starts forming and its selectivity increases upto 2% over a period of 12 h (Fig. 3.9. (c)). However, it is significant to note that on increasing the reaction temperature to

110 °C product 1b starts forming after 50 min. and the selectivity for product 1b increased and that of product 1a decreased with time (Fig. 3.9. (b-c)). It is noteworthy that the reaction is feasible even at 85 °C and the selectivity towards linear mono addition product is significantly better at lower temperature (Fig. 3.9. (b)).
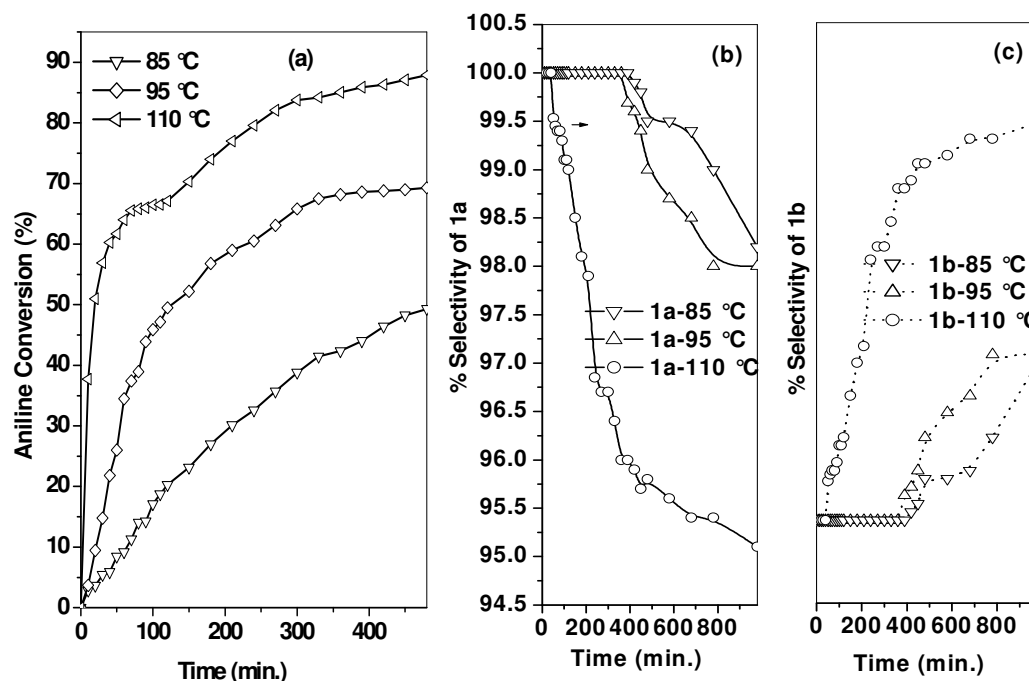
Figure 3.9. Dependence of reaction temperature on the conversion of aniline and selectivity of mono addition product (1a) and di-addition product (1b) as a function of time in the hydroamination of EA over K-10.

The kinetic investigations results revealed a first order reaction rate dependence with respect to amine concentrations. The standard equations for a first-order series reaction $C_A/C_{Ao} = e^{-K_1 t}$ has been used for the determination of rate constant, where C_A and C_{Ao} are the concentration of aniline at initial time and at time t, respectively. From the plot of ln(rate) versus 1000/T, by applying the initial rate approach model, the activation energy was evaluated to be $E_a = 24$ kcal mol^{-1}.

91

Table 3.12. Influence of stoichiometric ratio of aniline with EA for hydroamination over K-10 at a reaction temperature of 95 °C.

Aniline to EA molar ratio	Conversion (%)[*]	Selectivity (%)[#]		Rate constant k_1 x 10^{-4} min^{-1}
		(Mono-addition) [1a]	(Di-addition) [1b]	
1 : 1	49.5	100	0	56.90
1 : 2	53.58	99.6	0.35	64.17
1 : 4	67.1	98.36	1.5	92.77

Reaction conditions: Amount of catalyst = 0.3 g (10 wt.% of total reaction mixture, Time = 2h., [*] Conversion determined by GC analysis with respect to aniline, [#] Selectivity was determined by GC analysis. [1a] N-[2-(ethoxycarbonyl) ethyl]aniline (mono-addition product) , [1b] N,N-bis[2--(ethoxycarbonyl)ethyl]aniline,

The effect of catalyst weight % on the conversion and product selectivity was also studied between 5-10 wt.% of the total reaction mixture over clay K-10 at a reaction temperature of 95 °C and with aniline to EA molar ratio of 1. An increase in catalyst loading from 5-10 wt.% is associated with a decrease in reaction time from 120 min to 70 min for a conversion of 50 % and a decrease in selectivity for 1a from 100 % to 96 % over a period of 2 h.

The effect of the stoichiometric ratios of aniline with EA on conversion and product selectivity was also studied over clay K-10 catalyst at a reaction temperature of 95 °C. The molar ratio of aniline with EA was varied in the range of 1 – 4 and the product distribution at various aniline to EA ratios is shown in Table 3.12. It was found that both activity and selectivity were influenced drastically by the change of reactant molar ratio. The results show that the conversion of aniline increases from 49.5 to 67.1 % on varying the molar ratio from 1 to 4 over a period of 2h. It can also be seen from Table 3.12 that the selectivity for 1b increases and that of 1a reduces with increasing EA concentration. Availability of excess of EA leads to the addition of another molecule of EA with 1a to form double addition product.

Under the optimized condition, the hydroamination of EA with aniline was carried out with K-10, 0.3 g (10 wt.% of total reaction mixture), aniline/EA molar ratio 1 at 95 °C for 12 h to see the effect aniline conversion and products selectivity as

a function of time (Fig. 3.9.). With increase in time, conversion of aniline increases to a maximum of 85% after 12 h with selectivity for 1a = 98 %, and 1b = 2 %.

3.2.4.2.4. Catalyst recyclibility study

Recycling of the clay K-10 was attempted at 95 °C by separating the catalysts by filtration followed by washing with toluene and refluxing in methanol (methanol has great affinity to clay surface, hence used for regeneration of the catalyst) for 2h to remove products remaining from the first run and drying in oven at 100 °C for 15 h in air. The catalyst was used for hydroamination of EA with aniline under selected reaction conditions. The extent of catalyst regeneration was studied for three consecutive runs by refluxing the catalysts with methanol each time followed by drying. Same procedure is repeated for second cycle and the data on the conversion of amine are presented in Table 3.11. From the result it is concluded that there is no appreciable loss in the catalytic activity and product selectivities in the two cycles and catalyst could be reused. The conversions of the amine were 48.4%, 48.9% and 48% for the first, second and third reuse after methanol wash, respectively with 100 % selectivity for mono-addition product. From the result it is concluded that there is no appreciable loss in the catalytic activity and product selectivities in the four cycles and catalyst could be reused.

In order to check the leaching of any active sites into the reaction mixture, the reaction was carried out for 2 h under selected reaction conditions using fresh K-10 clay activated at 100 °C. The reaction was stopped and catalyst was separated by filtration and then the filtrate was stirred for 1 h under same reaction conditions. It was found that in the absence of the catalyst, there was no further increase in the conversion of amine, which indicated the absence of leaching of any acid into the reaction mixture. This observation confirmed that the reaction was catalyzed heterogeneously.

3.2.4.2.5. Proposed reaction mechanism

The data obtained from the kinetic experiments and literature suggests the mechanism shown in Scheme 3.5. for the intermolecular hydroamination of EA with anilines using clay as catalyst. The carbonyl group of EA combines with the electron deficient centers in the acidic clay (either Brönsted or Lewis acid sites), which makes β-carbon electron deficient, which attacks the electron rich center in the amine (Scheme 3.5. step I and II). This is followed by 1,3-proton shift in step III with the release of *anti*-Markovnikov product in step IV to regenerate the acidic clay.
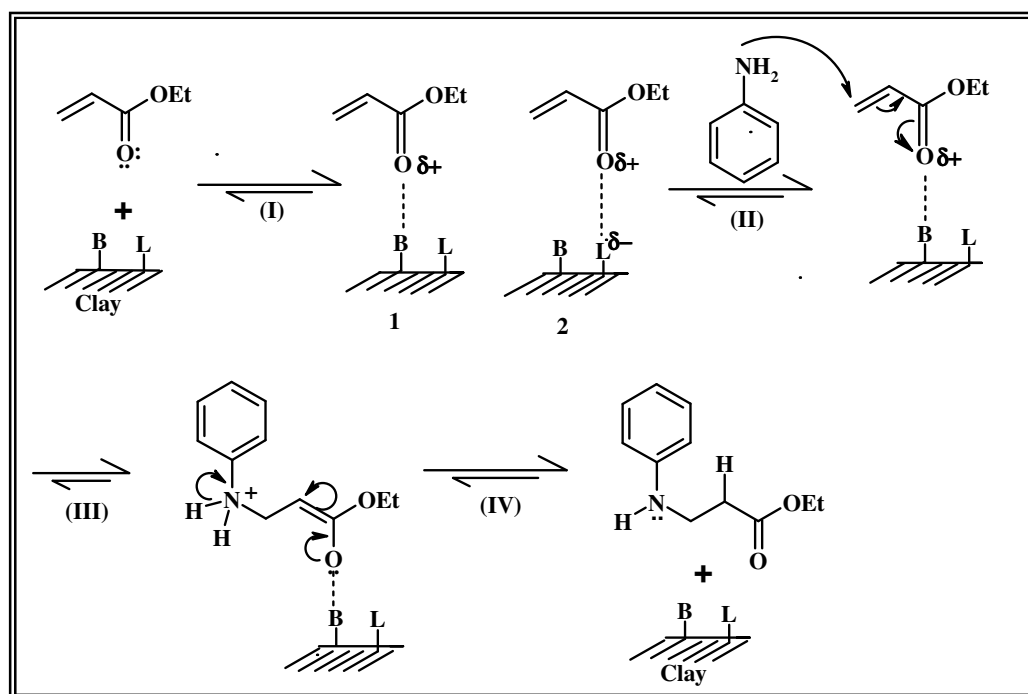
Scheme 3.5. Proposed reaction mechanism for the hydroamination of EA with aniline by clay.

3.3. References

1.   R. S. Varma, Tetrahedron 58 (2002) 1235.

2.   J. H. Clark, Catalysis Of Organic Reactions by Supported Inorganic Reagents, VCH Publishers, New York, 1994.

3.   J. A. Ballantine, J. H. Purnell and J. M. Thomas, J. Mol. Catal. A: Chemical 27 (1984) 157.

4.   L. Jankovic and P. Komadel, J. Catal. 218 (2003) 227.

5.   B.M. Choudary, M. Sateesh, M.L. Kantam, K.V.R. Prasad, Appl. Catal. A: Gen.171 (1998) 155.

6.   K. Kaneda, 7 (2007) Synlett 999.

7.   J. Barluenga, F. Aznar, Synthesis (1975) 704.

8.   J. Barluenga, F. Aznar, Synthesis (1977) 195.

9.   J. Barluenga, F. Aznar, R. Liz, R. Rodes, J. Chem. Soc., Perkin Trans. 1 (1980) 2732.

10   D. Tzalis, C. Koradin, P. Knochel, Tetrahedron Lett. 40 (1999) 6193.

11.   P. Walsh, A.M. Baranger, R.G. Bergman, J. Am. Chem. Soc. 114 (1992) 1708.

12.   Y. Li, T. J. Marks, Organometallics 15 (1996) 3770.

13.   A. Haskel, T. Straub, M.S. Eisen, Organometallics 15 (1996) 3773.

14.   M.S. Eisen, T. Straub, A. Haskel, J. Alloys Compd. 1998, 116.

15.   T. Straub, A. Haskel, T.G. Neyroud, M. Kapon, M. Botoshansky, M.S. Eisen, Organometallics 20 (2001) 5017.

16.   I. Bytschkov, S. Doye, Eur. J. Org. Chem. (2003) 935.

17.   S. Doye, Synlett. (2004) 1653.

18.   A. Heutling, F. Pohlki, I. Bytschkov, S. Doye, Angew. Chem. Int. Ed. 44 (2005) 2.

19.   Y. Uchimaru, Chem. Commun. (1999) 1133.

20.   M. Tokunaga, M. Eckert, Y. Wakatsuki, Angew. Chem. Int. Ed. 38 (1999) 3222.

21.   M. Tokunaga, M. Ota, M. Haga, Y. Wakatsuki, Tetrahedron Lett. 42 (2001) 3865.

22.   D.P. Klein, A. Ellern, R. Angelici, J. Organometallics 23 (2004) 5662.

23.   C.G. Hartung, A. Tillack, H. Trauthwein, M. Beller, J. Org. Chem. 66 (2001) 6339.

24. M. Beller, C. Breindl, M. Eichberger, C.G. Hartung, J. Seayad, O.R. Thiel, A. Tillack, H. Trauthwein, Synlett 10 (2002) 1579.

25. L.D. Field, B.A. Messerle, K.Q. Vuong, P. Turner, Organometallics 24 (2005) 4241.

26. I. Kadota, A. Shibuya, L. M. Lutete, Y. Yamamoto, J. Org. Chem. 64 (1999) 4570.

27. T. Shimada, Y. Yamamoto, J. Am. Chem. Soc. 124 (2002) 12670.

28. E. Mizushima, T. Hayashi, M. Tanaka, Org. Lett. 5 (2003) 3349.

29. J. Penzien, T.E.Muller, J.A.Lercher, Chem.Commun. (2000) 1753.

30. J.Penzien, C. Haeβner, A.Jentys, K. Köhler, T.E.Müller, J.Lercher, J.Catal. 221 (2004) 302.

31. J. Penzien, R.Q.Su, T.E.Muller J. Mol. Catal A: Chemical 182 (2002) 489.

32. M.K. Richmond, S.L. Scott, H. Alper, J. Am. Chem. Soc. 123 (2001) 10521.

33. L. W. Xu, J-W. Li, C-G. Xia, S-L. Zhou, X-X. Hu, Synlett 15 (2003) 2425.

34. J. S. Yadav, B. V. S. Reddy, A. K. Basak, A. V. Narsaiah, Chem. Lett. 32 (2003) 988.

35   M. Kawatsura, J. F. Hartwig, Organometallics 20 (2001) 1960.

36. N. S. Shaikh, V. H. Deshpande, A. V. Bedekar Tetrahedron 57 (2001) 9045.

37. L. Fandini, A. Togni Chem. Commun. (2003) 30.

38. J. Horniakova, K. Komura, H. Osaki, Y. Kubota and Y. Sugi, Catal. Lett. 102 (2005) 191.

39. O. Löber, M. Kawatsura and J. F. Hartwig, J. Am. Chem. Soc 123 (2001) 4366.

40. O. Jemenez, T. E. Müller, W. Schwieger, and J. A. Lercher, in: Proceedings of the 14th international Zeolite Conference (25-30 April, 2004, Cape Town, South Africa, 2788).

CHAPTER IV

4.1. Chemoselective synthesis of β-amino acid derivatives by hydroamination of activated olefins using AlSBA-15 catalyst

4.1.1. Introduction

Hydroamination of olefins with amines is an industrially very important reaction which converts readily available olefins into value added products such as alkylated amines, β-amino acid derivatives and N-heterocycles [1]. There are several reports on hydroamination of unactivated alkenes especially catalyzed by transition metal complexes in homogeneous conditions [2-5]. On the other hand, hydroamination of activated olefins (acrylate derivatives) is a Michael type addition reaction, which is a simple approach to synthesize amino acid derivatives. These amino acid derivatives have a wide variety of applications *viz.* in the synthesis of peptide analogues, precursor for amino alcohols, optically active amino acids, lactums and diamines [6, 7]. In earlier studies, Brönsted and Lewis acids such as H_2SO_4, HBF_4 and $FeCl_3$ have been used for this reaction [8, 9]. Recently hydroamination of acrylates with amines has been reported with copper and bismuth salts [10,11], and complexes of Ni(II) and Pd(II) [12,13]. However, homogeneous methods suffer from tedious work-up procedures, low catalyst recyclability and above all the environmental problems. Surprisingly there are very few reports available on the use of heterogeneous catalysts for hydroamination of activated olefins. Zeolite beta and clays have been reported so far for this reaction [14-17]. Zeolites cannot be used for larger substrates because of their smaller pore sizes where as clays have low thermal stability which affects the catalyst regeneration. Mesoporous materials such as MCM-41 and SBA-15 have advantages over zeolites for their larger pore size and higher surface area [18]. The isomorphous substitution of aluminium into the mesoporous framework of MCM-41 and SBA-15 induces the Brönsted and Lewis acidity [19]. AlSBA-15 has a larger pore diameter, thicker pore walls, and higher hydrothermal stability compared to MCM-41. Hence AlSBA-15 has been used for hydroamination of activated olefins and the results are compared with that of AlMCM-41.

To create Brönsted and Lewis acidic sites in SBA-15, much effort has been made on the incorporation of heteroatom, such as Al, in the framework of mesoporous silica by post grafting or doping (one-pot synthesis). However, it is very difficult to introduce the metals directly into SBA-15 due to the easy dissociation of metal-O–Si bonds under strong acidic conditions. Only a few studies on the direct synthesis of Al-SBA-15 have been reported so far [20-25]. Thus, the post-synthesis method for the alumination of mesoporous silicas, which are obtained by ion exchange, becomes a useful alternative. The researchers have demonstrated that Al can be effectively incorporated into siliceous MCM-41 and MCM-48 materials via various post-synthesis procedures [26-28]. The authors claimed that the materials produced via the post-synthesis method have structural integrity, acidity, and catalytic activity similar to those of materials prepared by *in-situ* method. However, as of present, very few post synthesis alumination methods for SBA-15 have been reported [29-33]. The present section deals with the synthesis, characterization and applications of AlSBA-15 in the synthesis of β-amino acid derivatives by the hydroamination of activated olefins with amines.

4.1.2. Experimental

4.1.2.1 Materials

Amines, solvents and metal acetates were purchased from Merck India Ltd. Activated olefins and montmorillonite K-10 were procured from Aldrich, USA. Zeolite H-beta was obtained from CPP, NCL, Pune. All the chemicals were of research grade and were used after drying following standard procedures.

4.1.2.2. Catalyst preparation

Syntheses of SBA-15, AlSBA-15 and AlMCM-41 were discussed in Chapter II.

Synthesis of Cu^{2+} and Zn^{2+} exchanged AlSBA-15: A known amount of 1 g of AlSBA-15 (Si/Al=10) was stirred with 0.05 M cupric acetate solution prepared in water (20 ml) at 80 °C for 6 h and then cooled to room temperature and the exchanged CuAlSBA-15 (10) was filtered, washed repeatedly with distilled water and dried in air. The above procedure was repeated to ensure maximum copper exchange. Then it was dried at 120 °C for 12 h and calcined (RT-500 °C, 4 °C min^{-1}; for 4 h at 500 °C). Similar procedure was followed for the preparation of ZnAlSBA-15 (10). These materials are designated as AlSBA-15-(X), MAlSBA-15 (X), where M is the

exchanged metal ion and X is the Si/Al ratio of the chemical stoichiometric composition taken in the post synthesis mixtures.
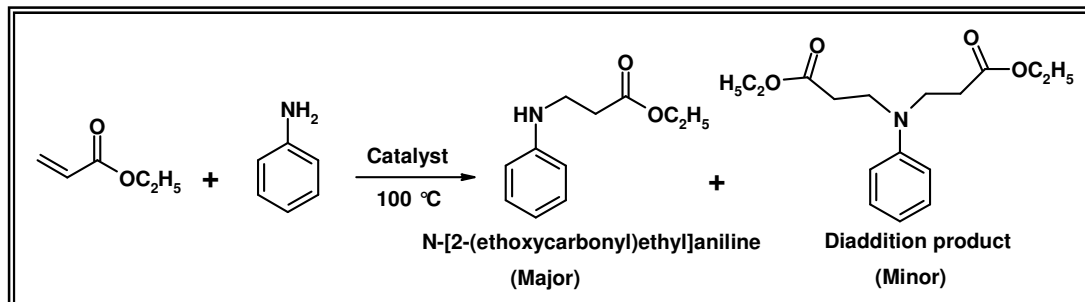
Scheme 4.1. Hydroamination of ethyl acrylate with aniline

4.1.2.3. Catalytic activity measurements

Experiments were carried out in a two-necked round bottom flask fitted with a water condenser connected to a balloon filled with N_2 and kept in a thermostatic oil bath at a temperature of 100 °C at atmospheric pressure. In a typical reaction, ethyl acrylate (hereafter EA) (1.04 g), aniline (0.96 g), toluene (3 ml) and catalyst (0.05 g, activated at 500 °C prior to reaction) were heated in the flask. Samples were withdrawn at regular intervals of time and analyzed by gas chromatography (Shimadzu 14B) equipped with a cross linked 5% diphenyl-95% dimethylpolysiloxane capillary column (30m) and a flame ionization detector. The identity of products were confirmed by GCMS (Shimadzu GCMS QP 5000) equipped with an identical column and a mass selective detector. Conversions were calculated with respect to weight percentage of ethyl acrylate. The product was separated by column chromatography using neutral alumina as stationary phase and petroleum ether/ethyl acetate, 95: 5 as eluent. The single product was characterized by NMR, FTIR and GCMS analysis which confirmed the product to be N-[2-(ethoxycarbonyl)ethyl]aniline. Yield: 95%, ^{1}HNMR (200MHz, CDCl$_3$): 7.21-7.06 (m, 2H), 6.68-6.53 (m, 3H), 5.21 (1H), 4.13-4.01 (m, J=3.72 Hz, 2H), 3.41-3.34 (t, J= 6.45 Hz, 2H), 2.57-2.47 (q, J= 6.32 Hz, 2H), 1.22-1.14 (t, J= 7.07Hz, 3H), FT-IR (neat, cm^{-1}) υ 3409, 2985, 1731, 1604, 1504, 1373, 1319, 1249, 1176, 1099, 1029, 1864, 748, 694. GCMS: *m/z* (relative intensity): 193 (11.83), 118 (2.55), 106 (100), 93 (2.46), 77 (11.26), 65 (6.57), 51 (7.79).

4.1.3. Results and discussion

4.1.3.1. Characterization of the catalysts

4.1.3.1.1. X-ray diffraction

XRD patterns of calcined AlSBA-15 catalysts with different Si /Al ratios (shown in Fig. 4.1, (a), (b), (c) and (d)) consist of three well-resolved peaks in the 2θ range of 0.8 to 1.8 correspond to the (100), (110), (200) reflections which are associated with p6mm hexagonal symmetry in the materials. Isomorphous substitution of Al into the framework of siliceous SBA-15 by the post synthesis method did not show any changes in the XRD pattern implying that the hexagonal mesoporous structure is retained after modification. It is evident from the XRD profile of the samples that they do not contain any other phase or amorphous matter. Also XRD pattern of AlMCM-41 (15) (Fig. 4.1 (e)) shows the appearance of the (100), (110) and (200) reflections in lower 2θ region which demonstrates the well ordered nature of phases in the AlMCM-41.

4.1.3.1.2. N_2 sorption measurements

Textural properties such as specific surface area, specific pore volume, and mesopore size distribution are typically obtained from low-temperature (-196 °C) nitrogen adsorption isotherms. The nitrogen adsorption-desorption isotherms of AlSBA-15 (10) is shown in Fig. 4.2. and the textural properties of all the samples are presented in Table 1. All isotherms were of type IV, as defined by IUPAC and exhibited a H1-type broad hysteresis loop, which was typical of large-pore mesoporous solids. As the relative pressure increases ($p/p_o > 0.6$), all isotherms exhibit a sharp step characteristic of capillary condensation of nitrogen within uniform mesopores, where the p/p_o position of the inflection point is correlated to the diameter of the mesopore.

Table 4.1. Structural characteristics and acidity of different catalysts and their catalytic activities.

SL No	Catalyst	Si/Al (XRF)	Surface area BET (m^2g^{-1})	Pore volume (cm^3/g)	Average pore diameter (Å)	Total acidity (mmol NH_3/g)	EA[a] convn wt.%	Mono addition select-ivity (%)	TOF[b]
1	SBA-15	∞	745	1.03	66.6	0.08	05	100	-
2	AlSBA-15 (10)	17	685	1.31	76.7	0.23	77	100	46
3	AlSBA-15 (20)	26	730	1.16	66.3	0.20	60	100	45
4	AlSBA-15 (30)	36	720	0.99	63.5	0.16	41	100	38
5	AlSBA-15 (40)	43	620	0.98	63.4	0.12	33	100	37
6	AlMCM-41 (15)	15	962	0.80	33.6	0.26	82	100	43
7	H-beta	15	530	0.28	-	-	41	99	18
8	Clay	-	230	-	-	-	39	99	-
9	CuAlSBA-15(10)	20	664	1.09	67.9	-	50	100	32
10	ZnAlSBA-15 (10)	21	671	1.12	69.1	-	53	100	33

[a] Conditions: temperature = 100 °C, aniline to EA mole ratio = 1, catalyst wt. = 0.05 g, total reactants wt. = 2 g, Toluene = 3 ml, time = 6 h.

[b] TOF = moles of EA converted per mole Al per hour.
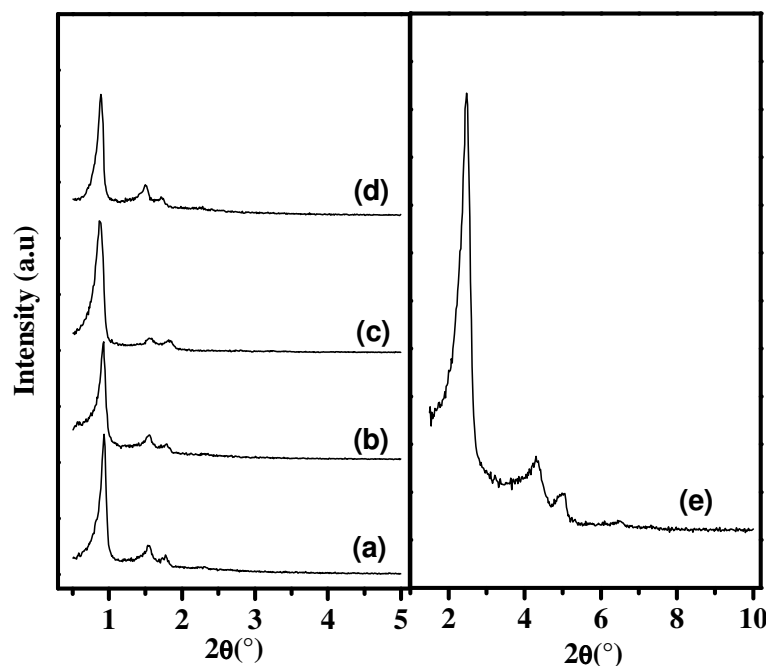
Fig. 4.1. Low angle XRD patterns of (a) AlSBA-15 (10), (b) AlSBA-15 (20), (c) AlSBA-15 (30), (d) AlSBA-15 (40), (e) AlMCM-41.

The pore size distribution was calculated from the Kelvin equation and is presented as a BJH plot (inset picture, Fig. 4.2.). It showed a narrow pore size distribution with average mesopore size of 77 Å and a high surface area ABJH of 685 m^2/g. The overall N_2 adsorption amounts decreased depending on the aluminum loading though no particular trend was observed.

Low alumination of SBA-15 did not affect the original pore structure of the parent SBA-15 while the surface areas slightly decreased with increase in aluminium loadings (Table 4.1.). AlMCM-41 (15) had a higher surface area but lower average pore diameter than AlSBA-15 (10) (962 vs 685 m^2/g and 33.6 vs 77 Å, respectively). Surface areas of H-beta (480 m^2/g) and montmorillonite K-10 (207 m^2/g) are low compared to AlSBA-15 catalysts.

102
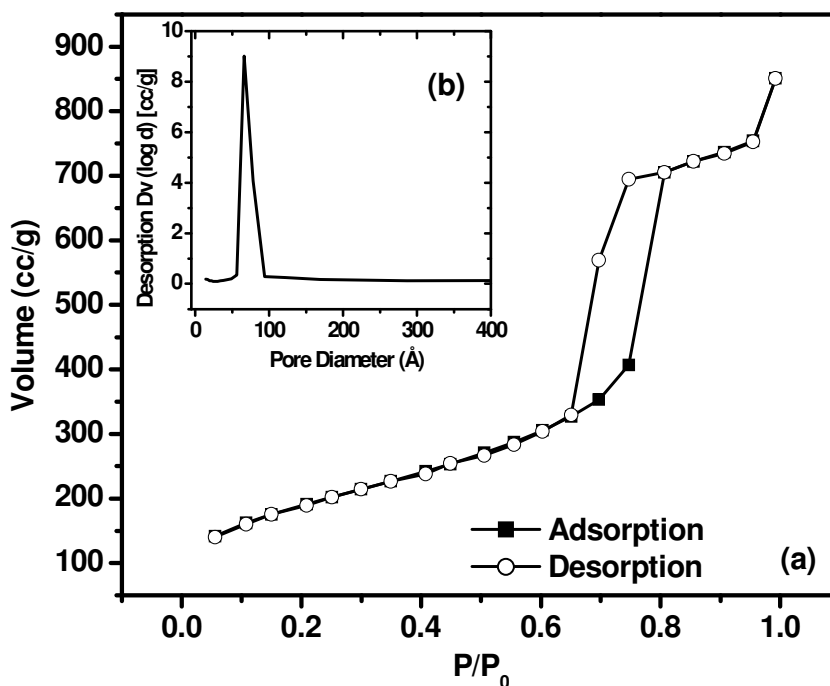
Fig. 4.2. N_2 adsorption and desorption isotherm (a) AlSBA-15 (10), (b) Inset picture: Pore size distribution of. AlSBA-15 (10).

4.1.3.1.3. Microscopic analysis

SEM images of AlSBA-15 with different magnifications (2000 and 7500) shown in Fig. 4.3.(A). The photos reveal that the of rope like micromorphology remained the same even after the modification of SBA-15 with post synthesis Al incorporation.

TEM measurements were carried out to study the morphology of AlSBA-15 (10) (Fig. 4.3. (B)). TEM images of these catalysts show the retention of the periodic structure of parent SBA-15 precursor. It indicates that hexagonally arranged mesopores of SBA-15 are retained after modification with aluminium.
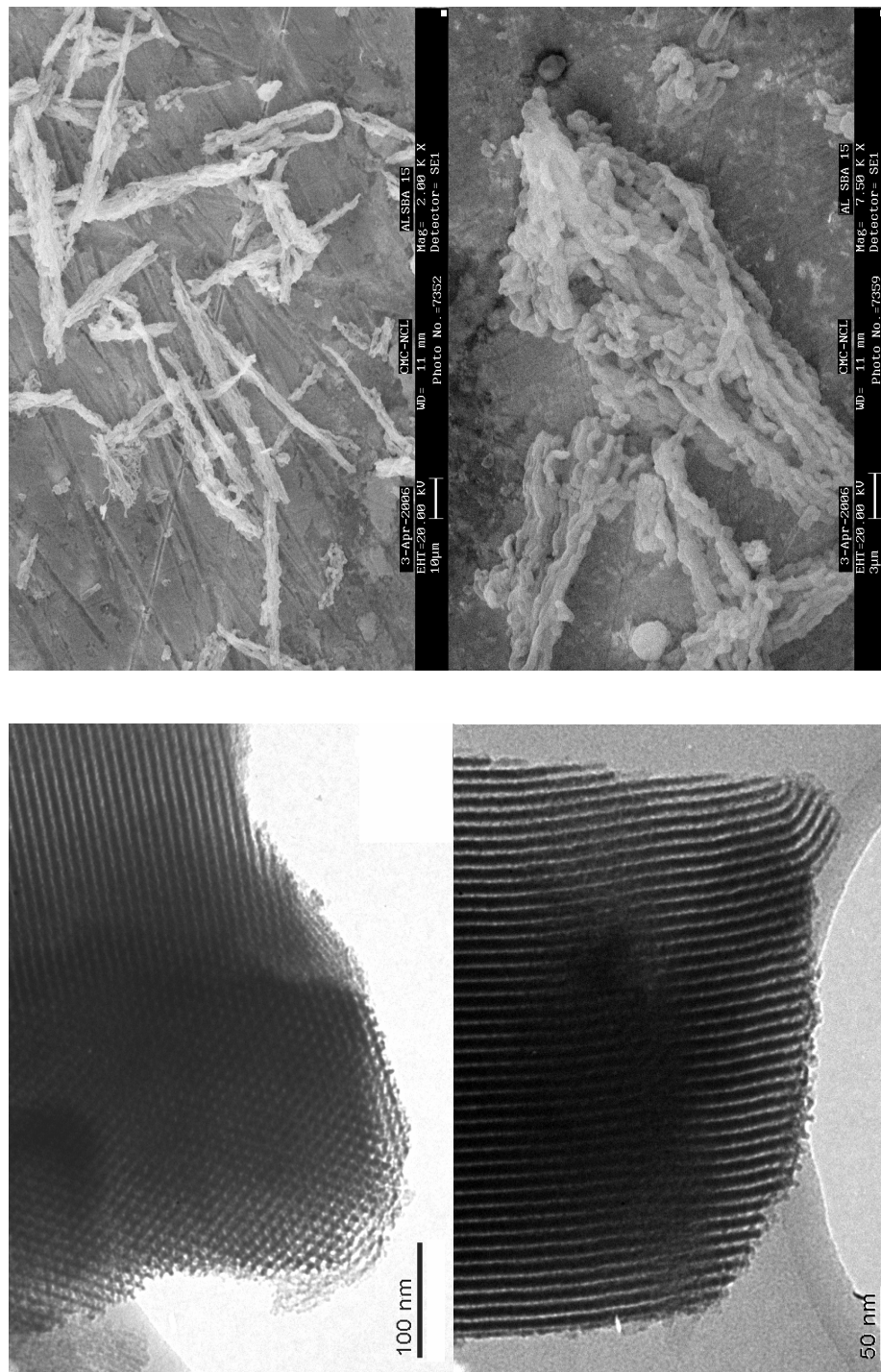
(B) SEM photograph of AlSBA-15 (10).

Fig. 4.3. (A) TEM photographs of AlSBA-15 (10)

4.1.3.1.4. Solid state NMR measurements

Solid-state ^{27}Al MAS NMR was used to determine the local environment of aluminium in the AlSBA-15 samples. The spectra of AlSBA-15 (10) (Fig. 4.4. (ii) (a)) and AlSBA-15 (30) (Fig. 4.4. (ii) (b)) samples show that the majority of Al atoms are incorporated into the framework of SBA-15 (tetrahedrally coordinated, 53 ppm) in which Al is covalently bound to four Si atoms via oxygen bridges. The peak at 0 ppm is attributed to distorted or octahedrally coordinated aluminium species in extra-framework positions. In addition, low intensity signals were observed around 30 ppm which indicated the presence of distorted tetrahedral or five coordinated aluminum in SBA-15 [34].
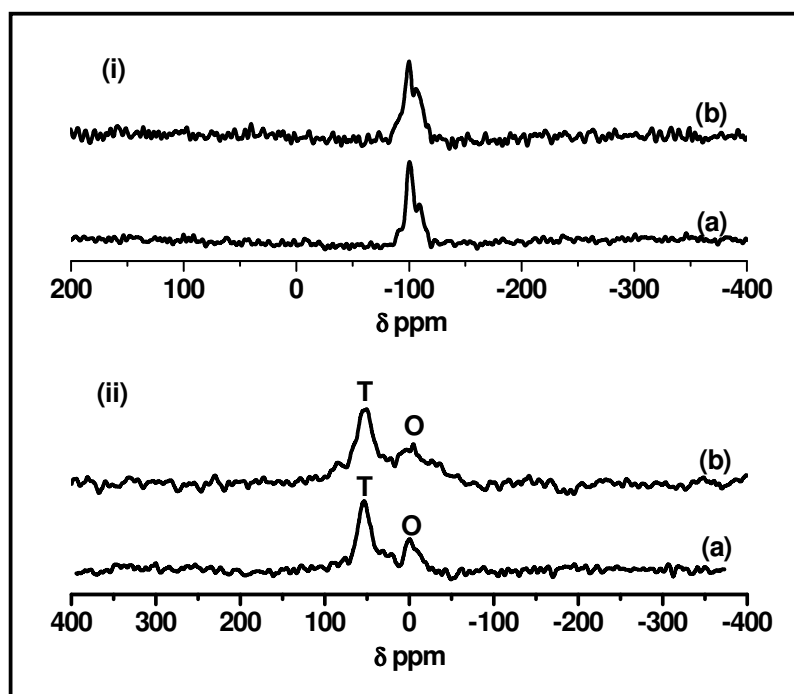
Fig. 4.4. (i) ^{29}Si MAS NMR profile of (a) SBA-15, (b) AlSBA-15 (10).
(ii) ^{27}Al MAS NMR profile of (a) AlSBA-15 (10), (b) AlSBA-15 (30), (T = tetrahedral Al sites and O = octahedral Al sites.

^{29}Si MAS NMR spectra (Fig. 4.4 (i)) of SBA-15 (a) and AlSBA-15 (b) the samples contain a broad signal at -100 ppm and some shoulders at -90, -107, -110 ppm. The main signal at -100 ppm is due to $Si(OSi)_3OH$ species (Q_3), while the shoulders at -90, -107 and -110 ppm are attributed to $Si(OSi)_2(OH)_2$ (Q_2), Si(3Si,1Al) and $Si(OSi)_4$ (Q_4) structural units respectively as reported Kolodziejski et al [35]. There are no significant differences between ^{29}Si MAS NMR spectra of AlSBA-15 and SBA15. Moreover, the broadness of the ^{29}Si signals has been attributed to the large distribution of the T–O–T angle.
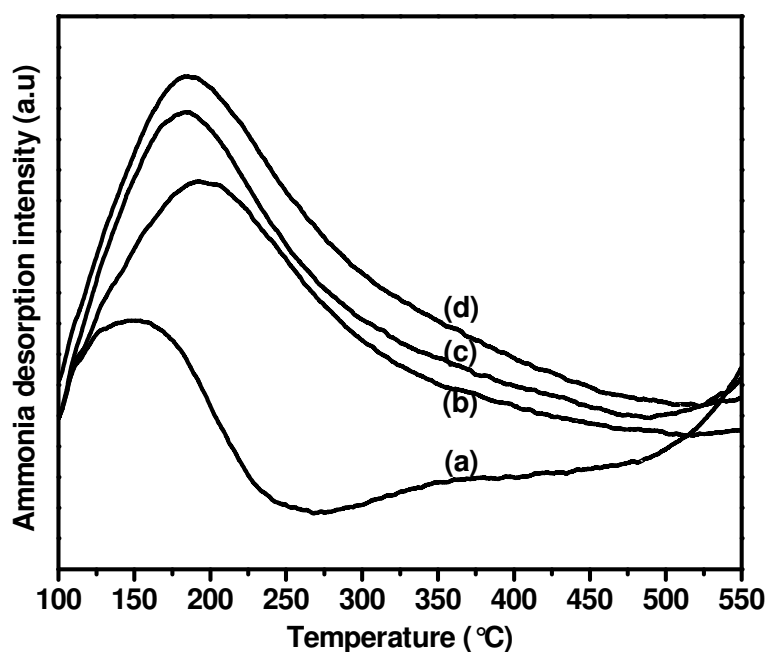
Fig. 4.5. NH_3-TPD profile of (a) SBA-15, (b) AlSBA-15 (30), (c) AlSBA-15 (20), (d) AlSBA-15 (10).

4.1.3.1.5. Acidity measurements by NH_3-TPD

The acidities of the AlSBA-15 and SBA-15 samples were measured by NH_3-TPD method and TPD profiles are depicted in Fig. 4.5. The total acidity data of SBA-15 and AlSBA-15 with different Si/Al expressed in mmol/g of desorbed ammonia are listed in Table 4.1. Comparison of the TPD curves of SBA-15 with that of AlSBA-15 showed a dramatic increase in acidity and acid strength after alumination. There is only one asymmetric broad peak on the TPD profiles of the AlSBA-15 samples. Total acidity increased with decrease in Si/Al ratio. This is due to the increase in number of

106

acid sites on AlSBA-15 with a decrease in Si/Al ratio. Highest acidity was found to be 0.23 mmol/g for AlSBA-15 with high Al content (Si/Al = 17). It is to be noted that pure mesoporous silica is acidic in nature though the acidity is low compared to AlSBA-15. SBA-15 showed total acidity of 0.08mmol/g of NH_3. These experiments clearly showed that acid sites were formed after alumination on the surface of the solid.

4.1.3.2. Catalytic results

Intermolecular hydroamination of EA with aniline was carried out using AlSBA-15 with different Si/Al and results are depicted in Table 4.1. It is seen that AlSBA-15 (10) showed highest activity with 77% EA conversion and the others followed as AlSBA-15 (20) (60%), AlSBA-15 (30) (41%) and AlSBA-15 (40) (33%) after 6 h of reaction. The results indicate that the conversion increases with decrease in Si/Al ratios i.e. increase in acidity. AlMCM-41 (Si/Al = 15) gave slightly more conversion compared to AlSBA-15 (10) (Si/Al = 17) but lower TOF (43) (expressed as moles of EA converted per mole Al per hour). The activities of well known heterogeneous catalysts such as H-beta and montmorillonite K-10 were compared with mesoporous solid acids. Interestingly highly acidic H-beta was only half as active as AlSBA-15 (conversion = 41% and TOF = 18). Lower activity of H-beta can be attributed to its smaller pore size which restricts the mobility of the molecules. Previous reports on Zn-beta and CuAlSBA-15 catalysts showed that Lewis acidic Cu^{2+} and Zn^{2+} catalyze hydroamination of alkynes by aromatic amines [36]. So, we compared the activities of ZnAlSBA-15 and CuAlSBA-15 catalysts with unexchanged AlSBA-15 catalysts. Interestingly, there is a decrease in EA conversion after Cu and Zn exchange with AlSBA-15. The result clearly shows that the Brönsted acidity in AlSBA-15 catalyzes the hydroamination of activated olefins. It is also to be noted that after metal exchange, the catalyst still showed considerable activity. Hence, it is apparent that lewis acidic sites in the catalyst also act as active centers in hydroamination reaction of activated olefins.
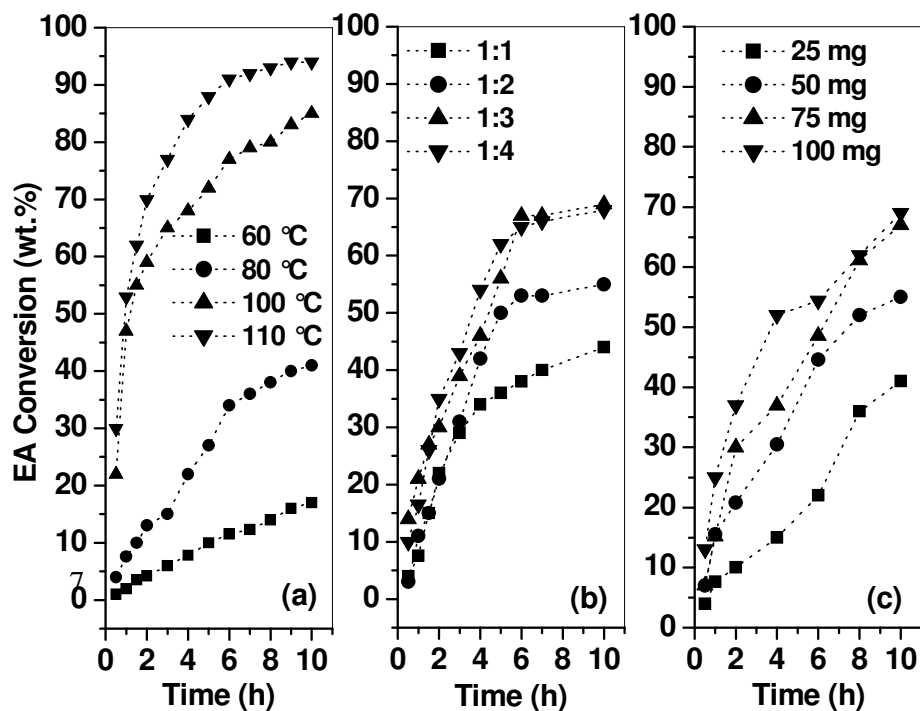
Fig. 4.6. Effect of reaction conditions (a) Effect of reaction temperature. Conditions: catalyst = AlSBA-15 (10), aniline to EA mole ratio = 1, catalyst wt. = 0.05 g, total reactants wt. = 2 g, toluene = 3 ml, (b) Effect of aniline to EA mole ratio. Conditions: catalyst = AlSBA-15 (10), temperature = 80 °C, catalyst wt. = 0.05 g, total reactants wt. = 2 g, toluene = 3 ml (c) Effect of catalyst concentration. Conditions: catalyst = AlSBA-15 (10), temperature = 80 °C, aniline to EA mole ratio = 1, total reactants wt. = 2 g, toluene = 3 ml.

Hydroamination of EA with aniline was studied by varying the temperatures (60-110 °C), keeping constant catalyst 0.05 g (2% of the total reactant weight) and aniline to EA mole ratio as 1. Conversion of EA as a function of time is shown in Fig. 4.6(a). The *anti*-Markovnikov addition product N-[2 (ethoxycarbonyl)ethyl]aniline formed with 100% selectivity. The results show that the activity (conversion of EA) of the catalyst increases substantially with increasing reaction temperature. At 60 °C, the conversion was only 17%, which increased to 94% at 110 °C in 10 h of reaction. Following the initial rate approach, the graph of ln(rate) versus 1/T was plotted, which gave a straight line and the activation energy calculated from the slope was found to be 20 kcal /mol.

The reaction was also carried out with aniline to EA molar ratios ranging from 1 to 4 keeping catalyst wt. (0.05 g) and temperature (80 °C) constant and the results

are shown in Fig. 4.6 (b). The results show that the conversion of EA increased from 36 to 62 % on varying the molar ratio from 1 to 4 over a period of 5 h. However, the change in the mole ratio did not affect the selectivity. The *anti*-Markovnikov addition product formed with 100% selectivity. But excess of EA in the reaction decreases the selectivity of mono-addition product because it reacts further with another molecule of EA to form di-addition product.

The effect of catalyst concentration on EA conversion was studied at 80 °C with aniline/ EA mole ratio of 1 (Fig. 4.6. (c)). It shows that as the catalyst concentration increased, the conversion of EA increased as expected. There was linear increase in conversion up to 8 h and the reaction is slowed down with marginal increase in the range of 8–10 h. At optimized reaction conditions; 100 °C, aniline to EA molar ratio of 2, catalyst weight 0.1 g and total reactant weight 2 g and 3 ml of toluene as a solvent, the conversion of EA was found to be 99% with 98 % selectivity for mono-addition product after 15 h reaction.

In order to check the leaching of framework Al into the reaction mixture during the course of the reaction, reaction was carried out for 2 h under selected reaction conditions. The reaction was then stopped and catalyst was separated by filtration of hot reaction mixture and same reaction mixture was stirred further for 10 h. It was found that in the absence of the catalyst, there was no further increase in the conversion of EA, which indicated the absence of leaching of Al. The above study ensured that the reaction was catalyzed purely by a heterogeneous catalyst.

Table 4.2. Hydroamination of different activated olefins and amines catalyzed by AlSBA-15 (10).

Aromatic Amine	Activated olefin	Time (h)	Yield (%)	anti-Markovnikov product selectivity (%)	
				Mono-addition	Di-addition
Aniline	Ethyl acrylate	4	75	99	1
		10	93	98	2
4-Bromoaniline	Ethyl acrylate	4	40	100	0
		10	68	98	2
p-Anisidine	Ethyl acrylate	4	65	99	1
		10	91	97	3
2,4-Xylidene	Ethyl acrylate	4	59	99	1
		10	85	98	2
o-Nitroaniline	Ethyl acrylate	20	NR	-	-
p-Ethylaniline	Ethyl acrylate	4	82	100	0
		10	95	99	1
N-Methylaniline	Ethyl acrylate	4	50	100	0
		10	71	99	1
1-Naphthylamine	Ethyl acrylate	4	40	100	0
		10	65	100	0
Cyclohexylamine	Ethyl acrylate	2	95	100	0
Aniline	Methyl acrylate	10	65	100	0
Aniline	Acrylonitrile	10	21	100	0
Aniline	Acrylic acid	10	40	100	0

Reaction conditions: temperature = 100 °C, amine: activated olefin =1 (molar ratio), catalyst wt. = 0.1 g, total reactants wt. = 2 g, yield of mono addition product was determined by GC analysis, NR = No reaction.

The recyclability of AlSBA-15 (10) catalyst was tested in the hydroamination of EA with aniline by conducting five runs (~85% conversion after 10h) using selected reaction conditions. After each run, the catalyst was repeatedly washed with toluene, dried at 120 °C for 2 h and calcined at 500 °C in air for 2 h. It was then used in the hydroamination reaction with a fresh reaction mixture. It was found that the conversion was practically the same in all the five cycles.

To further investigate the reaction, we carried out the reaction of aniline with different α, β-ethylenic compounds like methyl acrylate, acrylonitrile, and acrylic acid with 5 wt % AlSBA-15 (10), at 100 °C and molar ratio of 1 (Table 4.2). The yield for mono-addition product was obtained in the order EA (93%) > methyl acrylate (65%) > acrylic acid (40%) > acrylo nitrile (18%) after 10 h of reaction. Since aniline is basic, it undergoes a side reaction with acrylic acid to form acrylanilide.

To explore the general applicability of the catalyst, hydroaminations of EA with different amines were carried out and the mono addition product yield after 10 h of reaction was compared (Table 4.2). The nature of substituents on the aromatic ring of aniline derivatives has considerable effect over the reactivity. The electron-donating groups at the *-ortho* and *-para* positions gave higher yields of mono addition, anti-Markovnikov products. Large molecule such as 1-naphthylamine gave a higher yield (65%), which indicates that the bulky amines can easily pass through the mesopores of AlSBA-15. The aromatic amines with electron withdrawing substituents such as 4-bromoaniline (21%) were less reactive where as *p*-nitroaniline did not undergo reaction with EA. The results showed that AlSBA-15 can also be used for hydroamination using secondary amine (N-methyl aniline, 71% yield) and aliphatic amines (cyclohexyl amine, 95% yield). These results indicate that the amine reactivity depends on their basicity. It is well known that aliphatic amines are more basic than aromatic amines where as amines with electron donating substituents are more basic than amines with electron withdrawing substituents. As the basicity of amines increased their reactivity also increased in hydroamination of activated olefins and *vice versa*.

4.2. Copper(II) ion exchanged AlSBA-15: a versatile catalyst for intermolecular hydroamination of alkynes with aromatic amines

4.2.1. Introduction

The earliest report on hydroamination of alkynes dates back to 1939, when Loritsch and Vogt used mercuric oxide and boron fluoride in stoichiometric amounts for hydroamination of alkynes with anilines [37]. Since then various approaches using homogeneous catalysts such as transition metal salts, lanthanide and actinide complexes, and transition metal complexes have been extensively studied for this seemingly simple but challenging transformation [38-44]. However, homogeneous methods suffer from their tedious work-up procedure and low catalyst recyclability. There is a need to develop efficient, sustainable, recyclable and eco-friendly solid catalysts for hydroamination reactions. Compared to homogeneous catalysts, only a handful of heterogeneous catalysts have been reported till date. Penzien et al. have developed metal exchanged zeolites for alkyne hydroamination, which favored Markovnikov addition products [36, 45-47]. But zeolite based catalysts normally show low activity towards bulkier substrates due to pore size restrictions. Pd complex immobilized on silica has been reported for intramolecular cyclization of amino-alkynes [48]. Ionic liquids supported on diatomic earth and silver-exchanged tungstophosphoric acid have also been reported for heterogeneous hydroamination of terminal alkynes [49, 50].

Mesoporous materials such as MCM-41 and SBA-15 have advantages over zeolites for their larger pore size and higher surface area. The isomorphous substitution of aluminium into the mesoporous framework of MCM-41 and SBA-15 induces the Brönsted acidity which can act as ion exchange site [19]. Mesoporous solids such as AlSBA-15 and AlMCM-41 possess ordered porous structure, and the active components tailored in their nano-ordered spaces will improve their catalytic performances. Transition metal ions can be introduced by ion-exchange method in different states and coordinations on their surfaces as well as inside the pores. Metal cations located at different ion exchange positions will have distinct stability as well as reactivity. Over the past few decades, several catalytic studies have been made using transition metal ion-exchanged porous solids and clays [51-56]. Recently, CuMCM-41 was reported for 1–butene isomerization and hydroxylation of phenol

[57, 58]. There are very few reports available in the literature on CuAlSBA-15. In one such report, aluminium has been incorporated in the framework of SiSBA-15 by post synthesis method and Cu^{2+} ions were exchanged to evaluate the ion exchange property of AlSBA-15 [29]. The present section deals with the synthesis, characterization and the applications of metal ions exchanged catalysts such as CuAlSBA-15 in the synthesis of imines from the hydroamination of alkynes with aromatic amines.

4.2.2. Experimental

4.2.2.1. Materials

Amines and solvents were purchased from Merck India Ltd; Alkynes and montmorillonite K-10 were procured from Aldrich, USA. Zeolite H-beta was obtained from CPP, NCL, Pune. All the chemicals were of research grade and were used after drying by following the standard procedures.

4.2.2.2. Catalyst preparation

Synthesis of SBA-15 and AlSBA-15 was discussed in Chapter II, section 2.2.

Synthesis of M^{n+}AlSBA-15: In a typical synthesis of CuAlSBA-15, a known amount of AlSBA-15 (1 g) was stirred with 0.03 M cupric acetate solution prepared in water (20 ml) at 80 °C for 6 h and then cooled to room temperature and the exchanged AlSBA-15 was filtered, washed repeatedly with distilled water and dried in air. The above procedure was repeated to ensure maximum copper exchange. Then it was dried at 120 °C for 12 h and calcined at 500 °C for 5 h. (RT-500 °C, 4 °C min^{-1}; for 4 h at 500 °C). This procedure was applied to all the other catalyst preparations. Similarly, all other metal exchanged catalysts with different supports were prepared by exchanging with the pre decided stock solutions of the corresponding metal acetate by following the above procedure except for La and Fe where $LaCl_3$ and $FeCl_3$ solutions were used. For comparative study with the exchanged catalysts, 2 wt. % copper was loaded over SBA-15 (hereafter CuO/SBA-15) by wet impregnation method. SBA-15 was added to aqueous copper acetate solution, stirred well for 10h, evaporated to dryness and calcined at 500 °C. These materials are designated as AlSBA-15-(X), MAlSBA-15 (X), where M is the exchanged metal ion and X is the Si/Al ratio of the chemical stoichiometric composition taken in the post synthesis mixtures.
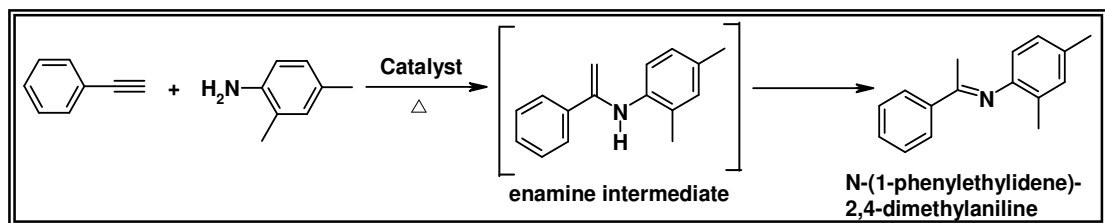
Scheme 4.2.

4.2.2.3. Catalyst testing

In a typical reaction, the reaction mixture consisting of phenyl acetylene (here after PhAc) (0.59 g), 2,4-xylidine (1.41 g), toluene (2 ml) and catalyst (0.1 g) (activated at 300 °C for 4 h prior to its use) placed in a 50 ml round bottom flask in an oil bath, which was refluxed (110 °C) under N_2 atmosphere. Samples were withdrawn at regular intervals of time and analyzed for its contents by Shimadzu 14B gas chromatograph, equipped with a flame ionization detector using a capillary column. Reactions at temperatures above the boiling point of toluene or substrate were performed in a 50 ml Parr autoclave. To find the general applicability of the catalyst, the reactions were carried out with different alkynes and aromatic amines. Conversion of PhAc was expressed in mole percentage. To determine the authenticity of the product, the reaction mixture was cooled and filtered to remove the catalyst and the solvent was removed by distillation. The mixture was dried *in vacuo* and purified by column chromatography on silica gel (petroleum ether/ethyl acetate, 200/1). N-(1-phenylethylidene)-2,4-dimethylaniline. Light brown oil: ^{1}H NMR (CDCl$_3$, 200 MHz): δ = 7.93-8.02 (m, 2H), 7.43-7.57 (m, 3H), 7.02 (d, 1H), 6.86 (m, 1H), 6.56 (m, 1H), 2.31 (s, 3H), 2.16 (s, 3H), 2.06 (s, 3H). FTIR (neat, cm^{-1}): 3020, 2951, 1639, 1209, 847, 764, 631. GCMS *m/z* (relative intensity): 223 (54) [M$^+$], 208 (100), 193 (35), 146 (12), 103 (35), 77 (67), 51 (25).

Hydration of alkyne with water (the addition of H-OH over the triple bond and subsequent rearrangement gives a ketone) is the side reaction which may occur in the presence of an acid catalyst at a faster rate than hydroamination. Hence, the chemicals and reaction set up must be free from water to avoid hydration reaction.

4.2.3. Results and Discussion

4.2.3.1. Physico-chemical characterization

4.2.3.1.1. X-ray diffraction

The well-defined XRD patterns were obtained for all the samples which are similar to those recorded for SBA-15 materials as described by Zhao et al [59]. XRD patterns of calcined SBA-15, Al-SBA-15 (10) and CuAlSBA-15 (10) materials with different Si /Al ratios (shown in Fig. 4.7. (a), (b) and (c) respectively) consists of three well-resolved peaks in the 2θ range of 0.8 to 1.8 correspond to the (100), (110), (200) reflections which are associated with p6mm hexagonal symmetry in the materials. It is noteworthy that no obvious change can be observed after the isomorphous substitution of Al into the framework of siliceous SBA-15 by the post synthesis method implying that the hexagonal mesoporous structure is well preserved. It is evident from the XRD profile of the samples that they do not contain any other phase or amorphous matter. Also XRD pattern of CuMCM-41 (15) (Fig. 4.7 (d)) shows the appearance of the (100), (110) and (200) reflections in lower 2θ region which demonstrates the well ordered nature of phases in the CuAlMCM-41.
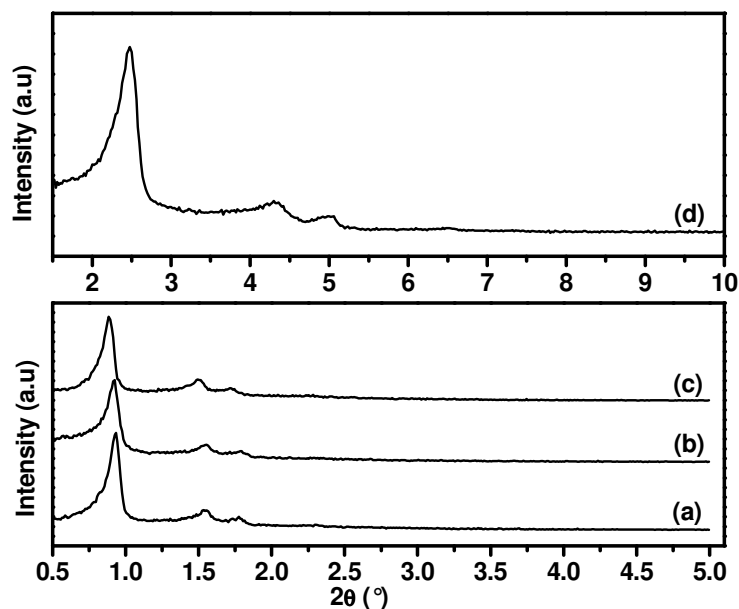

Fig. 4.7. Low angle XRD patterns of (a) SBA-15, (b) AlSBA-15, (c) CuAlSBA-15 (10), (d) CuAlMCM-41.

Table 4.3. Structural characteristics of different catalysts and their catalytic activities

	Catalyst	Si/Al (XRF)	Surface area BET $(m^2 g^{-1})$	Pore volume (cm^3/g)	Average pore diameter	Copper Conc. mmol/g	PhAc Convn[a] mol %	TOF[b]
1	SBA-15	∞	745	1.03	66.6	-	1.2	-
2	AlSBA-15 (10)	17	685	1.31	76.7	-	2.0	-
3	AlSBA-15 (20)	26	730	1.16	66.3	-	1.8	-
4	AlSBA-15 (30)	36	720	0.99	63.5	-	1.5	-
5	AlSBA-15 (40)	43	620	0.98	63.4	-	1.3	-
6	AlMCM-41 (15)	15	962	0.80	33.6	-	2.1	-
7	H-beta	15	530	0.28	-	-	1.5	-
8	Clay	-	230	-	-	-	1.2	-
9	CuAlSBA-15 (10)	-	664	1.09	67.9	0.21	48	22
10	CuAlSBA-15 (20)	-	685	0.95	65.8	0.15	37	24
11	CuAlSBA-15 (30)	-	603	0.98	67.7	0.11	27	25
12	CuAlSBA-15 (40)	-	652	1.1	67.6	0.09	21	23
13	CuO/SBA-15	-	685	0.95	66.0	0.31	08	03
14	CuAlMCM-41 (15)	-	820	0.72	33.1	0.26	52	21
15	Cu-Clay	-	208	-	-	0.22	28	9
16	Cu-beta (15)	-	480	-	-	0.25	31	7
17	$Cu(CF_3SO_3)_2$	-	-	-	-	-	37	17
18	CuO	-	-	-	-	-	00	-

[a] Conditions: temperature = 110 °C, 2,4-xylidine to PhAc mole ratio = 2, catalyst wt. = 0.15 g, total reactants wt. = 2 g, time = 6 h.
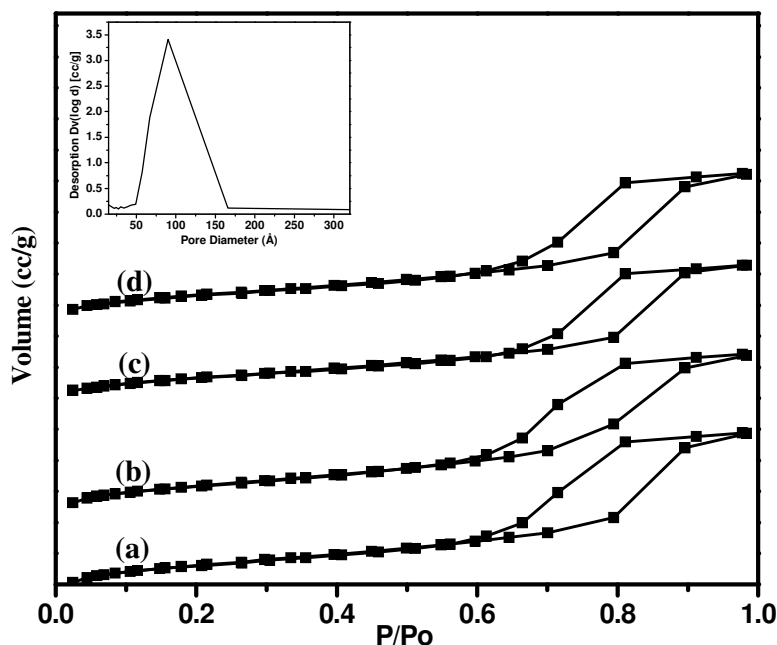[b] TOF = mole of PhAc converted per mole copper per hour

Fig. 4.8. N_2 adsorption and desorption isotherms of nitrogen on samples (a) AlSBA-15 (10), (b) CuAlSBA-15 (10), c) CuAlSBA-15 (30) (d) CuAlSBA-15 (40); Inset picture: Pore size distribution of. CuAlSBA-15 (10).

4.2.3.1.2. Nitrogen sorption studies

Textural properties of porous solids are typically obtained from low-temperature (-196 °C) nitrogen adsorption isotherms, which allow the computation of the specific surface area, specific pore volume, and mesopore size distribution. The nitrogen adsorption-desorption isotherms of AlSBA-15 (10) and CuSBA-15 samples of different Si/Al ratios are shown in Fig. 4.8. and the textural properties of all the samples are presented in Table 4.3. All isotherms were of type IV, as defined by IUPAC and exhibited a H1-type broad hysteresis loop, which was typical of large-pore mesoporous solids. As the relative pressure increases ($p/p_o > 0.6$), all isotherms exhibit a sharp step characteristic of capillary condensation of nitrogen within uniform mesopores, where the p/p_o position of the inflection point is correlated to the diameter of the mesopore. The pore size distribution was calculated from the Kelvin equation and is presented as a BJH plot (inset picture, Fig. 4.8.) [60]. It showed a narrow pore size distribution with an average mesopore size of 91 Å and a high surface area of 685 m^2/g. N_2 adsorption isotherms of all CuAlSBA-15 materials are

quite similar to that of AlSBA-15. The overall N_2 adsorption amounts decreased depending on the aluminum loading though no particular trend was observed. The calculated BET specific surface areas, total pore volume and average mesopore parameters based on BJH plots are listed in Table 4.3. Low alumination of SBA-15 does not affect the original pore structure of the parent SBA-15 while the surface areas slightly decrease as the aluminum loadings increase. Further modification of AlSBA-15 materials with copper exchange and calcination reduces the surface areas by small margin as expected. The surface area of CuAlMCM-41 (15) (820 m^2/g) is higher than CuAlSBA-15 (664 m^2/g) whereas average pore diameter is 33.1 Å which is lower than CuAlSBA-15 (10) (67.9 Å). Surface areas of Cu-beta (480 m^2/g) and Cu-clay (207 m^2/g) are low compared to CuAlSBA-15 catalysts.

4.2.3.1.3. Microscopic analysis

SEM images of CuAlSBA-15 shown in Fig. 4.9. (A) reveal that the micromorphology remained the same, which was rope like structures even after modification of SBA-15 with post synthesis Al incorporation and Cu^{2+} exchange. TEM measurements were carried out to study the morphology of AlSBA-15 and CuAlSBA-15 catalysts (Fig. 4.9 (B)). TEM images of these catalysts show the retention of the periodic structure of parent SBA-15 precursor (not shown) which confirms hexagonally arranged mesopores of SBA-15 are retained after modification with aluminium and copper.
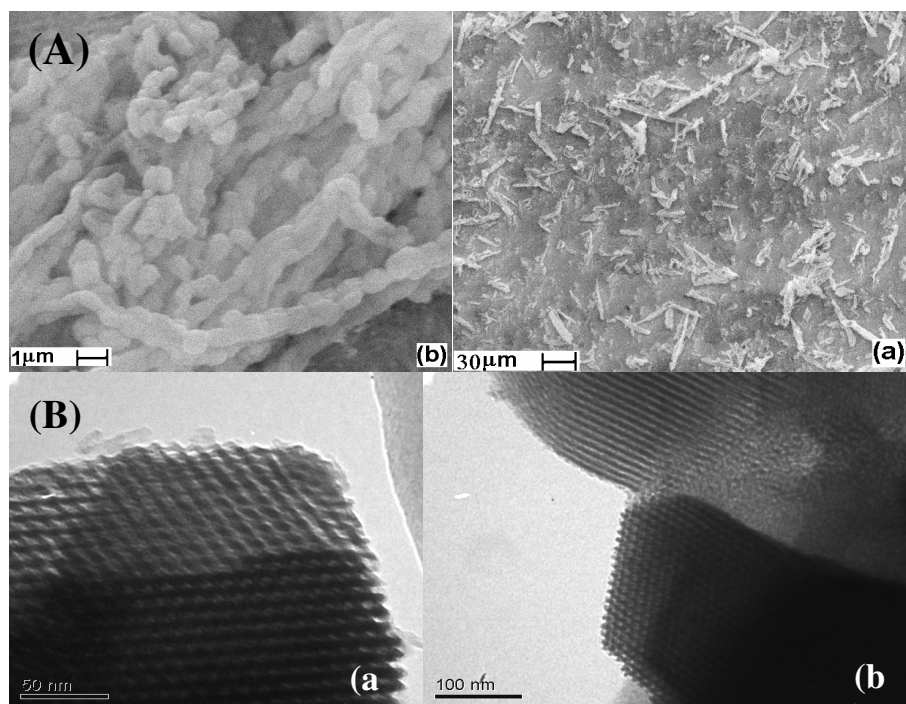
Fig. 4.9. (A) SEM photographs of (a) and (b) CuAlSBA-15 (10).
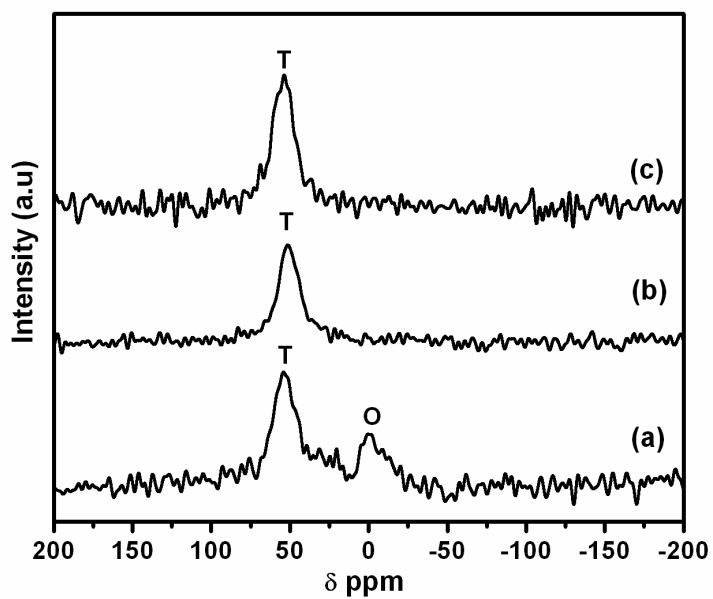(B) TEM photographs of (a) and (b) CuAlSBA-15 (10).

Fig. 4.10. ^{27}Al MAS NMR profile of (a) AlSBA-15 (10), (b) CuAlSBA-15 (10), (c) ZnAlSBA-15 (10). T = tetrahedral Al sites and O = octahedral Al sites.

4.2.3.1.4. Nuclear Magnetic Resonance

Solid-state ^{27}Al MAS NMR was used to investigate the local environment of aluminium species (Fig. 4.10.). The sharp peak observed at 53 ppm correspond to tetrahedrally coordinated framework aluminium in which Al is covalently bound to four Si atoms via oxygen bridges indicates that most of the aluminum has been incorporated into the framework. The peak at 0 ppm was attributed to distorted or octahedrally coordinated aluminium species in extra-framework positions. In addition, the presence of distorted tetrahedral or five coordinated aluminum cannot be discarded due to the signals of low intensity observed around 30 ppm [34]. In comparison to the ZnAlSBA-15 (10) sample, CuAlSBA-15 (10) exhibits a larger line width and lower intensity of ^{27}Al NMR signal at 53 ppm indicating the presence of paramagnetic Cu^{2+} ions near the aluminium sites in AlSBA-15. It is seen that the intensity of octahedral Al signal at 0 ppm is reduced after metal ion exchange which may be due to the removal of extra framework aluminium during the ion exchange of AlSBA-15 with the metal acetate solution. The material retained its structure after the metal ion exchange and calcination.
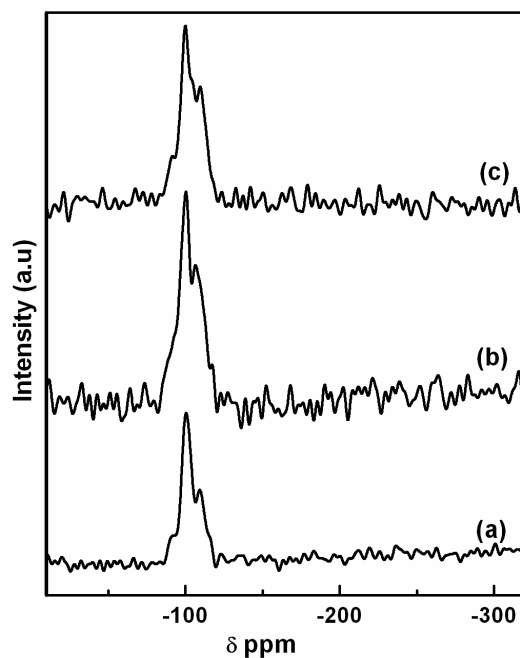
Fig. 4.11. ^{29}Si MAS NMR profile of (a) SBA-15, (b) AlSBA-15 (10), (c) CuAlSBA-15.

^{29}Si MAS NMR spectra (Fig. 4.11.) of all the samples contain a broad signal at -100 ppm and some shoulders at -90, -107, -110 ppm. According to Kolodziejski et al the main signal at -100 ppm is due to $Si(OSi)_3OH$ sites, while the shoulders at -90, -107 and -110 ppm are attributed to $Si(OSi)_2(OH)_2$, $Si(3Si,1Al)$ and $Si(OSi)_4$ structural units, respectively [35]. There are no significant differences between ^{29}Si MAS NMR spectra of CuAlSBA-15, AlSBA-15 and SBA15.
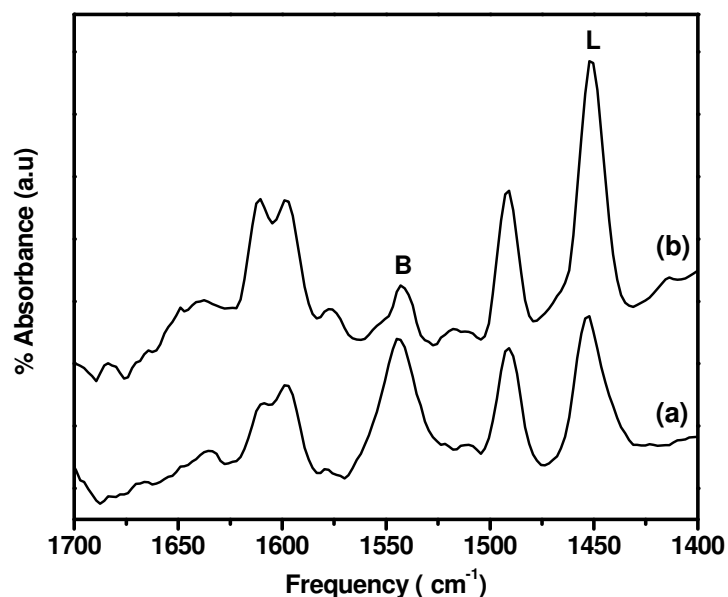
Fig. 4.12. FT-IR pyridine adsorption of (a) AlSBA-15 (10) and (b) CuAlSBA-15 (10) catalysts with Brönsted (B) and Lewis acid (L) peaks.

4.2.3.1.5. Acidity measurements

Pyridine adsorption *in-situ* FT-IR spectroscopy was performed for AlSBA-15 and Cu incorporated AlSBA-15 catalysts and the spectra recorded after out gassing at 200 °C are represented in Fig. 4.12. Adsorption of pyridine on the parent AlSBA-15 resulted in absorption bands at 1542 and 1451cm^{-1}, which can be assigned to pyridine molecules interacting with Brönsted (B) and Lewis (L) acid sites, respectively. Incorporation of copper led to an increase in Lewis acidity. CuAlSBA-15 (10) catalysts prepared by exchanging with different copper acetate concentrations and the ratio of B/L obtained by intensities measurements are listed in Table 4.4. It is seen

that B/L ratio increased as copper concentration increased in mesoporous support upto 0.21 mmol/g of Cu and decreased further. This suggests that there is an optimum amount of copper exchange at lower concentration of copper acetate (0.03 M). For over exchanged catalysts, the extra copper present in catalysts is due to the formation of CuO clusters inside the pores and the surface of the catalyst [55].

Table 4.4. Effect of copper acetate concentrations on Cu^{2+} exchange and their acidities.

Catalyst	Copper acetate solution (mol/l)	Total exchange time (h)	Copper Conc. (mmol/g)	Brönsted acidity I_{1542}	Lewis acidity I_{1451}	B/L I_{1542}/I_{1451}
AlSBA15 (10)	-	-	-	2.23	2.44	0.91
CuAlSBA15 (10)	0.01	18	0.14	1.68	3.23	0.52
CuAlSBA15 (10)	0.03	18	0.21	1.05	5.01	0.21
CuAlSBA15 (10)	0.06	18	0.26	1.14	4.56	0.25
CuAlSBA15 (10)	0.1	18	0.33	1.56	3.47	0.45
CuSBA-15 (10)	0.03	40	0.40	0.79	3.91	0.20

4.2.3.1.6. Temperature programmed reduction

H_2-TPR studies were performed for the identification of copper species in AlSBA-15 materials modified with copper. According to the literature [54, 58, 61] the following reduction processes can be considered.

$$CuO + H_2 \longrightarrow Cu^0 + H_2O \quad (1)$$

$$Cu^{2+} + \frac{1}{2}H_2 \longrightarrow Cu^+ + H^+ \quad (2)$$

$$Cu^+ + \frac{1}{2}H_2 \longrightarrow Cu^0 + H^+ \quad (3)$$
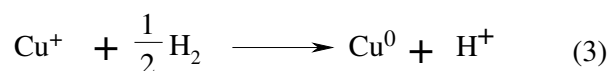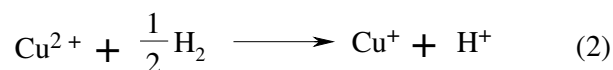
The reactions (1) and (2) occur at lower temperatures than reaction (3). TPR profiles of CuAlSBA-15 catalysts with different Si/Al ratios and CuO/SBA-15 are depicted in Fig. 4.13. The TPR graph of pure CuO gave a peak maximum at 207 °C (Inset picture). Cu^{2+} exchanged AlSBA-15 samples show different peaks from 160 to 650 °C.
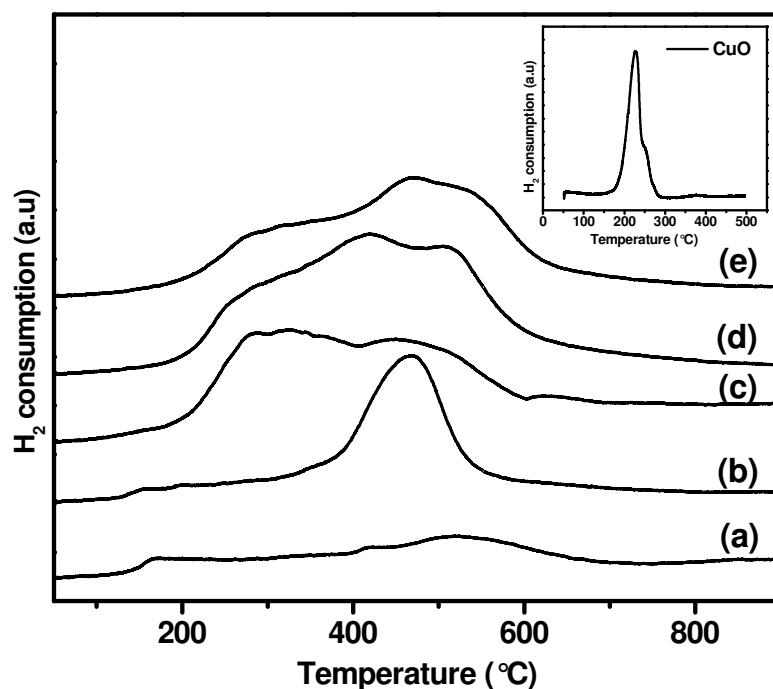
Fig. 4.13. H$_2$-TPR profiles of (a) CuO /SBA-15, (b) CuAlSBA-15 (40), (c) CuAlSBA-15 (30), (d) CuAlSBA-15 (20) and (e) CuAlSBA-15 (10)

The low temperature peaks below 210 °C for copper containing samples may be due to the reduction of copper-oxygen phase (not necessarily CuO) (Reaction (1)). The peaks at > 210 and > 330 °C indicate the reduction of isolated Cu^{2+} cations in step (2) and step (3) respectively. The results indicate that the copper ions are mostly located in the extra framework positions which are in the exchanged form. Different shoulders observed for these solids indicate that they contain isolated Cu^{2+} species present in small clusters in different environments. It is also seen that as the Si/Al increases, the temperature at the peak maximum of the first peak is shifted to a higher temperature. CuO/ SBA-15 ((Fig. 4.13. (a)) catalyst showed a weak TPR profile which suggests that it contains very low exchanged copper sites and all the isolated Cu^{2+} site observed for CuAlSBA-15 catalysts are due to the exchange with the Brönsted acid sites in AlSBA-15 samples.

4.2.3.1.7. Electron Paramagnetic Spectroscopy

EPR spectra of Cu(II) ion exchanged AlSBA-15 materials are illustrated in Figure 4.14. The spectra recorded at 25°C are well-resolved and show a single Cu(II) species described by g ll = 2.30, g perpendicular = 2.06 and A ll = 0.0141 cm^{-1} with A perpendicular unresolved where A is the hyperfine coupling. All the CuSBA-15 materials with different Si/Al ratio exhibit the same Cu^{2+} species with identical g ll and A ll values. As expected the intensity of the Cu^{2+} EPR signal increases with increase in aluminium content.
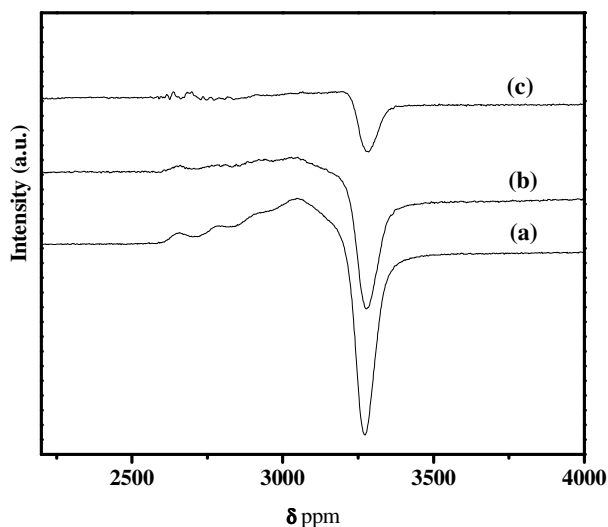
Fig. 4.14. EPR spectra of (a) CuAlSBA-15(10), (b) CuAlSBA-15 (20) and CuAlSBA-15 (40)

4.2.3.2. Hydroamination reaction

4.2.3.2.1. Influence of metal ions and supports on catalyst activity

The hydroamination of phenylacetylene with 2,4-xylidine to give an enamine as an intermediate (not observed) which rearranges itself to form N-(1-phenylethylidene)-2,4-dimethylaniline (Scheme 4.2.) was used as a model reaction for testing the catalytic activities of various catalysts. The reaction was highly selective and only the preferred Markovnikov addition product was observed. The different transition metal ions such as Cu^{2+}, Zn^{2+}, Pd^{2+}, Co^{2+}, Mn^{2+}, La^{3+} and Fe^{3+} were exchanged with AlSBA-15 (10) and the catalytic activities in hydroamination of PhAc with 2,4-xylidine were compared (Fig. 4.15.). CuAlSBA-15 showed the highest activity with 44 mol% conversion of PhAc after 4 h reaction and the others followed

in the decreasing order: CuAlSBA-15 > ZnAlSBA-15 > PdAlSBA-15 > LaAlSBA-15
> CoAlSBA-15 > MnAlSBA-15 > FeAlSBA-15.
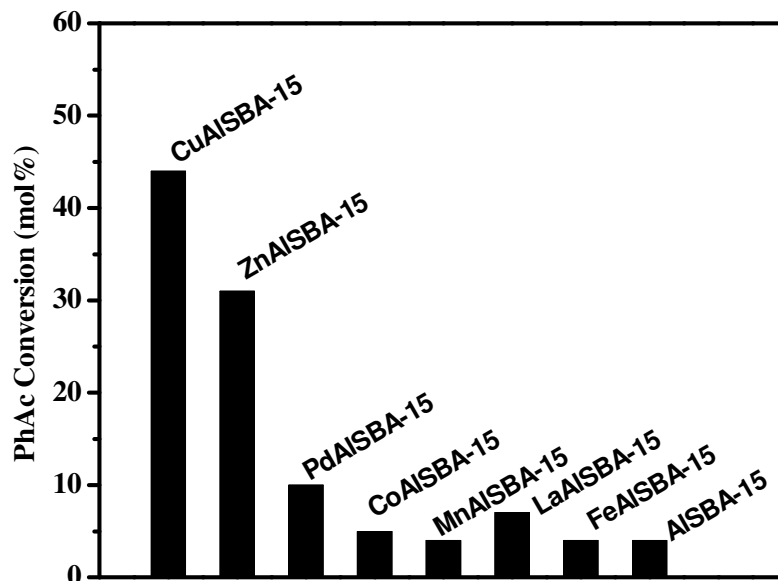
Fig. 4.15. Catalytic activities of M^{n+}AlSBA-15 (10) in hydroamination of PhAc with 2,4-xylidine (Reactin conditions: temperature = 110 °C, 2,4-xylidine to PhAc mole ratio = 2, catalyst wt. = 0.1 g, total reactants wt. = 2 g, time = 8 h).

As reported in the literature, the catalysts with Cu^{2+} and Zn^{2+} sites are highly active for hydroamination of alkynes by amines compared to other metal ions due to their moderately hard Lewis acidic properties [46]. Cu^{2+} ions exchanged with different supports such as AlSBA-15, AlMCM-41, H-beta, montmorillonite K-10 and the catalytic activities hydroamination of PhAc were compared (Table 4.3.). The unexchanged catalysts (supports) showed very low catalytic activity. The turnover frequencies (TOF = mole of PhAc converted per mole of Cu^{2+} per hour) were the highest with CuAlSBA-15 (10) (TOF= 22) and CuAlMCM-41 (15) (TOF = 21) in the hydroamination of PhAc by 2,4-xylidine compared to clay and zeolite supported catalysts. The higher activities of mesoporous supported catalysts could be attributed to their higher surface area and larger pore sizes.
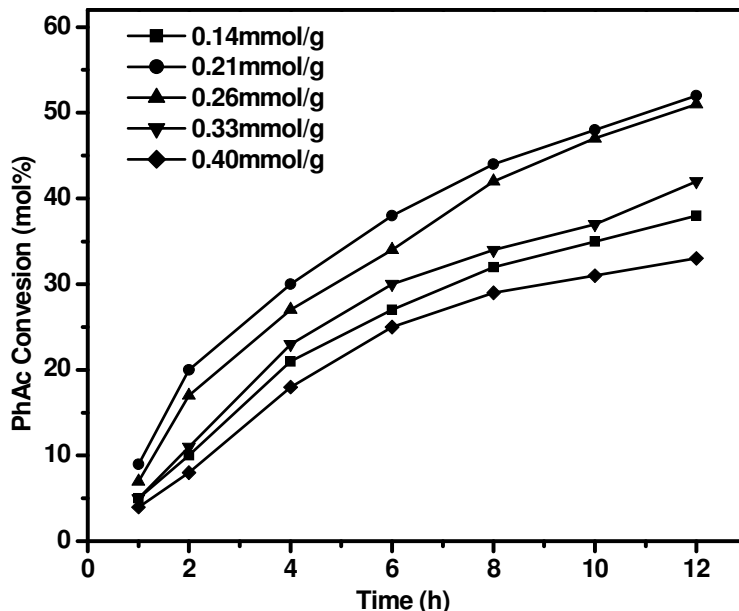
Fig. 4.16. Influence of Cu^{2+} concentration on catalytic activity Conditions: : catalyst = CuAlSBA-15 (10), temperature = 110 °C, 2,4-xylidine to PhAc mole ratio = 2, catalyst wt. = 0.1 g, total reactants wt. = 2 g.

Copper triflate was tested for its catalytic activity as the corresponding homogeneous counterpart by keeping the same copper amount as that of CuAlSBA-15 (10). This catalyst was less active compared to CuAlSBA-15 (10) (by ~10 %). This observation is contrary to the expectation that porous catalysts are often assumed to be less active than the corresponding homogeneous catalysts as diffusion within the pores may slow down the overall reaction. The higher activity of porous catalysts may be due to the presence of some Brönsted acid sites left unexchanged which may act as a promoter in hydroamination which is absent in copper salt [62]. In contrast to the Cu^{2+} ion exchanged materials, CuO did not show any catalytic activity in hydroamination reaction, which could be attributed to its basic nature. However, CuO/SBA-15 showed some activity (TOF = 3), which could be due to some exchangeable protons present in SBA-15. H_2-TPR results show that CuAlSBA-15 catalysts contain insignificant amount of CuO and it is present mostly in Cu^{2+} state, which is the active site for hydroamination reaction in the present study.
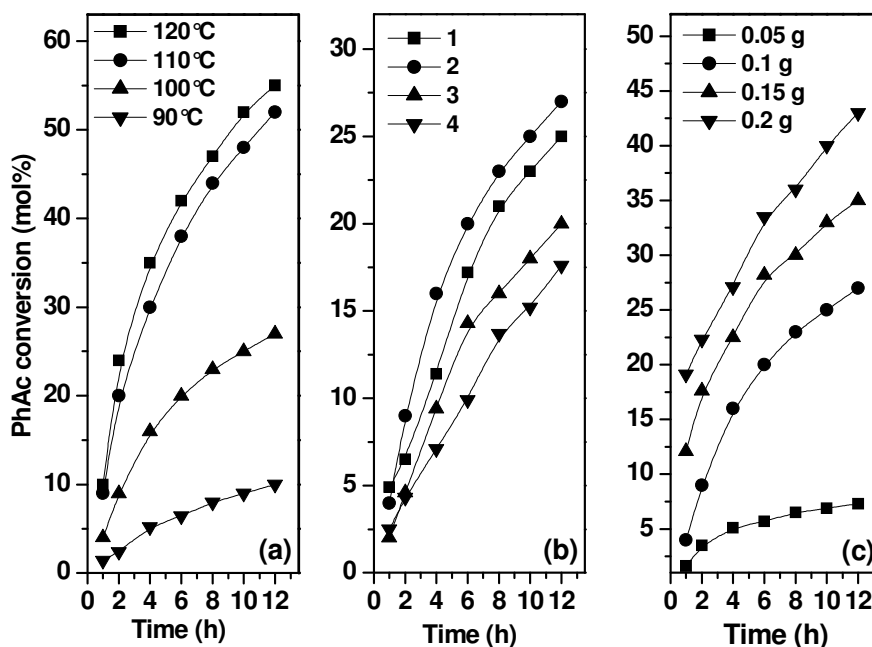
Fig. 4.17. Effect of reaction conditions (a) Effect of reaction temperature. Conditions: catalyst = CuAlSBA-15 (10), 2,4-xylidine to PhAc mole ratio = 2, catalyst wt. = 0.1 g, total reactants wt. = 2g, (b) Effect of 2,4-xylidine to PhAc mole ratio. Conditions: catalyst = CuAlSBA-15 (10), temperature = 100 °C, catalyst wt. = 0.1g, total reactants wt. = 2 g. (c) Effect of catalyst concentration. Conditions: catalyst = CuAlSBA-15 (10), temperature = 100 °C, 2,4-xylidine to PhAc mole ratio = 2, total reactants wt. = 2 g.

4.2.3.2.2. Effect of Si/Al ratio on catalytic activity.

Among CuAlSBA-15 with different Si/Al ratios (shown in the parenthesis), the activity increased with decrease in Si/Al ratio (Table 4.3.). Brönsted acidity increases with decrease in the Si/Al ratio, which in turn increases the ion exchange capacity and subsequently enhances the number of exchanged Cu^{2+} ions. To know the effect of Cu^{2+} concentration on the catalytic activity, the catalysts with different Cu^{2+} concentrations (0.14 - 0.40 mmol/g) were tested in the hydroamination of PhAc with 2,4-xylidine and the results are shown in Fig. 4.16. Conversion of PhAc increased upto 0.21 mmol/g of copper and then decreased at higher concentrations. The results are in agreement with the acidity data listed in Table 4.4. Brönsted acidity decreased with increase in Cu^{2+} concentration upto 0.21mmol/g and then decreased with further increase. The nature of the copper species depends on the concentration of copper

acetate solution as well as the time of exchange. Thus in over-exchanged catalysts, copper oxide clusters may be formed inside the channels as well as on the surface, which affects the activity.

4.2.3.2.3. Optimization of reaction conditions

CuAlSBA-15 (10) was used to study the effect of temperature (80–120 °C ranges) in the hydroamination of phenylacetylene with 2,4-xylidine. The results indicate that temperature has a remarkable effect on the conversion of PhAc (Fig. 4.17, (a)). At 90 °C, the conversion was only 10 mol%, which increased to 52 mol% at 110 °C after 12 h. Following the initial rate approach, the graph of ln(rate) versus $1/T$ was plotted and from the slope of the straight line (slope = -Ea/R), the activation energy calculated was found to be 65 kJ/mol.

The effect of substrate concentrations on PhAc conversion was studied at 100 °C by keeping the total weight of the reaction mixture constant (Fig. 4.17. (b)). As the mole ratio of 2,4-xylidine to PhAc was increased from 1 to 2, the PhAc conversion increased from 11 to 16 % after 4 h. But further increase in the mole ratio of 2,4-xylidine to PhAc, decreased the PhAc conversion. The higher conversions of PhAc are observed at 2,4-xylidine to PhAc mole ratio 2.

The effect of catalyst concentration on PhAc conversion was studied at 100 °C with mole ratio of 2 (Fig. 4.17. (c)) shows that as the catalyst concentration increased, the conversion of PhAc increased. There was linear increase in conversion up to 6 h and the reaction is slowed down with marginal increase in the range of 6–12 h. At optimized reaction conditions ; 110 °C, 2,4-xylidine / PhAc 2, catalyst weight 0.15 g and total reactant weight 2g with 2ml of toluene as a solvent, the conversion of PhAc was found to be 88 mol% after 20 h reaction.

4.2.3.2.4. Leaching and recyclability test.

To know if any active species of the catalyst are leaching into the reaction mixture, hydroamination of phenylacetylene with 2,4-xylidine to give an imine was carried out at optimized conditions taking CuAlSBA-15 (10) catalyst. After 2 h (20 mol% conversion), the reaction was stopped, filtered hot and reaction was continued with the filtrate under identical conditions. Conversion remained the same even after 20h, which indicates that there is no leaching of any active species of the catalyst. The

recyclability of CuAlSBA-15 catalyst was tested in the hydroamination of phenyl acetylene and 2,4-xylidine by conducting five runs (~ 80 mol% conversion after 20 h) using optimized reaction conditions. After each run, the catalyst (brown in color) was repeatedly washed with toluene, dried at 120 °C for 2 h and calcined at 500 °C in air for 4 h (turned white). It was then used in the hydroamination reaction with a fresh reaction mixture and it was found that the conversion of PhAc was practically the same in all the five cycles.

4.2.3.2.5. Hydroamination of different alkynes and amines.

To check the general applicability of the catalyst, two sets of reactions were carried out and the conversions were expressed as the conversion of alkyne. In the first set, different amines were reacted with phenyl acetylene (Table 4.5.). The nature of substituents on the aromatic ring of aniline derivatives has significant effect over the reactivity. The electron-donating groups at the *-ortho* and *-para* positions gave higher conversions to yield the corresponding imines, which are comparable to that of aniline reaction. The sterically hindered amines such as 2,4,6-trimethylaniline (37 %) and 2-isopropylaniline (35 %) and large molecule 1-naphthylamine (58 mol %) gave higher conversions, which indicates that the bulky amines can easily pass through the mesopores of CuAlSBA-15. The amines with electron withdrawing substituents such as 2-chloroaniline (15%), 4-bromoaniline (21 %) were least reactive. No reactivity was observed when phenylacetylene was reacted with a secondary aromatic amine (N-methylaniline) and an aliphatic amine (cyclohexylamine), which suggests that CuAlSBA-15 is suitable only for aromatic primary amines for the hydroamination of alkynes.

Table 4.5. Hydroamination of different alkynes and amines catalyzed by CuAlSBA-15

Entry[a]	Amine	Convn (mol %)	Entry[b]	Alkynes	Convn (mol %)
1	Aniline	61	1	1-Hexyne	15
2	*o*-Toluidine	38	2	1-Heptyne	31
3	*p*-Toluidine	52	3	3-Hexyne	NR
4	2,4-Xylidine	48	4	Phenylacetylene	61
5	2,4,6-Trimethylaniline	37	5	Diphenylacetylene	NR
6	2-Isopropylaniline	35	6	4-Ethynyltouene	52
7	4-Isopropylaniline	38	7	4-Ethynylanisole	55
8	4-Methoxyaniline	45	8	1-Ethynylnaphthalene	46
9	2-Chloroaniline	15			
10	4-Bromoaniline	21			
11	4-Nitroaniline	NR			
12	1-Naphthylamine	58			
13	N-Methylaniline	NR			
14	Cyclohexylamine	NR			

[a] Hydroamination of PhAc with amines: Conditions: catalyst = CuSBA-15 (10), Amine to PhAc mole ratio = 2, toluene = 2 ml, temperature = 110 °C, catalyst wt. = 0.15 g, total reactants wt. = 2 g, time = 6 h, 100 % selectivity for Markovnikov product.
[b] Hydroamination of alkynes with 2,4-xylidine: Conditions: catalyst = CuSBA-15 (10), 2,4-xylidine to alkyne mole ratio = 2, toluene = 2 ml, temperature = 110 °C, catalyst wt. = 0.15 g, total reactants wt. = 2 g., time = 6 h, NR = no reaction, 100% selectivity for Markovnikov product.

In the second set, the reactions were carried out by reacting different alkynes with 2,4-xylidine (Table 4.5.). Aromatic alkynes were more reactive than aliphatic alkynes while terminal alkynes gave the higher yields. Internal alkynes (entries 3, 5) did not undergo the reaction indicating that this catalyst is only suitable for hydroamination of terminal alkynes. The activated alkynes with electron-donating substituents, $-CH_3$ and CH_3O- gave better yields (entries 6, 7) where as the bigger molecule like 1-ethynylnaphthalene showed high conversion (46 %).

4.3. References

1.   T.E.Müller, M. Beller, Chem. Rev. 98 (1998) 675.

2.   L.L. Anderson, J. Arnold, R.G. Bergman, J. Am. Chem. Soc. 127 (2005) 14543.

3.   J.A. Bexrud, J.D. Beard, D.C. Leitch, L.L. Schafer, Org. Lett. 7 (2005) 1959.

4.   L. Ackermann, L.T. Kaspar, A. Althammer, Org. Biomol. Chem. 5 (2007) 1975 and references cited there in.

5.   K. Marcsekova, S. Doye, Synthesis 1 (2007) 145.

6.   N. Sewald, Amino Acids 11 (1996) 397.

7.   E. Juaristi, H. L. Ruiz, Curr. Med. Chem. 6 (1999) 983.

8.   M. Perez, R. Pleixats, Tetrahedron 51 (1995) 8355.

9.   T.C. Wabnitz, J.B. Spencer, Org. Lett. 5 (2003) 2141.

10.   L.W. Xu, J.W. Li, C.G. Xia, S.L. Zhou, X.X. Hu, Syn. Lett. 15 (2003) 2425.

11.   J. Monfray, A.M.P. Koskinen, Lett. Org. Chem. 3 (2006) 324.

12.   J.J. Bozell, L.S. Hegedus, J. Org. Chem. 46 (1981) 2561.

13.   L. Fadini, A. Togni, Chem.Commun. (2003) 30.

14.   N.S. Shaikh, V.H. Deshpande, A.V. Bedekar, Tetrahedron 57 (2001) 9045.

15.   J. Horniakova, K. Komura, H. Osaki, Y. Kubota and Y. Sugi, Catal. Lett. 102 (2005) 191.

16.   M.L. Kantam, B. Nilima, C.V. Reddy, J. Mol. Catal. A Chem. 241 (2005) 147.

17.   T. Joseph, G.V. Shanbhag, D.P. Sawant, S.B. Halligudi , J. Mol. Catal. A Chem. 250 (2006) 210.

18.   S. Lin, L.F. Wang, Y. Han, Y. Yu, Y. Di, R.W. Wang, D.Z. Jiang, F.S. Xiao, Chin. J. Chem. 22 (2004) 9.

19.   R. Ryoo, S. Jun, J.M. Kim, M.J. Kim, Chem. Commun. (1997) 2225.

20.   Y. Yue, A. Cedeon, J.L. Bonardet, N. Melosh, J.B. Despinose, J. Fraissard, Chem. Commun. (1999) 1967.

21.   A. Vinu, V. Murugesan, W. Böhlmann, M. Hartmann, J. Phys. Chem. B 108 (2004) 11496.

22.   A. Vinu, B.M. Devassy, S.B. Halligudi, W. Böhlmann, M. Hartmann, Appl. Catal. A: Gen. 281 (2005) 207.

23.   A. Vinu, G.S. Kumar, K. Ariga, V. Murugesan, J. Mol. Catal. A: Chem. 235 (2005) 57.

24.   W. Li, S.J. Huang, S.B. Liu, M.O. Coppens, Langmuir 21 (2005) 2078.

25.   Y. Li, Q. Yang, J. Yang, C. Li, J. Porous Mater. 13 (2006) 187.

26.   M. Xu, W. Wang, M. Seiler, A. Buchholz, M. Hunger, J. Phys. Chem. B 106 (2002) 3202.

27.   M.A. Zanjanchi, S. Asgari, Solid State Ionics 171 (2004) 277.

28.   R. Luque, J.M. Campelo, D. Luna, J.M. Marinas, A.A. Romero, Micropor. Mesopor. Mater. 84 (2005) 11.

29.   Z. Luan, M. Hartmann, D. Zhao, W. Zhou, L. Kevan, Chem. Mater. 11 (1999) 1621.

30.   M. Cheng, Z. Wang, K. Sakurai, F. Kumata, T. Saito, T. Komatsu, T. Yashima, Chem. Lett. 2 (1999) 131.

31.   S. Sumiya, Y. Oumi, T. Uozumi, T. Sano, J. Mater. Chem. 11 (2001) 1111.

32.   H.M. Kao, C.C. Ting, S.W. Chao, J. Mol. Catal. A: Chem. 235 (2005) 200.

33.   M.G. Cazalilla, J.M.M. Robles, A. Gurbani, E. R. Castellon A. J. Lopez, J. Solid State Chem. 180 (2007) 1130.

34.   R. Anwander, C. Palm, G. Gerstberger, O. Groeger, G. Engelhardt, Chem. Commun. (1998) 1811.

35.   W. Kolodziejski, A. Corma, M.T. Navarro, J. Perez-Periente, Solid State Nucl. Magn. Reson. 2 (1993) 253.

36.   J. Penzien, T.E.Muller, J.A.Lercher, Micropor. Mesopor. mater. 48 (2001) 285.

37.   J.A.Loritsch, R.R.Vogt, J. Am. Chem. Soc. 61 (1939) 1462.

38.   J. Barluenga, F. Aznar, R. Liz, R. Rodes, J. Chem. Soc., Perkin Trans. 1 (1980) 2732.

39.   D. Tzalis, C. Koradin, P. Knochel, Tetrahedron Lett. 40 (1999) 6193.

40.   Y. Li, T.J. Marks, Organometallics 15 (1996) 3770.

41.   Y. Li, T.J. Marks, J. Am. Chem. Soc. 120 (1998) 1757.

42.   A. Haskel, T. Straub, M. S. Eisen, Organometallics 15 (1996) 3773.

43.   P.J. Walsh, A.M. Baranger, R.G. Bergman, J. Am. Chem. Soc. 114 (1992) 1708.

44.   F. Pohlki, S. Doye, Chem. Soc. Rev. 32 (2003) 104.

45.   J. Penzien, T.E. Muller, J.A.Lercher, Chem.Commun. (2000) 1753.

46.   J. Penzien, C. Haeβner, A. Jentys, K. Köhler, T.E. Müller, J. Lercher, J. Catal. 221 (2004) 302.

47.   J. Penzien, R.Q. Su, T.E.Muller J. Mol. Catal A Chem. 182 (2002) 489.

48.   M.K. Richmond, S.L. Scott, H. Alper, J. Am. Chem. Soc. 123 (2001) 10521.

49.   S. Breitenlechner, M. Fleck, T.E. Müller, A. Suppan, J.Mol. Catal. A Chem. 214 (2004) 175.

50.   N. Lingaiah, N.S. Babu, K.M. Reddy, P.S.S. Prasad, I. Suryanarayana, Chem. Commun. (2007) 278.

51.   B.Z. Zhan, B. Moden, J. Dakka, J.G. Santiesteban, E. Iglesia J. Catal. 245 (2007) 316.

52.   M.F. Ribeiro, J.M. Silva, S. Brimaud, A.P. Antunes, E.R. Silva, A. Fernandes, P. Magnoux, D.M. Murphy, Appl. Catal. B 70 (2007) 384.

53.   B.M. Choudary, M. Sateesh, M.L. Kantam, K.V.R. Prasad, Appl. Catal, A 171 (1998) 155.

54.   C.T. Abreu, M.F. Ribeiro, C. Henriques, G. Delahay, Appl. Catal. B 12 (1997) 249.

55.   V.A. Matyashak, A.N. Ilichev, A.A. Ukharsky, V.N. Korchak, J. Catal. 171 (1997) 245.

56.   H. Yahiro, M. Iwamoto, Appl. Catal. A 222 (2001) 163.

57.   V. Nieminen, N. Kumar, J. Datka, J. Paivarinta, M. Hotokka, E. Laine, T. Salmi, D.Y. Murzin, Micropor. Mesopor. Mat. 60 (2003) 159.

58.   I. Sobczak, M. Ziolek, M. Renn, P. Decyk, I. Nowak, M. Daturi, J. Lavalley, Micropor. Mesopor. Mat. 74 (2004) 23.

59.   D. Zhao, J. Feng, Q. Huo, N. Melosh, G.H. Fredrickson, B.F. Chmelka, G.D. Stucky, Science 279 (1998) 548.

60.   E.P. Barrett, L.G. Joyner, P.P. Halenda, J. Am. Chem. Soc. 73 (1951) 373

61.   T.F. Guidry, G.L. Price, J. Catal. 181 (1999) 16.

62.   R.Q. Su, T.E. Muller, Tetrahedron 57 (2001) 6027.

CHAPTER V

5.1. Introduction

Heteropolyacids (HPA) and their salts are effective catalysts systems for various organic transformations such as acid-catalyzed as well as oxidation reactions [1-6]. They are effective heterogeneous catalysts systems for gas-phase selective oxidation of organic substrates [7-9]. It has been reported that metal and organic salts of heteropoly acids are more active or selective than their acid forms in some organic transformations [10-11]. Heteropoly compounds with Keggin-type structure possess special characteristics that make them very active in catalytic applications [5]. The solubility of these compounds in turn is closely connected to their ability to absorb various reactants. Nonpolar molecules are absorbed on the surface of bulk HPAs, while most polar molecules are mainly absorbed in the bulk, forming what Misono has described as a "pseudoliquid" phase [12]. This characteristic leads to two typical catalytic reaction types involving heteropoly compounds: surface-type and bulk-type reactions.

Since the use of heteropoly compounds as homogenous catalysts has its own drawbacks including recovery and recyclibility issues, lot of effort has been made to heterogenise them [13-19]. Most of the heteropoly salts are insoluble in non-polar solvents such as benzene, toluene and hydrocarbons. They are known to act as catalysts even in insoluble reaction medium [20-25]. Copper salts of HPA (CuHPA) have been used in some organic transformations [26-30]. Copper salt of silicotungstic acid (CuSTA) has been used as a catalyst in hydroxylation of phenol [31]. There is only a single report in the literature on the application of heteropoly salts in hydroamination reactions where silver heteropoly salt has been reported for intermolecular hydroamination of alkynes [32].

This chapter deals with the preparation of copper salt of HPA and characterization of catalysts (copper salt of HPA) by techniques such as X-ray diffraction, N_2 sorption, FTIR and TG-DTA. These catalysts have been used in the liquid-phase intra and intermolecular hydroamination reactions. The general application of the catalyst has been determined by carrying out hydroamination of

different alkynes and amines. Possibility of mesoporous solid acids as promoters has also been explored.
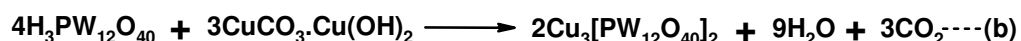
5.2. Experimental

5.2.1. Chemicals and reagents

All alkynes were purchased from Aldrich. Amines, cupric carbonate, other metal salts and toluene were purchased from local suppliers. All the chemicals were used as received. Dry toluene was prepared by distilling and storing over sodium wire. 6-Amino-1-hexyne was prepared from the reduction of 5-cyanopent-1-yne using the procedure described elsewhere [33].

5.2.2. Catalyst preparation

5.2.2.1. $M^{n+}HPA$

Stoichiometric amounts of metal carbonates and HPA are used for the synthesis of copper salts of HPAs [34]. In a typical synthesis of $Cu_2SiW_{12}O_{40}$, 10 g (0.0026 mole) of $H_4[SiW_{12}O_{40}].28H_2O$ was dissolved in 20 ml of water and 0.58 g (0.0026 mole) of $CuCO_3.Cu(OH)_2$ was added to the acid solution. Since no apparent evolution of gas occurred after the addition of the carbonate, the mixture was heated slowly to 65 °C at which point evolution of carbon dioxide began to occur. The reaction mixture was then stirred for 0.5 h with cooling and filtered. A solid was obtained upon evaporation of the solution to dryness in the open. Then it was calcined to 250 °C for 5h. Similarly, $Cu_1H_2SiW_{12}O_{40}$ (Cu_1H_2STA) was prepared by using appropriate amount of copper in the procedure. The similar procedure was followed for the synthesis of copper salts of $H_3[PW_{12}O_{40}]$ and $H_3[PMo_{12}O_{40}]$ (hereafter CuTPA and CuMPA). Similarly, Mn, Co, Ni, Pd and Zn salts of silicotungstic acid catalysts were prepared by employing similar procedures to those used for copper salts by taking metal carbonate or metal acetate salts as precursors. All the catalysts were calcined at 250 °C.

$$H_4SiW_{12}O_{40} \ + \ CuCO_3.Cu(OH)_2 \longrightarrow Cu_2SiW_{12}O_{40} \ + \ 3H_2O \ + \ CO_2 \cdots (a)$$

$$4H_3PW_{12}O_{40} \ + \ 3CuCO_3.Cu(OH)_2 \longrightarrow 2Cu_3[PW_{12}O_{40}]_2 \ + \ 9H_2O \ + \ 3CO_2 \cdots (b)$$

$$4H_3PMo_{12}O_{40} \ + \ 3CuCO_3.Cu(OH)_2 \longrightarrow 2Cu_3[PMo_{12}O_{40}]_2 \ + \ 9H_2O \ + \ 3CO_2 \cdots (c)$$

**Scheme 5.1.** Preparation of heteropoly salts of copper

5.2.2.2. 20 wt.% CuSTA/SBA-15 and 20 wt.% CuSTA/AlSBA-15

Synthesis of SBA-15 and AlSBA-15 (Si/Al = 17) is illustrated in Chapter II. Samples were prepared by wet impregnation method. 1 g of CuSTA (20 wt.% of. SBA-15) was dissolved in 25ml water. It was then added to 5 g of SBA-15 and stirred for 2 h at room temperature. Solvent was the evaporated on a rotary evaporator and resultant powder was dried and calcined at 250 °C in static air.

The above procedure was followed for the preparation of 20 wt.% CuSTA/AlSBA-15 (10) (hereafter 20CuSTA/AlSBA-15).

### 5.2.3. Experimental procedure.

5.2.3.1. Intermolecular hydroamination reaction.

Experiments were carried out in a two-necked round bottom flask fitted with a water condenser connected to a balloon filled with N_2 and kept in a thermostatic oil bath. In a typical procedure, the reaction mixture containing phenyl acetylene (1.04 g.), aniline (0.96 g.), toluene (3 ml) and catalyst (0.1 g., catalyst calcined at 250 °C prior to use) was placed in the flask. The flask was then flushed twice with N_2 before it was finally connected to balloon filled with N_2 and the reaction was carried out at 110 °C. Samples were withdrawn at regular intervals of time were analyzed by gas chromatography (Shimadzu 14B) equipped with a cross-linked 5% diphenyl-95% dimethylpolysiloxane capillary column (30m) and a flame ionization detector and the identity of the product was confirmed by GCIR and GCMS (Shimadzu GCMS QP5000) equipped with an identical column and a mass selective detector. The conversion is expressed as the weight percentage of alkyne converted into products.
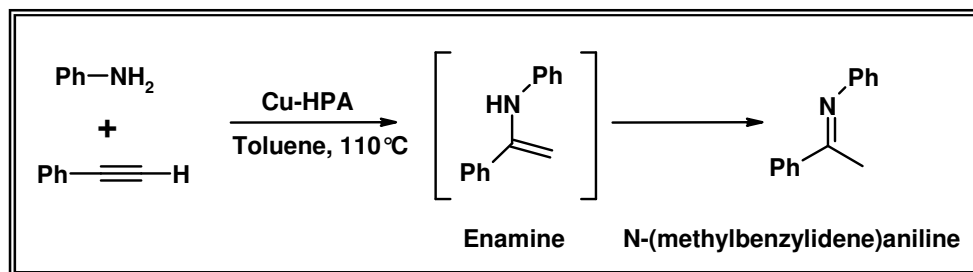
Scheme 5.2. Intermolecular hydroamination of phenyl acetylene with aniline

5.2.3.2. Intramolecular hydroamination reaction

The catalyst (0.03 g) and solvent toluene (5 ml) was placed in a round bottom flask fitted with a magnetic stirrer and N_2 balloon. The reaction was started by the addition of 6-amino-1-hexyne (0.1 g) and the mixture was refluxed. The samples were analyzed by gas chromatography. The product was confirmed by GCMS and GCIR as 2-methyl-1,2-dehydropiperidine.
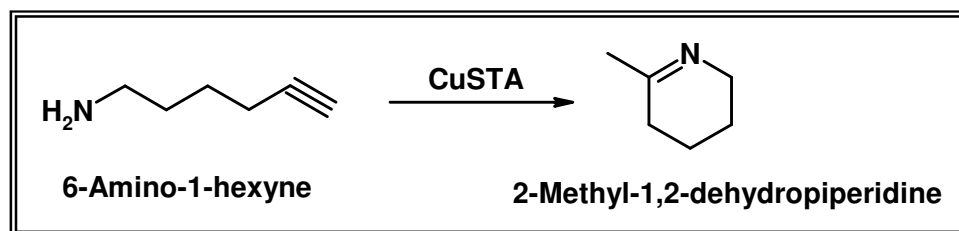
Scheme 5.3. Intramolecular hydroamination of 6-amino-1-hexyne

5.3. Results and Discussion-characterization

5.3.1. X-ray diffraction

Low angle XRD patterns of SBA-15, AlSBA-15 and 20CuSTA/SBA-15 and 20CuSTA/AlSBA-15 are depicted in Fig. 5.1. Peaks in the *2θ* range of 0.8 to 1.8 correspond to the (100), (110), (200) reflections which are associated with p6mm hexagonal symmetry in the materials were observed in all the catalysts. The impregnation of 20wt.% CuSTA did not harm the structure of mesoporous supports. XRD patterns of impregnated catalysts were compared with CuSTA at wide angle range. No diffraction peaks characteristic for CuSTA appears in the spectra of impregnated catalysts. This is a consequence of finely dispersed CuSTA in the porous structure of mesoporous silica and the composite shows amorphous nature at wide angle range. Staiti et al made similar observations when they impregnated HPA in porous silica [35].

5.3.2. N_2 sorption measurements

Specific surface area of HPA and salts of HPA represented in Table 5.1. are typically obtained from low-temperature (-196 °C) nitrogen adsorption isotherms. HPAs have low surface area (~12 m^2/g) whereas salts of HPAs showed still lower surface area (~6 m^2/g). The N_2 sorption analyses of mesoporous catalysts are represented in Table 5.2. Surface area of SBA-15 and AlSBA-15 (745 and 685 m^2/g respectively) decreased with impregnation of CuSTA on them (700 and 662 m^2/g respectively). Pore volume and pore diameter of 20CuSTA/SBA-15 and 20CuSTA/AlSBA-15 were slightly lower than that of their supports.
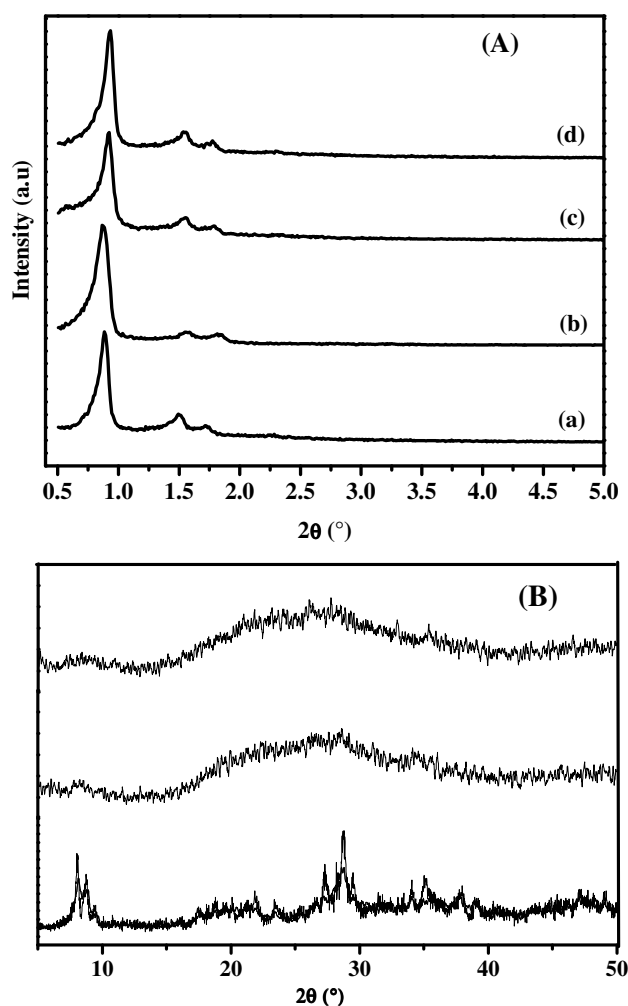

Fig. 5.1. (A) Low angle XRD patterns of (a) SBA-15, (b)AlSBA-15, (c) 20CuSTA/SBA-15 (d) 20CuSTA/AlSBA-15; (B) Wide angle XRD patterns of (a) CuSTA, (b) 20CuSTA/SBA-15, (c) 20CuSTA/AlSBA-15

Table 5.1. Surface area and catalytic activities of different catalysts in hydroamination of PhAc with aniline

Catalysts	Surface area (m^2/g)	Time (h)	PhAc Conversion (wt.%)
TPA	10	20	04
STA	12	20	03
MPA	12	20	03
CuSTA	6	1	35
CuSTA	6	8	99
Cu_1H_2STA	6	1	21
CuTPA	7	1	28
CuTPA	7	8	99
CuMPA	6	1	27
CuMPA	6	8	99
ZnSTA	-	8	45
PdSTA	-	20	21
CoSTA	-	20	08
NiSTA	-	20	06
MnSTA	-	20	05
$CuCO_3.Cu(OH)_2$	-	20	NR
$Cu(CH_3COO)_2$	-	20	NR

Reaction conditions: temperature = 110 °C, aniline to PhAc mole ratio = 2, catalyst wt. = 0.3 g, total reactants wt. = 2 g. toluene = 3 ml, NR = no reaction

5.3.3. FTIR measurements

The FTIR spectra of neat STA, TPA and MPA, and their copper salts are presented in Fig. 5.2. Detailed inspection of the bands in the range 1200–400cm^{-1} show characteristic bands for the structure of both pure heteropoly acids and salts. All

the characteristic bands of HPA and CuHPA catalysts are represented in Table 5.2. STA: 786 vs (W-O-W (edge)), 925 s (W-O-W (corner)), 984 s (W=O), 1021 w (Si-O). CuSTA: 782 vs (W-O-W (edge)), 924 s (W-O-W (corner)), 980 s (W=O), 1020 w (Si-O). FTIR spectrum of CuSTA shows that all the characteristics for parent STA is retained after salt formation and subsequent calcinations at 250 °C. Similar observations were made for CuTPA and CuMPA catalysts. They demonstrate that all the bands representing fingerprints of the Keggin unit structure of both acids and their salts are preserved.

Table 5.2. N_2 sorption analysis of CuSTA impregnated on mesoporous silica catalysts

SL No	Catalyst	Specific surface area (m^2g^{-1})	Pore volume (cm^3g^{-1})	Average pore diameter (Å)
1	SBA-15	745	1.03	66.6
2	AlSBA-15 (Si/Al = 17)	685	1.31	76.7
3	20CuSTA/SBA-15	700	0.96	62.1
4	20CuSTA/AlSBA-15 (Si/Al = 17)	662	0.99	70.2

Table 5.3. Keggin unit IR bands of HPA and CuHPA catalysts

IR bands (cm^{-1})	STA	CuSTA	TPA	CuTPA	MPA	CuMPA
M-O-M (edge)	786	782	801	798	787	786
M-O-M (corner)	925	924	889	892	868	869
M=O	984	980	983	983	963	961
Si-O or P-O	1021	1020	1080	1080	1065	1065

M = W or Mo
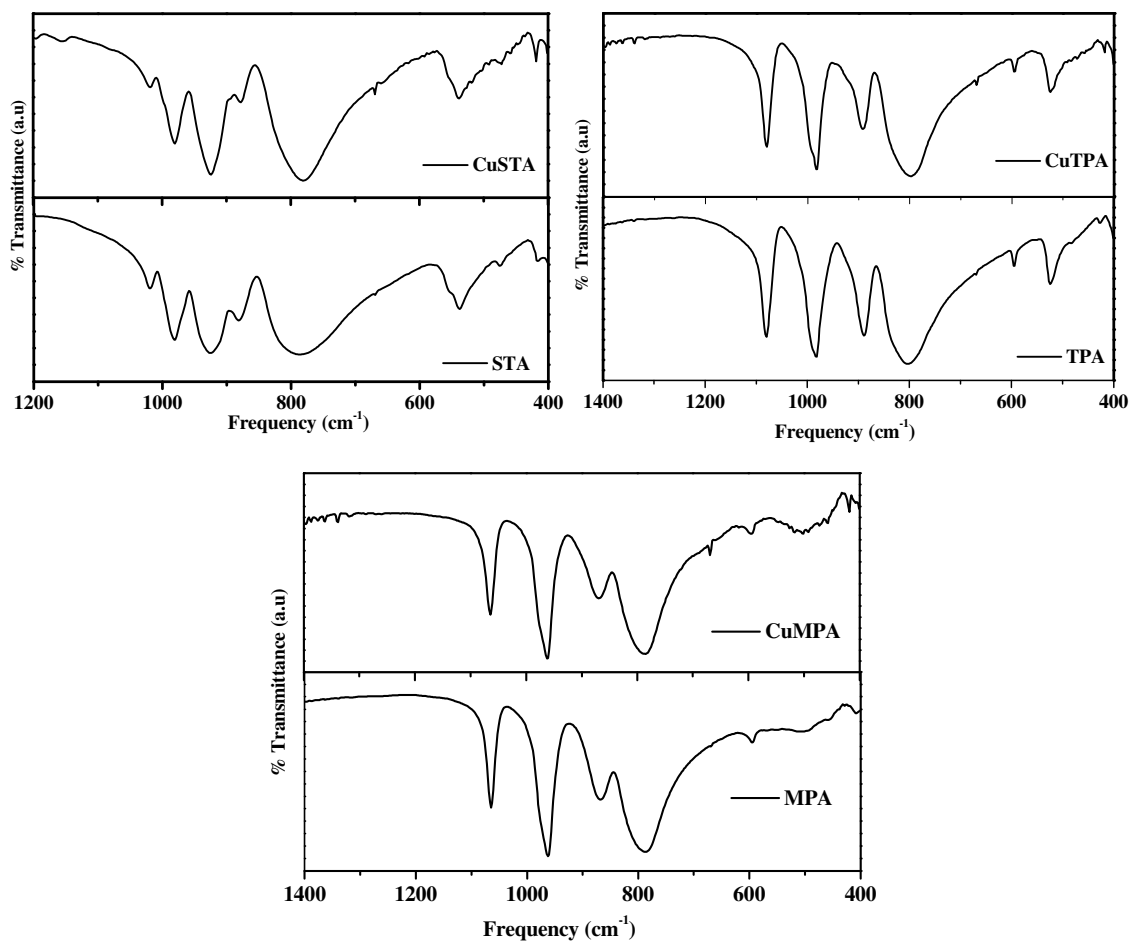
Fig. 5.2. FTIR spectra of HPA and CuHPA catalysts

5.3.4. Thermal analysis

The thermal stability of the bulk STA and CuSTA were investigated by means of TGA-DTA (Figures 5.3 and 5.4). The TGA profile of the STA shows a weight loss in three steps, which are due to the removal of physisorbed water, crystalline water and constitutional water respectively. The DTA profile of the STA also shows two endothermic peaks, which correspond to water loss at 103 °C and 225 °C in the first two steps. The small endothermic peak at 346 °C corresponds to the loss of constitutional water. The decomposition of the bulk STA is verified by an exothermic

peak at around 520 °C, which is associated with the decomposition of STA to corresponding oxides.
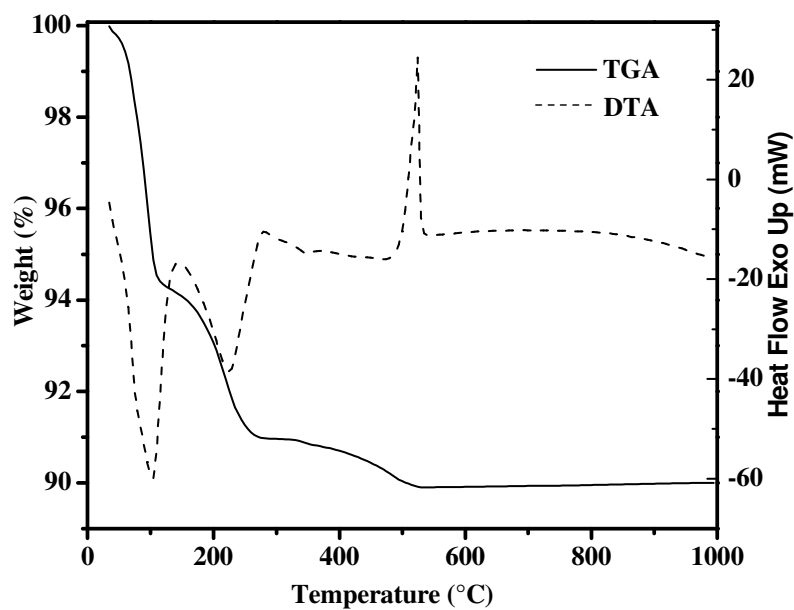

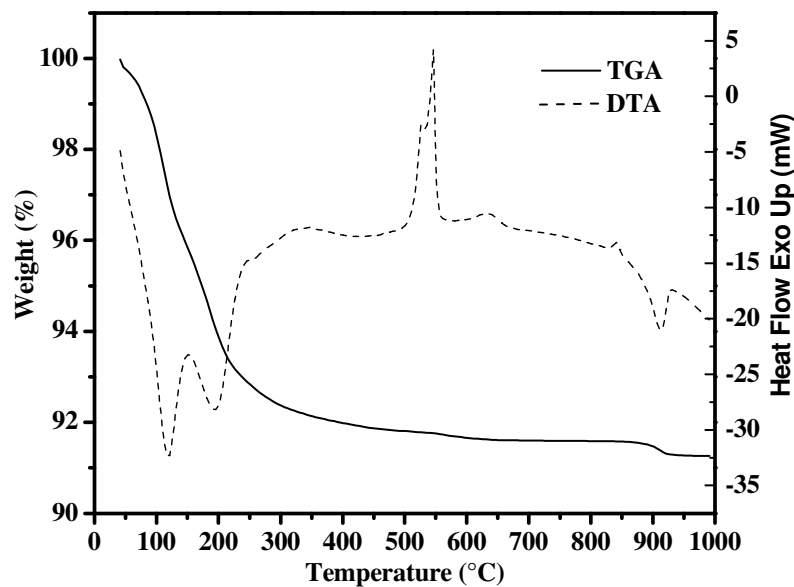**Fig. 5.3.** TGA-DTA profile of STA

Fig. 5.4. TGA-DTA profile of CuSTA

The TGA profile of the CuSTA showed a weight loss in two steps, which are due to the removal of physisorbed water and crystalline water as shown in Fig. 5.4. The third step is absent in CuSTA because the absence of constitutional water. The DTA profile of CuSTA showed two types of endothermic peaks responsible for the loss of water. The first peak observed at about 116 °C, related to the removal of the physisorbed water whereas the second endothermic peak originates from removal of crystalline water at 192 °C. The complete decomposition of CuSTA with the formation of oxides corresponds to the large exothermic effect at 546 °C and another small exothermic peak at 634 °C results from exothermic crystallization of oxides.

5.4.   Result and discussion-catalytic activity

5.4.1. Catalytic activities of different HPA and salts of HPA.

Since transition metal salts of heteropoly acids are insoluble in nonpolar reaction medium, they were used as heterogeneous catalysts in hydroamination of alkynes with amines. The reaction of phenylacetylene with aniline to give phenyl-(1-phenylethylidene)amine was used as a model reaction. The reaction was carried out by taking heteropoly acids TPA, MPA and STA as catalysts. These acids showed very poor activities (> 4%) towards hydroamination even after 20h reaction (Table 5.1). Activities of different copper salts of heteropoly acids were compared after 1h of reaction. CuSTA gave highest conversion (35%) followed by CuTPA (28%) and CuMPA (27%). The higher activity of copper heteropoly salts compared to heteropoly acids suggests that copper is the active species in hydroamination reactions. The higher activity of CuSTA could be attributed to its higher copper content viz. 2 moles of copper in each mole of CuSTA salt compared to 1.5 moles of copper in CuTPA and CuMPA. The role of copper was further explored by conducting reaction with Cu_1H_2STA which showed almost half of the activity (21% in 1 h) compared to CuSTA. Other copper salts such as copper acetate and basic copper carbonate did not show any activity as heterogeneous catalysts. Cu^{2+} in these salts are so strongly bound with the anion that they cannot take part in the reaction whereas copper ion in heteropoly salts are loosely bound to the bulky Keggin anion, which enables it to catalyze the reaction.

In order to find the influence of metals on the intermolecular hydroamination of phenyl acetylene by aniline, silicotungstic salt prepared with different divalent transition metals such as Zn, Cu, Pd, Co, Mn were tested (Table 5.1). It is seen that CuSTA showed the highest activity with 99% PhAc conversion while ZnSTA showed 45% conversion in 8 h. The other catalysts followed as PdSTA (21 %), CoSTA (8 %) and MnSTA (6 %) after 20 h of reaction.

5.4.2. Optimization of reaction conditions using CuSTA catalyst

For exploring the potential of CuSTA as catalyst, the hydroamination of phenyl acetylene was carried out in toluene and the conditions were optimized. The effects of catalyst and substrate concentrations, and temperature on hydroamination of phenyl acetylene with aniline over CuSTA were investigated. The following observations were noted when studies were carried out at the following reaction conditions:
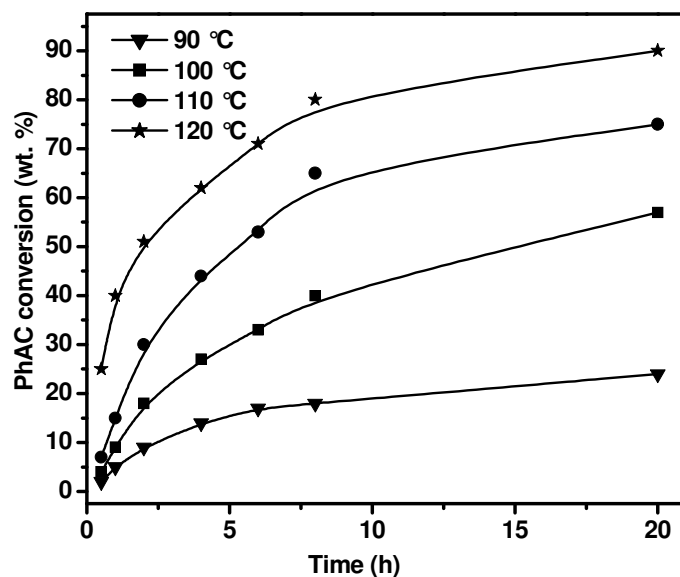
Fig. 5.5. Effect of reaction temperature. (Conditions: catalyst = CuSTA, aniline to PhAc mole ratio = 1, catalyst wt. = 0.1 g, total reactant wt. = 2 g, toluene = 3 ml).

5.4.2.1. Effect of temperature

Temperature was varied between 90 – 120 °C, by keeping total reactant weight (2 g), amount of solvent (3 ml), catalyst (0.1 g) and phenylacetylene and aniline ratio (1) constant (Fig 5.5.). The PhAc conversion increased with increase in

temperature as expected. There was a linear increase in conversion up to 6 h and the reaction proceeded steadily thereafter. 100% product selectivity was observed for Markovnikov addition product. Activation energy (Ea) was calculated by using initial rate approach which was found to be 18 kcal/mol.

5.4.2.2. Effect of mole ratio

Aniline to phenyl acetylene mole ratio was varied between 1 to 10, by keeping the temperature (100 °C), amount of solvent (3 ml) and catalyst (0.1g) constant (Fig. 5.6.). It is observed that an increase in the concentration of aniline favors the conversion for phenyl acetylene. There was a 20% increase in conversion when the mole ratio was changed from 1 to 10 after 4 h of reaction. Hence higher aniline concentrations facilitate the hydroamination reaction with CuSTA catalyst.
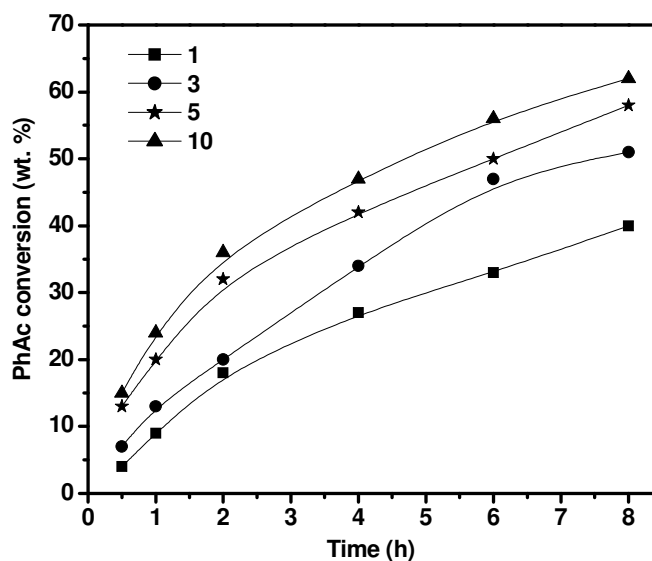
Fig. 5.6. Effect of anline to PhAc mole ratio. (Conditions: catalyst = CuSTA, temp = 100 °C, catalyst wt. = 0.1 g, total reactants wt. = 2 g, toluene = 3ml).

5.4.2.3. Effect of catalyst concentration

The concentration of the catalyst was varied between 0.025 – 0.1 5g by keeping the temperature (100 °C), amount of solvent (3 ml) and mole ratio of phenyl acetylene and aniline (1) constant and results are depicted in Fig. 5.7. An increase in the rate of phenyl acetylene conversion was observed over a period of 8h upon

increasing the catalyst concentration. It is expected since an increase in catalyst concentration increases the number of active species in the reaction.
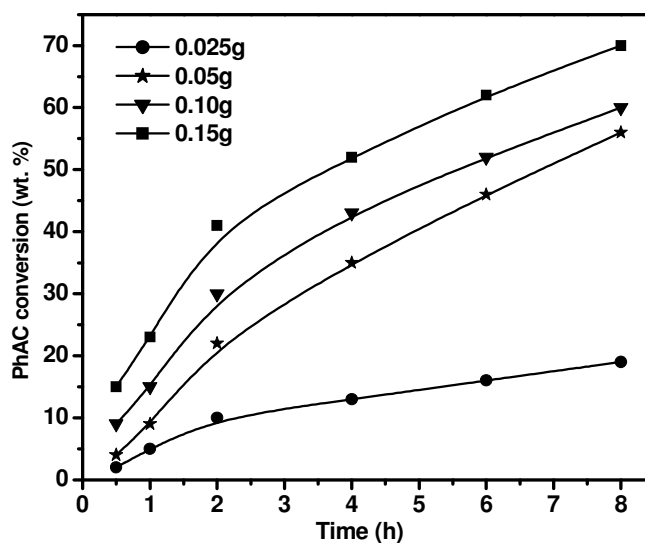

Fig. 5.7. Effect of catalyst concentration. (Conditions: catalyst = CuSTA, temp = 100 °C, aniline to PhAc mole ratio = 1, total reactants wt. = 2 g, toluene = 3 ml).

5.4.3. Catalyst leaching, regeneration and recyclability studies

In order to check the leaching of active species from CuSTA into the reaction medium during hydroamination reaction, the reaction mixture was hot filtered after 2 h of the reaction (22% conversion). The reaction was continued with the filtrate for 10h. The conversion remained the same even after 10 h of reaction, which indicates that no active species is leached into the reaction medium.

CuSTA catalyst, which gave complete conversion of PhAc, was separated from the reaction mixture and washed with toluene several times to remove adsorbed reactants and products. The catalyst was further refluxed in toluene for 2 h, filtered and washed with toluene. The catalyst was then dried and calcined at 250 °C for 5 h. This regenerated catalyst was then used for first recycle. After every recycle, the regeneration procedure was repeated and used for the next recycle. It is observed that after 5 recycles of CuSTA catalyst, the PhAc conversion decreased by 12 wt.% (Table 5.4). The decrease in activity is due to the progressive deactivation of the catalyst.

Table 5.4. Catalyst recyclibility studies

Recycles	PhAc conversion (wt.%)
1st	99
2nd	95
3rd	93
4th	91
5th	87

(Conditions: catalyst = CuSTA, temperature = 120 °C, aniline to PhAc mole ratio = 3, catalyst wt. = 0.2 g, total reactants wt. = 2 g, time = 8 h, toluene = 3 ml).

5.4.4. Reaction of different alkynes and amines

The nature of substituents on the aromatic ring of aniline derivatives has a significant effect over the reactivity (Table 5.5. (A)). The electron-donating groups at the -*ortho* and -*para* positions gave higher conversions to yield the corresponding imines whereas substrates with electron withdrawing groups gave lower conversions.

The sterically hindered amines such as 2,4,6-trimethylaniline (37%) and 2, 4-xylidine (35%) showed less reactivity. The amines with electron withdrawing substituents such as 4-chloroaniline (15%), 4-bromoaniline (21%) were least reactive. Interesting correlation of aromatic amine reactivity can be made with its basicity. It is observed that amine reactivity decreased with decrease in its basicity (Fig. 5.8.). *p*-Anisidene (pKb = 8.7) gave 89% conversion after 4h whereas 4-nitroaniline (pKb = 13) did not undergo reaction. Amine, being a nucleophile, should be strong enough to attack the electron deficient carbon of alkyne (Scheme 5.4.). Higher the basicity greater is the strength of the nucleophile.

The reactions were also carried out by reacting different alkynes with aniline (Table 5.5. (B)). Aromatic alkynes were more reactive than aliphatic alkynes while terminal alkynes showed higher conversions. Internal alkynes like diphenylacetylene did not undergo the reaction indicating that this catalyst is only suitable for

hydroamination of terminal alkynes. The alkynes with electron-donating substituents, -CH$_3$ and –OCH$_3$ gave better conversions (80 and 90% after 4 h respectively) whereas

Table 5.5. Hydroamination of different alkynes and amines[a]

(A) Intermolecular hydroamination of phenyl acetylene with aromatic amines				
Aromatic amine	Ring Substituent	pKb	Conversion (wt.%)	
			4h	8h
p-Anisidine	*p*-OCH$_3$	8.7	89	99
4-Ethylaniline	*p*-CH$_2$CH$_3$	8.9	88	99
Cumidine	*p*-CH(CH$_3$)$_2$	9.0	88	99
2,4-Xylidine	*o,p*-CH$_3$	9.1	80	97
Aniline	-H	9.4	77	99
2,4,6-Trimethylaniline	*o,m,p*-CH$_3$	9.6	75	95
4-Bromoaniline	*p*-Br	10.0	34	61
4-Chloroaniline	*p*-Cl	10.0	22	53
4-Nitroaniline	*p*-NO$_2$	13.0	0	0

(B) Intermolecular hydroamination of aniline with alkynes			
Alkyne	Ring substituent	Conversion (wt.%)	
		4h	8h
Phenylacetylene	-H	77	99
4-Ethynyltoluene	-CH$_3$	80	99
4-Ethynylanisole	-OCH$_3$	91	99
4-Ethynylbenzaldehyde[b]	-CHO	86	99
4-Ethynyl-2-nitrobenzene	-NO$_2$	22	38
4-Ethynyl-2-methoxynaphthalene	-	45	76
1-Heptyne	-	21	38
Diphenylacetylene	-	-	NR
6-Amino-1-hexyne[c]	-	82	99

[a]Reaction conditions: catalyst = CuSTA Amine to alkyne mole ratio = 2, toluene = 3 ml, temperature = 110 °C, catalyst wt. = 0.3 g, total reactants wt. = 2 g, conversion w.r.t. alkyne, 100 % selectivity for Markovnikov product.
[b] 55% selectivity for Markovnikov product
[c]Intramolecular hydroamination; conditions: catalyst = CuSTA, catalyst wt. = 0.075 g substrate wt. = 0.5 g, temp = 110 °C, toluene = 2 ml

the bigger molecule like 1-ethynyl-6-methoxynaphthalene showed comparatively lower conversion (76% after 8 h). The reaction of aniline with 4-ethynylbenzaldehyde gave 91% conversion after 4 h and 55% selectivity for hydroamination product. The second product formed was due to the condensation of -CHO group with $–NH_2$ of aniline to form an imine. 4-Ethynylnitrobenzene yielded only 38% of product after 8h of reaction.
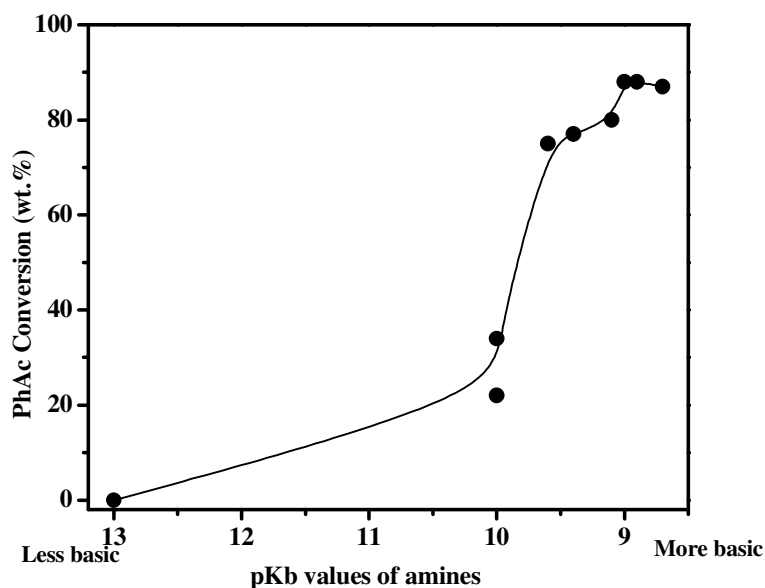

Fig. 5.8. Correlation between the conversion of PhAc and the basicity of aromatic amines

5.4.5. Application of acidity as promoter.

The effect of impregnation of CuSTA on mesoporous SBA-15 and AlSBA-15 (Si/Al = 17) was studied in hydroamination of PhAc with aniline at 110 °C, mole ratio of 1 using toluene as solvent. 20 wt% of CuSTA was impregnated on SBA-15 and AlSBA-15. The amount of CuSTA loading was not optimized. The catalysts weight was adjusted in these reactions to keep CuSTA content constant. For example, 0.1 g of neat CuSTA was used in the reaction whereas 0.5 g of 20CuSTA/SBA-15 is used for comparison. Fig. 5.4. represents the time plots of neat and impregnated catalysts in hydroamination of phenyl acetylene with aniline. The reaction proceeded with 100% selectivity for Markovnikov addition product. SBA-15 and AlSBA-15 catalysts

showed very low PhAc conversion (2% and 5% respectively). When 20CuSTA/SBA-15 was used, the PhAc conversion dropped by 10% compared to CuSTA after 8 h of reaction. The decrease in conversion after CuSTA impregnation on SBA-15 suggests that the higher surface area of the support has no positive effect on the activity whereas a small decrease in conversion may be attributed to a decrease in accessibility of the active sites after impregnation. On the other hand, 20CuSTA/AlSBA-15 catalyst showed about 2.5 times higher activity compared to CuSTA. The acidity (discussed in Chapter IV) present in AlSBA-15 possibly acts as a promoter in hydroamination of phenyl acetylene with aniline. Similar observation was made by T.E. Muller and co-workers when they found an enhancement in activity of $Zn(OTf)_2$ by using triflic acid (a Bronsted acid) as a promoter in homogeneous intramolecular hydroamination reactions [36]. But the use of such strong homogeneous acids as promoters could lead to the leaching of active sites in heterogeneous catalysts. Hence the acidity in solid acids such as AlSBA-15 can prove as good promoter for CuSTA catalyst in hydroamination reaction.
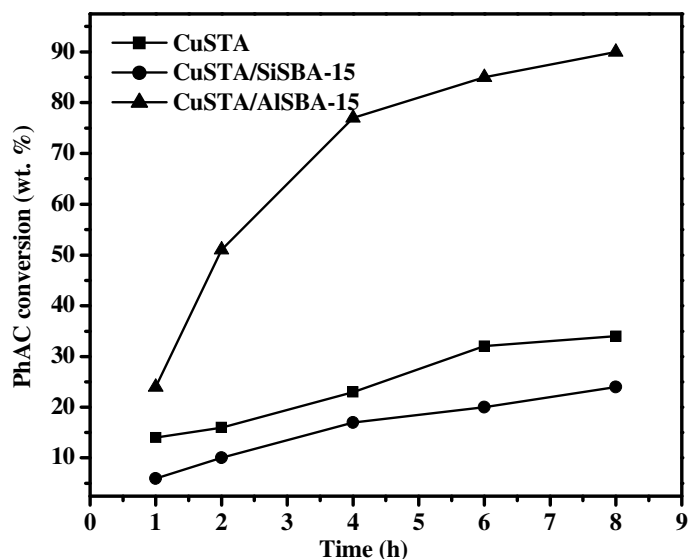

Fig 5.9. Effect of support on the activity of the catalyst in hydroamination of PhAc by aniline. (Conditions: temperature = 110 °C, aniline to PhAc mole ratio = 1, catalyst wt. = 0.1 g, total reactants wt. = 2 g, toluene = 3 ml).

5.4.6. Plausible mechanism

The above results show that Cu^{2+} ion is the active site in CuSTA catalyst for hydroamination reaction. Activity of a particular metal depends on the hardness property of metal cation [37]. Cu^{2+} ion is moderately hard acid and hence shows very high activity for hydroamination compared to other metals. The plausible mechanism involves the nucleophilic addition of amine to alkyne coordinated to Cu^{2+} ion. Alkyne forms a π-coordination complex with copper in step 1 (Scheme 5.4.). Amine attacks the electron deficient carbon atom on alkyne to form β-ammonioalkenyl complex in step 2. 1,3-Proton shift from nitrogen to β-carbon results in the formation of enamine in step 3. Enamine being unstable under the reaction conditions, rearranges itself to form imine in step 4. Brönsted acidity can facilitate step 3 and step 4 where migration of protons is involved.
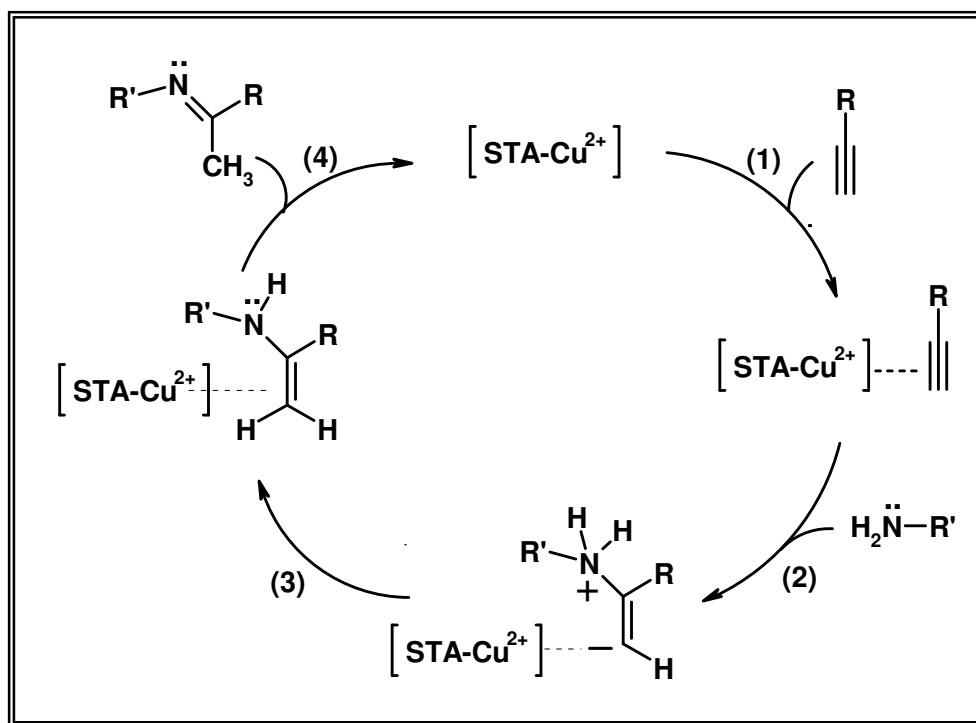
Scheme 5.4. Plausible mechanism of hydroamination of alkyne with amine catalyzed by CuSTA

5.5. References

1. H. Niiyama, Y. Saito, E. Echigoya, "Proceedings, 7th International Congress on Catalysis, Tokyo, 1980," p. 1416. Kodansha, Tokyo/Elsevier, Amsterdam, 1981.

2. H. Hayashi, J.B. Moffat, J. Catal. 77 (1982) 473.

3. T. Okuhara, T. Hashimoto, T. Hibi, M. Misono, J. Catal. 93 (1985) 224

4. M. Misono, Catal. Rev. Sci. Eng. 29 (1987) 269.

5. I.V. Kozhevnikov, Chem. Rev. 98 (1998), 171.

6. E. B. Crusson, M. Rigole, M. Fournier, A. Aboukais, F. Daubreged, G. Hecquet, Michel Guelton, Appl. Catal. A Gen. 178 (1999) 69.

7. J.S. Kim, J.M. Kim, G. Seo, N.C. Park, H. Niiyama, Appl. Catal. A Gen. 37 (1988) 45.

8. Y. Izumi, Catal. Today 33 (1997) 371.

9. N. Mizuno, M. Misono, Chem. Rev. 98 (1998), 199.

10. Y. Ono, T. Baba, J. Sakai, T. Keii, J. Chem. Soc. Chem. Commun. (1982) 400.

11. T. Okuhara, N. Hayakawa, A. Kasai, M. Misono, Y. Yoneda, J. Catal. 83 (1983) 121.

12. M. Misono, T. Okuhara, T. Ichiki, T. Arai, Y. Kanda, J. Am. Chem. Soc. 109 (1987) 5535.

13. A. Aboukais, D. Ghoussoub, E. B.Crusson, M. Rigole, M. Guelton, Appl. Catal. A: Gen. 111 (1994) 109.

14. J.M. Tatibouët, C. Montalescot, K. Brückman, Appl. Catal. A: Gen. 138 (1996) L1.

15. S. Damyanova, J.L.G. Fierro, Chem. Mater. 10 (1998) 871

16. A. Molnár, T. Beregszászi, A. Fudala, P. Lentz, J.B. Nagy, Z. Kónya, I. Kiricsi, J. Catal. 202 (2001) 379.

17. C. Yuan, F. Zhang, J. Wang, X. Ren, Catal.Commun. 6 (2005) 721.

18. K.M. Reddy, N. Lingaiah, P.S.S. Prasad, I. Suryanarayana, J. Sol. Chem.35 (2006) 407.

19. Y.B. Gu, R.P. Wei, X.Q. Ren, J. Wang, Catal. Lett. 113 (2007) 41.

20. T. Okuhara, T. Nishimura, H. Watanabe, M. Misono, J. Mol. Catal. A Chem. 74 (1992) 247.

21.   G.B. McGarvey, J.B. Moffat, Catal. Lett. 16 (1992) 173.

22.   A.W.S. Kreemers, M.V. D. Zon, M. Makkee, J.J.F. Scholten, J. Mol. Catal. A Chem. 107 (1996) 247.

23.   K. Nowinska, M. Sopa, D. Dudko, M. Mocna, Catal. Lett. 49 (1997) 43.

24.   K.A.S. Rocha, P.A. R. Dutenhefner, E.M.B. Sousa, E.F. Kozhevnikova, I.V. Kozhevnikov, E.V. Gusevskaya, Appl. Catal. A: Gen. 317 (2007) 171.

25.   B.Y. Giri, B.L.A.P. Devi, K.N. Gangadhar, K.V. Lakshmi, R.B.N. Prasad, N. Lingaiah, P.S.S. Prasad, Syn. Commun. 37 (2007) 2331.

26.   E. B. Crusson, M. Rigole, M. Fournier, A. Aboukaões, F. Daubrege, G. Hecquet, M. Guelton, Appl. Catal. A: Gen. 178 (1999) 69.

27.   N.A. Alekar, S. Gopinathan, C. Gopinathan, Ind. J. Chem. A 39 (2000) 439.

28.   A. Aouissi, L.A. Allaoui, D. Aldhayan, Asian J.Chem.18 (2006) 3009.

29.   L.A. Allaoui, A. Aouissi, J. Mol. Catal. A Chem. 259 (2006) 281.

30.   G. Zhou, X. Yang, J. Liu, K. Zhen, H. Wang, T. Cheng, J. Phys. Chem. B 110 (2006) 9831.

31.   H. Zhang, X. Zhang, Y. Ding, L. Yan, T. Ren, J. Suo, New J. Chem. 26 (2002) 376.

32.   N. Lingaiah, N. S. Babu, K. M. Reddy, P. S. S. Prasad, I. Suryanarayana, Chem. Commun. (2007) 278.

33.   T.E. Muller, J.A. Lercher, N.V. Nhu, AIChE, 49 (2003) 214.

34.   G. A. Tsigdinos, Ind. Eng. Chem., Prod. Res. Develop. 13 (1974) 267.

35.   P. Staiti, S. Freni, S. Hocevar, J. Power Sources 79 (1999) 250.

36.   J. Penzien, R.Q. Su, T.E. Muller, J.Mol. Catal. A Chem. 182 (2002) 489.

37.   J.Penzien, C. Haeβner, A.Jentys, K. Köhler, T.E.Müller, J.Lercher, J.Catal. 221 (2004) 302.

CHAPTER VI

6.1. Summary

This thesis describes hydroamination reactions of alkynes and activated olefins with amines catalyzed by metal ion exchanged montmorillonite clays, AlSBA-15, CuAlSBA-15 and copper salts of Keggin heteropoly acids and their applications in hydroamination reactions of alkynes and activated olefins. This chapter present a brief summary of the work described in previous chapters and general conclusions arrived from the work.

Chapter I gives a general introduction about hydroamination reactions, mechanisms and literature survey of the homogeneous and heterogeneous catalysts employed in hydroamination reactions. It also gives brief introduction to clays, M41S and SBA-15 mesoporous solids and heteropoly compounds. Finally the aim of the thesis is given to explore the efficacy of the above heterogeneous catalyst systems in hydroamination reactions.

Chapter II describes the procedure for the preparation of metal ion exchanged montmorillonite clays, SBA-15, AlSBA-15 and M^{n+}AlSBA-15 and transition metal salts of heteropoly acids. A brief discussion of theory and experimental procedures of all characterization techniques such as N_2 sorption, X-ray diffraction, TEM, SEM, FTIR pyridine adsorption, TPD of ammonia, H_2-TPR, UV-vis spectroscopy, ^{27}AlNMR, ^{29}SiNMR, TG-DTA whichever applicable to particular catalysts were discussed in this section.

Chapter III Part A describes the preparation of transition metal ion incorporated montmorillonite K-10 clay by ion-exchanged method. The catalyst material was well characterized by XRD, AAS, sorption analysis, UV-vis spectroscopy and FTIR pyridine adsorption. The hydroamination of phenylacetylene with aniline was used as a model reaction. Activities of different metal ion (Zn^{2+}, Cu^{2+}, Pd^{2+}, Co^{2+}, Mn^{2+}) exchanged clays were compared. Correlation of acidity with catalytic activity was addressed. Reactions conditions were optimized with Zn^{2+}-K-10 clay. The

performance of Cu^{2+}-K-10 clay in hydroamination of different alkynes and amines were explored.

Part B describes the applications of commercially available montmorillonite clays like K-10, K-20, K-30, Al pillared and untreated clays in hydroamination of activated olefins. The catalysts were characterized by AAS, surface area and FTIR pyridine adsorption. Hydroamination of ethylacrylate with aniline was studied as a model reaction. Performance of montmorillonite K-10 with hydroamination of different amines and olefins was also discussed.

Chapter IV First part of the chapter describes the synthesis of AlSBA-15 materials with different Si/Al ratio, by post synthesis modification of SBA-15 and the structure of the catalysts systems were diagnosed with different technique such as small angle XRD, N_2 sorption measurements, SEM, TEM, ^{27}AlNMR, ^{29}SiNMR and acidity of the materials were estimated by TPD of ammonia and FTIR pyridine adsorption. Application of AlSBA-15 as a catalyst in hydroamination of activated olefins with amines was studied. The activity of AlSBA-15 was compared with AlMCM-41, H-beta and montmorillonite K-10 clay in the hydroamination of ethyl acrylate with aniline. The catalyst was employed in the reactions of other amines and α, β-unsaturated compounds such as methylacrylate, acrylonitrile and acrylic acid.

Second part of the chapter deals with the synthesis of CuAlSBA-15 (with different Si/Al ratio) catalyst by ion exchange method and characterization by the techniques such as XRD, N_2 sorption measurements, SEM, TEM, ^{27}AlNMR, ^{29}SiNMR, H_2-TPR and FTIR pyridine adsorption. The catalytic activity of CuAlSBA-15 was studied in the intermolecular hydroamination of terminal alkynes and aromatic amines.

Chapter V illustrates the preparation of copper salts of heteropoly acids and their characterizations by XRD, surface area, FTIR and TGDTA measurements. The application of salts of heteropoly acids as heterogeneous catalyst was scrutinized in the intra and intermolecular hydroamination of alkynes with amines. The role of acidity promoter is addressed.

Chapter VI summarizes the conclusions made in this thesis.

6.2. Conclusions

- Lewis acidity of the montmorillonite K-10 increased with the Zn^{2+} ion exchange whereas Bronsted acidity decreased. Zn/K-10 and Cu/K-10 catalysts were highly active in intermolecular hydroamination of phenyl acetylene with aniline to give N-(1-phenylethylidene)aniline. The reaction was highly regioselective and only the Markovnikov addition product was formed. The activity of Zn / H-beta and Zn / K-10 were nearly the same and others followed the order Zn / silica > H-beta > clay > silica. Metal ions with moderately hard Lewis acidity (e.g. Cu^{2+} and Zn^{2+}) are required to catalyze hydroamination of alkynes.

- The hydroamination of different alkynes and amines by Cu/K-10 showed that the catalyst is active for the reactions of terminal alkynes with aromatic amines. Bulky molecules such as naphthylamine and sterically hindered amines such as xylidine undergo hydroamination with high product yields with Cu/K-10 catalyst.

- Taking into account of surface area, the acidity per unit surface area of montmorillonite clays decreased in the order K10 ~ K20 > Al-pillared clay > K30 > untreated clay. Montmorillonite clay K-10 showed a superior catalytic performance in the hydroamination of ethylacrylate with aniline with a conversion of aniline to *anti*-Markovnikov mono-addition product with a very high rate constant. Clay showed high activity towards the hydroamination of ethylacrylate with both aliphatic and aromatic amines. The catalyst could easily be regenerated and recycled.

- AlSBA-15 and CuAlSBA-15 were successfully synthesized with a well-ordered nature of crystalline phases and hexagonal mesoporous structure, characterized by structural and textural characterizations such as XRD, N_2-sorption and TEM.

- FTIR pyridine adsorption of AlSBA-15 showed that Brönsted and Lewis acid sites were generated by the alumination of SBA-15 by post-synthesis method. In CuAlSBA-15, incorporation of copper led to an increase in Lewis acidity at the loss of Brönsted acidity.

- Solid-state ^{27}Al MAS NMR spectra of AlSBA-15 and CuAlSBA-15 catalysts showed a major peak at 53 ppm which corresponds to tetrahedrally coordinated framework aluminium in which Al is covalently bound to four Si atoms via

oxygen bridges indicates that most of the aluminum has been incorporated into the framework.

➢ In comparison to the ZnAlSBA-15 (10) sample, CuAlSBA-15 (10) exhibits a larger line width and lower intensity of ^{27}Al NMR signal at 53 ppm indicating the presence of paramagnetic Cu^{2+} ions near the aluminium sites in CuAlSBA-15.

➢ H_2-TPR profile of CuAlSBA-15 indicates that the copper ions are mostly located in the extra framework positions, which are in the exchanged form. Different shoulders observed for these solids indicate that they contain isolated Cu^{2+} species present in small clusters in different environments.

➢ Intermolecular hydroamination of activated olefins with amines catalyzed by AlSBA-15 was effectively used to synthesize β-amino acid derivatives. AlSBA-15 and AlMCM-41 catalysts showed around twice higher activities compared to H-beta and montmorillonite K-10. Hydroamination of ethylacrylate (EA) with aniline was used as a test reaction, which gave *anti*-Markovnikov product N-[2-(ethoxycarbonyl)ethyl]aniline with high selectivity. The reaction depends on the total acidity in the catalyst and both Brönsted and Lewis acid sites are active centers for this reaction. AlSBA-15 showed no leaching of the active sites and high recyclibility for the hydroamination reaction.

➢ The hydroamination of phenylacetylene with 2,4-xylidine catalyzed by CuAlSBA-15 was highly regioselective and only the preferred Markovnikov addition product was formed. The unexchanged catalysts like AlSBA-15 (supports) and CuO/SBA-15 showed very low catalytic activities in hydroamination, which indicate that copper in exchanged form is active species for this reaction.

➢ The activities of CuAlSBA-15 increased with decrease in Si/Al ratio since Cu^{2+} ion exchange increased with increase in aluminium content in the catalyst. AlSBA-15 and AlMCM-41 were the best supports compared to zeolite beta and clay, whereas Cu and Zn exchanged AlSBA-15 catalysts showed higher activity compared to other metals in the hydroamination of phenylacetylene with 2, 4-xylidine. The CuAlSBA-15 catalyst did not catalyze hydroamination reactions involving internal alkynes, aromatic secondary amines and aliphatic amines which shows that this catalyst is suitable for the hydroamination of terminal

alkynes with aromatic amines. CuAlSBA-15 showed no leaching of active species and could be regenerated and recycled.

➢ FTIR spectra of copper salts of heteropoly acids showed that all the characteristics for Keggin structure of parent HPA is retained after salt formation and subsequent calcinations at 250 °C. TGA-DTA analysis showed that STA and CuSTA are thermally stable upto ~500 °C. The absence of constitutional water in CuSTA shows that the protons of STA are replaced by copper, which confirms the salt formation.

➢ Copper salts of HPA were highly active as catalyst for the intermolecular hydroamination of phenylacetylene with aniline. CuSTA gave higher conversion that CuTPA and CuMPA due to the presence of more copper, which is an active species in the reaction.

➢ Other copper salts such as copper acetate and copper carbonate did not show any activity as heterogeneous catalysts. Cu^{2+} in these salts are so strongly bound with the anion that they cannot take part in the reaction whereas copper ion in heteropoly salts are loosely bound to the bulky Keggin anion, which enables it to catalyze the reaction.

➢ Aromatic amine reactivity decreased with decrease in its basicity in hydroamination reaction. Amine, being a nucleophile, should be strong enough to attack the electron deficient carbon of alkyne. Higher the basicity greater is the strength of the nucleophile.

➢ The decrease in conversion after CuSTA impregnation on SBA-15 suggests that the higher surface area of the support has no positive effect on the activity whereas a small decrease in conversion may be attributed to a decrease in accessibility of the active sites after impregnation. On the other hand, 20CuSTA/AlSBA-15 catalyst showed about 2.5 times higher activity compared to CuSTA. The acidity present in AlSBA-15 possibly acts as a promoter in hydroamination of phenyl acetylene with aniline.

   Thus, the present work showed heterogeneous catalysts such as Zn^{2+} and Cu^{2+} exchanged montmorillonite K-10 clay, CuAlSBA-15 and copper salts of STA can be effectively used as catalysts for hydroamination of terminal alkynes with aromatic amines. The acid catalysts like montmorillonite K-10 and AlSBA-15 are excellent catalysts for hydroamination of activated olefins with amines.

1. Copper(II) ion exchanged AlSBA-15: a versatile catalyst for intermolecular hydroamination of terminal alkynes with aromatic amines
   Ganapati V. Shanbhag, Trissa Joseph and S. B. Halligudi*
   Journal of Catalysis, *Volume 250 (2), 2007, 274-282.*

2. Heterogeneous intermolecular hydroamination of terminal alkynes with aromatic amines
   Ganapati V. Shanbhag, S.M. Kumbar, T. Joseph and S.B. Halligudi*
   Tetrahedron Letters, Volume 47 (2), 2006, 141-143.

3. Heteropoly acid supported on titania as solid acid catalyst in alkylation of p- cresol with tert-butanol
   S. M. Kumbar, **G. V. Shanbhag,** F. Lefebvre, S.B. Halligudi
   Journal of Molecular Catalysis A: Chemical, Volume 256 (*1-2),* 2006, 324-334.

4. Chemoselective *anti-*Markovnikov hydroamination of ,α, β-ethylenic compounds with amines using montmorillonite clay
   Trissa Joseph∗, **G.V. Shanbhag**, D.P. Sawant, S.B. Halligudi
   Journal of Molecular Catalysis A: Chemical, *Volume 250 (1-2),* 2006, 210-217.

5. Phenol tert-butylation over zirconia-supported 12-molybdophosphoric acid catalyst
   B.M. Devassy, **G. V. Shanbhag** and S. B. Halligudi*
   Journal of Molecular Catalysis A: Chemical, Volume 247 (1-2), 2006, 162-170.

6. Synthesis of monoallyl guaiacol via allylation using HY zeolite
   S.M. Kumbar, **G. V. Shanbhag** and S.B. Halligudi*
   Journal of Molecular Catalysis A: Chemical, Volume 244 (1-2), 2006, 278-282.

7. Mesoporous molecular sieve (MCM-41)-filled sodium alginate hybrid nanocomposite membranes for pervaporation separation of water–isopropanol mixtures
   S.D. Bhat, B.V.K. Naidu, **G.V. Shanbhag**, S.B. Halligudi, M. Sairam and T.M. Aminabhavi
   Separation and Purification Technology, Volume 49 (1), 2006, 56–63.

8. Copper(II) ion-exchanged montmorillonite as catalyst for the direct addition of NH bond to CC triple bond
   Trissa Joseph, **G.V. Shanbhag** and S.B. Halligudi*
   Journal of Molecular Catalysis A: Chemical, *Volume 236 (1-2), 2005, 139-144.*

9. Silicotungstate-modified zirconia as an efficient catalyst for phenol *tert-*butylation

B.M. Devassy, **G. V. Shanbhag**, S.P. Mirajkar, Walter Böhringer, Jack Fletcher and S.B. Halligudi*.
Journal of Molecular Catalysis A: Chemical, Volume 233 (1-2), 2005, 141-146.

10. Zirconia-supported phosphotungstic acid as catalyst for alkylation of phenol with benzyl alcohol.
B.M. Devassy, **G. V. Shanbhag**, F. Lefebvre, W. Böhringer, J. Fletcher and S.B. Halligudi*
Journal of Molecular Catalysis A: Chemical, Volume 230 (1-2), 2005, 113-119.

11. Intermolecular hydroamination of alkynes catalyzed by zinc-exchanged montmorillonite clay
Ganapati V. Shanbhag and S.B. Halligudi*
Journal of Molecular Catalysis A: Chemical, Volume 222 (1-2), 2004, 223-228.

12. Liquid phase allylation of anisole using TPA/ZrO2 catalyst
G. V. Shanbhag, B. M. Devassy and S. B. Halligudi*
Journal of Molecular Catalysis A: Chemical, Volume 218 (1), 2004, 67-72.

13. Alkylation of *p*-cresol with *tert*-butanol catalyzed by heteropoly acid supported on zirconia catalyst.
B.M. Devassy, **G. V. Shanbhag**, F. Lefebvre and S. B. Halligudi*
Journal of Molecular Catalysis A: Chemical, Volume 210 (1-2), 2004, 125-130.

14. Aerial oxidation of substituted aromatic hydrocarbons catalyzed by Co/Mn/Br– in water-dioxane medium
K. Nair, D.P. Sawant, **G. V. Shanbhag** and S. B. Halligudi*
Catalysis Communications, Volume 5 (1), 2004, 9-13.

15. Chemoselective synthesis of β-amino acid derivatives by hydroamination of activated olefins using AlSBA-15 catalyst
G. V. Shanbhag, S.M. Kumbar and S.B. Halligudi*
Journal of Molecular Catalysis A: Chemical, 2008 (In press)

16. Copper salts of heteropoly acids as heterogeneous catalysts for intra and intermolecular hydroamination reactions
G. V. Shanbhag, K. Palraj and S.B. Halligudi*
(Manuscript under preparation)